NOTICE

The quality of this microform is heavily dependent upon the quality of the original thesis submitted for microfilming. Every effort has been made to ensure the highest quality of reproduction possible.

If pages are missing, contact the university which granted the degree.

Some pages may have indistinct print especially if the original pages were typed with a poor typewriter ribbon or if the university sent us an inferior photocopy.

Reproduction in full or in part of this microform is governed by the Canadian Copyright Act, R.S.C. 1970, c. C-30, and subsequent amendments.

AVIS

La qualité de cette microforme dépend grandement de la qualité de la thèse soumise au microfilmage. Nous avons tout fait pour assurer une qualité supérieure de reproduction.

S'il manque des pages, veuillez communiquer avec l'université qui a conféré le grade

La qualité d'impression de certaines pages peut laisser a désirer, surtout si les pages originales ont été dactylographiées à l'aide d'un ruban usé ou si l'université nous a fait parvenir une photocopie de qualité inférieure

La reproduction, même partielle, de cette microforme est soumise à la Loi canadienne sur le droit d'auteur, SRC 1970, c. C-30, et ses amendements subséquents.

Electrochemical and Photoelectrochemical Studies on Electronic Conduction in an Ionomeric Polymer Blend

Mark Charles Lefebvre

A Thesis

in

The Department

of

Chemistry and Biochemistry

Presented in Partial Fulfilment of the Requirements
for the Degree of Master of Science at
Concordia University
Montreal, Quebec, Canada

August, 1991

ISBN 0-315-68732-0

Abstract

Electrochemical and Photoelectrochemical Studies on Electrical Conduction in an Ionomeric Polymer Blend

Mark C. Lefebvre

Ion exchange polymers can immobilize a large concentration of photoelectrochemically active molecules at an electrode's surface. One such cationic copolymer (**QP blend**) based upon a random copolymer of quaternized amines on poly(chloromethylstyrene-co-styrene) and poly(4-vinylpyridine-co-styrene) showed high in-partitioning of anions from solution and large diffusion coefficients (10^{-7} cm^2/s) for these across the film. When irradiated, films that contained bis(maleonitriledithiolato)-nickelate(II) produced photocurrent. Electronic conductivity along the polymeric backbone of the QP blend, however was poor and largely limited by electron traps.

Investigation of a superior electronic conducting ion exchange polymer, poly(xylylviologen) (**PXV**) featured poor ionic conductivity (10^{-9} cm^2/s) and illustrated the importance of supporting both electronic and ionic conductivity in these modifying films. A modifying layer of the PXV swollen with a polar hydrophobic solvent (tributylphosphate) gave high diffusion coefficients for ferri/ferrocyanide, but in-partitioning of the couple and overlap of adjacent polymer chains was limited.

Incorporation of PXV into dye modified QP blend films, a direction toward supporting electronic and ionic conductivities, met with limited success due to an inability to retain the PXV within the film or to preserve its electro-activity when anchored by crosslinking.

CdS particles offer high extinction coefficients, high surface area and

interparticle conductivity, but photocorrosion is a problem. Cells using small-sized surface-derivatized particles contained within the QP blend coating were limited by poor electronic conductivity along the QP blend and poor energetic coupling to solution species, despite successful passivation of CdS.

Acknowledgements

I wish to acknowledge and thank the following people without whom this work would not have been possible:

Dr Cooper Langford whose attitude toward research and researchers has stimulated enthusiasm in chemistry and science in many an uncertain wreck.

Dr Marcus Lawrence whose assistance and encouragement throughout this project is much appreciated.

Dr Roland Côté for his many free consultations on organic synthesis and fruit tree planting.

Drs Susan Mikkelsen and Ann English for agreeing to participate in this effort.

Ms Carole Coutts whose friendly and willing administrative assistance made the "final 90 feet to home plate" much easier.

All the technical staff in the Chemistry and Biochemistry department at Concordia whose help contributed to this work.

David Biro (PhD) whose help and friendship during the initial stages of my work at Concordia made the lab an enjoyable place to "do chemistry".

Paul Taslimi whose selflessness and great cooking will forever spoil me for other roommates (. Big Guy!).

The rest of my friends at Concordia who, when they weren't helping, at least weren't hindering (much).

Marie Ferland whose love has supported me through the difficult latter stages of this undertaking and whose fresh, realistic outlook prompted some self analysis and consequently a book (so blame it on her (heh heh)).

My sister, Jo and mother, Shirley for supporting me through this endeavour as well as through much of life. It is good to feel that there are people behind you, no matter what sort of derelict bum you are.

Table of Contents

List of Figures

List of Tables

List of Abbreviations in Text

ΔE_p	Separation (in volts) between anodic and cathodic peak potentials in a cyclic voltammogram
ϕ-CO_2^-	Benzoate
ϕ_m	Work function of a metal
ϕ_s	Work function of a semiconductor
ω	Molar water to surfactant ratio
A_p	Electron affinity
AOT	Surfactant dioctyl sulfosuccinate
D_{eff}	Effective diffusion coefficient
DMF	N,N-dimethylformamide
<E>	Centroid, representing the energy halfway between E_a and E_d
E_a	Energy of acceptor states
E_c	Minimum energy of conduction band
E_d	Energy of donor states
E_f	Fermi level
E_g	Energy difference between valence and conduction bands
E_o'	Formal reduction potential
E_{pa}	Potential of anodic peak
E_{pc}	Potential of cathodic peak
E_v	Maximum energy of valence band
E_{vac}	Reference vacuum energy level

FTIR	Fourier transform infrared
i_p	Voltammetric peak current
I_p	Ionization energy
$Ni(mnt)_2$	Bis(maleonitriledithiolato)nickelate(II)
OTE	Optically transparent electrode
P4VP	Poly(4-vinylpyridine-costyrene)
PXV	Poly(xylylviologen)
rR	Resonance Raman
SCE	Saturated calomel electrode
SCPC	Short-circuit photocurrent
QP	Quaternized random copolymer
QP blend	2:1 blend of quaternized random copolymer and poly(4-vinylpyridine-costyrene)
tbp	Tributylphosphate
Tris	Tris(hydroxymethyl)aminomethane
v	Scan rate
V_d	Potential created by band bending
V_{oc}	Potential measured at open circuit

Chapter 1

Introduction

1.1 Overview

With global non-renewable energy resources coming to a foreseeable end, oil in *ca.* 40 years and coal which is much more environmentally harmful in *ca.* 300 years, the drive toward alternative sources of energy continues. Solar energy represents a massive, largely untapped resource. Converting this abundant energy source into electricity or highly energetic products has been an active area of research (1-5).

The majority of solar energy lies in the visible and near IR region. Sensitized semiconductor photoelectrodes offer the potential of harvesting visible light. Efficiency may be realized by coupling a very large concentration of sensitizer to an electrode surface.

A series of publications (6-9) from this laboratory have described two ion-exchange polymer electrode coatings used to increase the effective electrode concentration of sensitizing dyes. One of these showed excellent ionic diffusion capabilities (6-8) while the other featured good electronic conductivity. The work has underlined the importance of efficiently supporting both ionic and electronic currents in a system which functions as a phototransducer between the two.

The subject of this thesis is bis(maleonitriledithiolato)nicke-late(II) sensitized SnO_2 optically transparent electrodes. Composite electrode coatings were prepared with the aim of incorporating good electronic conductors within polymeric matrices that display high mobilities for ionic species.

1.2 Sensitization of semiconductor electrodes

1.2.1 Solid state photovoltaics

When atoms form into molecules, their valence orbitals mix to give bonding and antibonding orbitals as per molecular orbital theory. The mixing of very many molecules into crystals causes mixing of the bonding and antibonding orbitals into very many closely spaced energy levels which, when the number of molecules approaches infinity, form into continuous energy bands, termed valence and conduction bands. If the energy difference between the valence and conduction bands (E_g) is small, electrons can be promoted to the conduction band upon input of a relatively small amount of energy such as might be found in a photon of visible light. The energy gap between conduction and valence bands is termed the forbidden region. Materials somewhat arbitrarily termed insulators have E_g's greater than 5 eV, semiconductors have E_g's less than 5 eV.

The Fermi level (E_f) is an important property of a material which can be thought of as a thermodynamic potential. The Fermi level is defined as the energy at which the probability of occupancy by an electron is 1/2. In a perfect single crystal intrinsic semiconductor which has no defect or doping states within the forbidden region, the Fermi level lies half way between the valence and conduction bands as in Figure 1.1a. Structural imperfections or impurities within the semiconductor lattice create energy levels or "states" which lie in the forbidden gap shifting the Fermi level either toward the bottom of the conduction band in the case of donor states or toward the top of the valence band in the case of acceptor states. A material's work function

(ϕ_s) is the energy necessary to remove an electron from it. The work function (Figure 1.1a for a semiconductor and Figure 1.1b for a metal) is simply the energy of the Fermi level relative to a reference vacuum level (E_{vac} - E_f). The work function of a metal (ϕ_m) is equivalent to its ionization potential (I_p).

Conductivity in semiconductors can be controlled by thermal and optical energies or an electric field. When an electron is displaced from the valence band a hole is left behind which can have a conductivity in the valence band as an electron can have a conductivity in the conduction band. Doping introduces a surplus of weakly bound holes or electrons which reduces the E_g by creating impurity states within the forbidden energy gap. Materials with a deficit of valence band electrons become conductors of holes, termed p-type (positive) semiconductors and those with a surplus of conduction band electrons become conductors of electrons, termed n-type (negative) semiconductors (shown in Figures 1.1c,d).

Semiconductors form the basis of photovoltaic solar cells as a result of their ability to create electron-hole pairs on absorption of electromagnetic radiation of energy equivalent to the near IR, visible, or near UV spectrum (Figure 1.1e). In the absence of an electric field, however, these pairs are likely to simply recombine giving no net current. In solid state semiconductor photovoltaic devices the electric field necessary to separate the electron hole pairs and therefore give net photocurrent is generated by the potential that arises when a metal, a semiconductor of different Fermi level, or an electrolyte solution forms a contact with the semiconductor. When such a contact is formed charge moves across the interface as the E_f of the two phases equil-

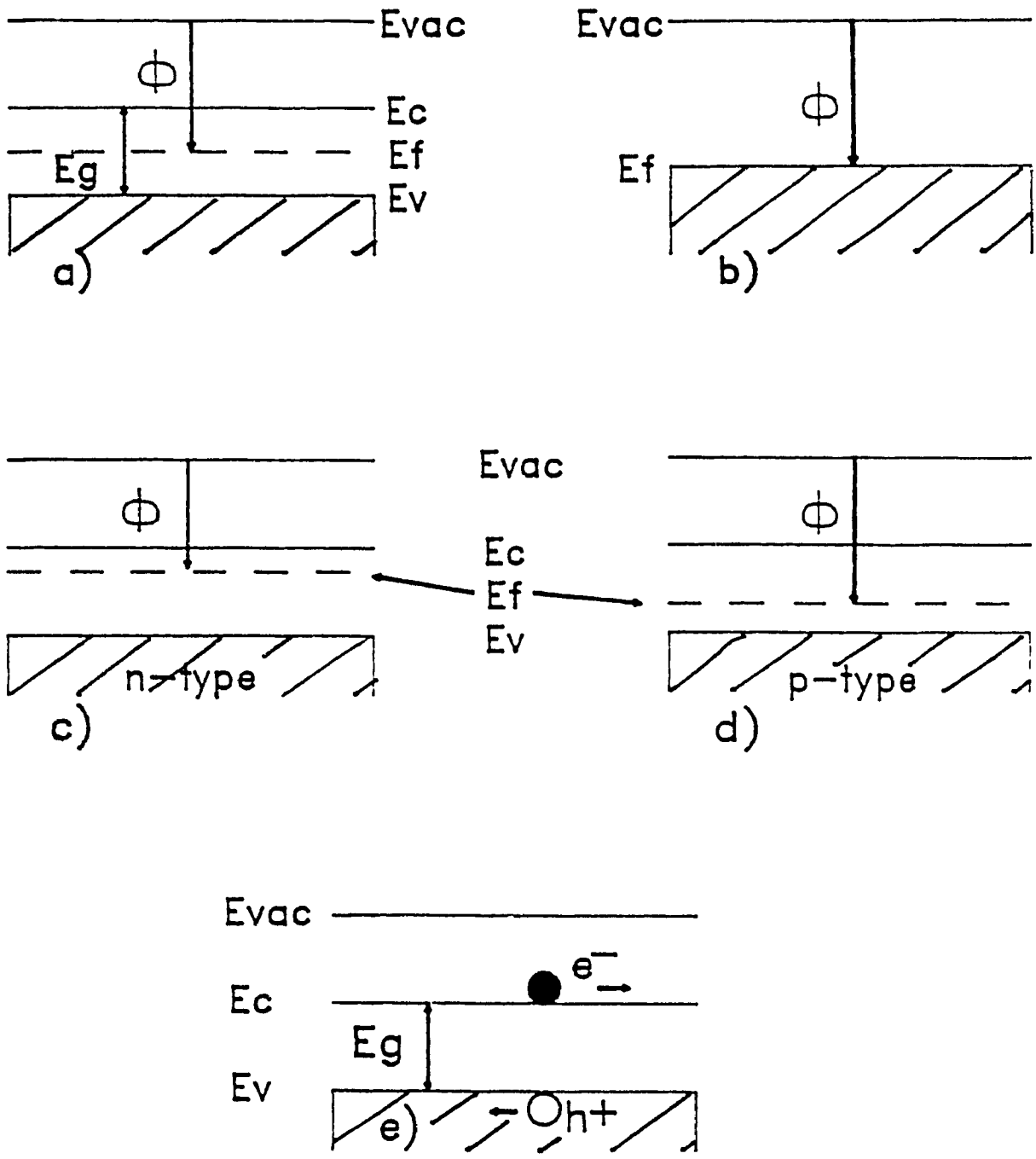

Figure 1.1 Energy band diagrams showing work function (Φ), vacuum (E_{vac}), conduction (E_c), Fermi (E_f), and valence (E_v) energy levels and band gap (ΔE_g) for (a) an intrinsic semiconductor, (b) a metal and (c and d) extrinsic n- and p-type semiconductors. (e) Diagram demonstrating electron hole pairs in an intrinsic semiconductor.

ibrates. In the bulk of the semiconductor the relative position of E_f to both E_c and E_v remains unchanged which causes bending of the bands in the semiconductor near the contact interface. Contact formation is illustrated in Figure 1.2. Band bending creates an electric field at the contact interface which is proportional to the potential created V_d, this region of the semiconductor being known as the space charge region. The E_f of metals and electrolytes remains unchanged since they are considered infinite electron sinks/sources relative to the semiconductor, i.e. their space charge regions are much narrower. Electron hole pairs created in the space charge region will be separated by the electric field developed by the band bending giving a net current. The photoelectrochemical process is very simple. Electron-hole pairs are created upon absorption of a photon of appropriate energy. These pairs are separated, minority carriers being transferred to ions in the electrolyte solution and majority carrier being transferred to the electrode.

1.2.2 Dye sensitization

Solid state photovoltaic devices offer the greatest efficiency and power output of the solar cells designed thus far (for example GaAlAs (10)). Research efforts are directed toward creating stable semiconductors with smaller band gaps and more energetically desirable junctions. The optimum bandgap for solar cell applications is between 1.5 and 2 eV which corresponds to visible light. Liquid/semiconductor junctions offer the potential for inexpensive, chemically based energy conversion devices which can be coupled to high energy products.

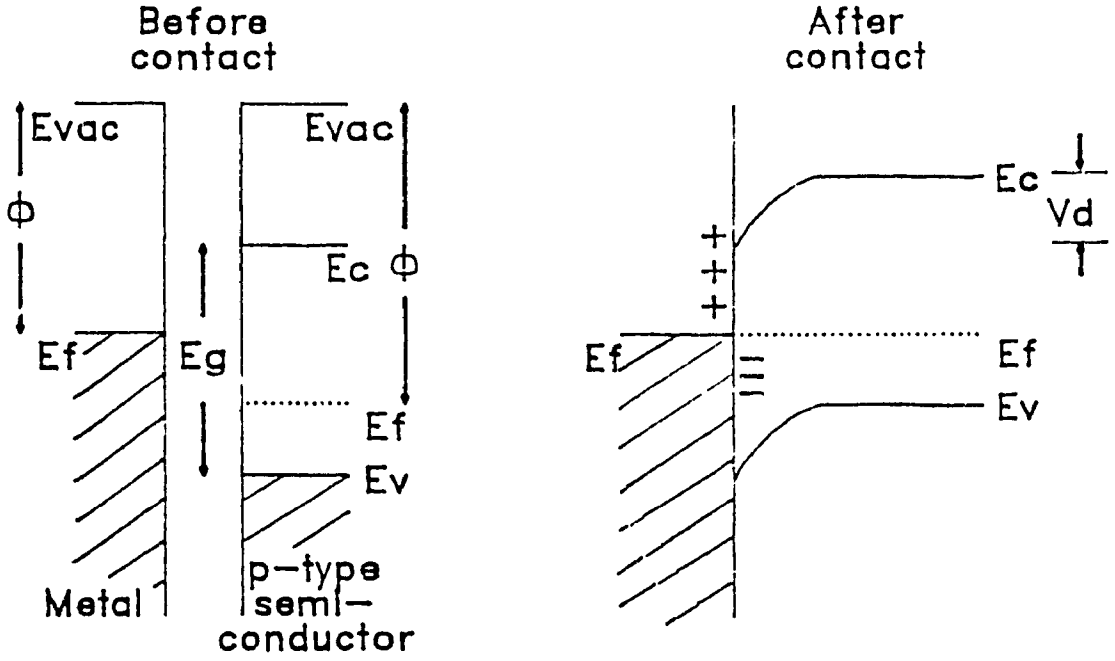

Figure 1.2 Energy diagram demonstrating a metal/semiconductor contact before and after contact. Φ and E_f of separate metal and semiconductor are illustrated. As well E_v, E_c and ΔE_g of semiconductor are shown. The contact causes shifting of the Fermi level of the semiconductor to that of the metal and band bending in the semiconductor close to the metal/semiconductor interface.

Table 1.1. Bandgaps of some common semiconductors.

Semiconductor	Bandgap (eV)	Wavelength equivalent (nm)
SnO_2	3.5	350
ZnO	3.2	390
TiO_2	3.0	410
CdS	2.4	520
Fe_2O_3	2.1	590
CdTe	1.4	890
Si	1.1	1130

An unfortunate reality for materials with small bandgaps capable of direct conversion of sunlight to usable energy is that they tend to be unstable when illuminated in electrolyte solutions. Illumination with photons of energy greater than or equal to the material's E_g creates electron-hole pairs. When a pair is separated in the space charge region the majority carrier is driven into the bulk of the semiconductor while the minority carrier is driven to the electrolyte interface. The minority carriers are, however, usually highly reactive and thus may oxidize or reduce the semiconductor itself. This is known as photocorrosion (4).

Large bandgap semiconductors such as the metal oxides (ie.SnO_2 or TiO_2) are not susceptible to corrosion but do not offer efficient use of the solar spectrum available on the surface of our planet. Photosen. .ization of these with dye molecules of appropriate energetics can permit broader use of the solar spectrum (Figure 1.3 is the spectral distribution of our sun). The dyes can be adsorbed or covalently bound to the electrode (11,12,13) or incorporated into polymeric matrices (7,8,14). Photosensi-

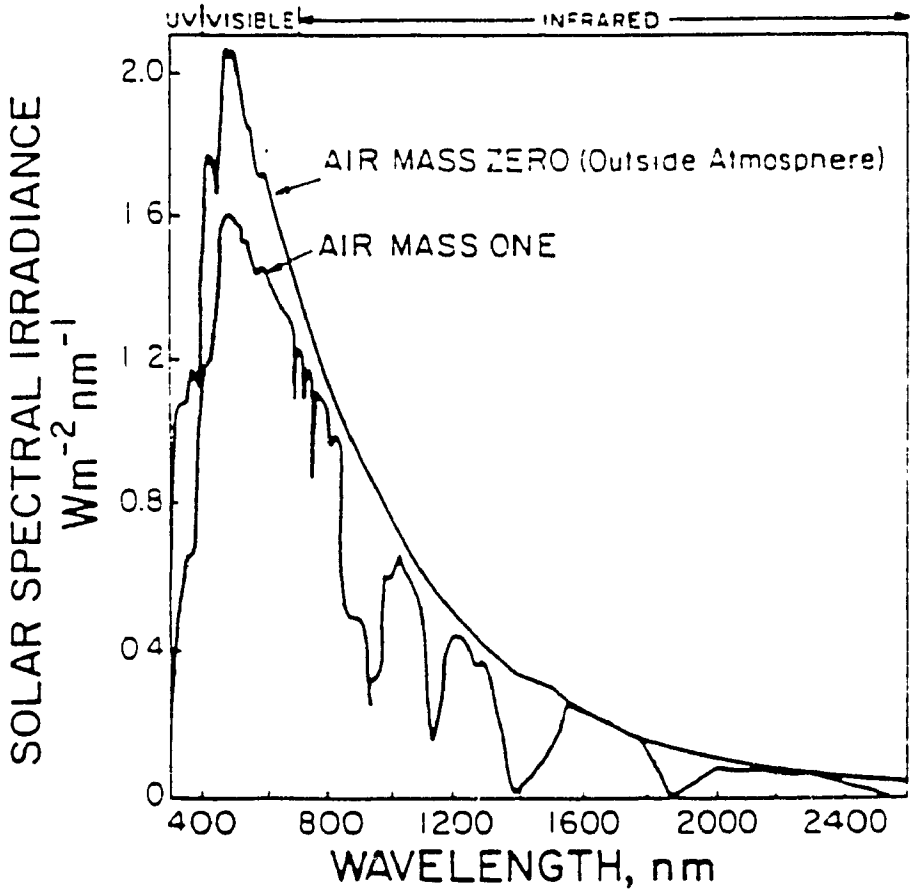

Figure 1.3 Solar spectral distribution on earth (air mass one) and outside atmosphere (air mass zero). From (71).

tized electrodes can only reach the efficiency of solid state devices in a form that allows absorption of a large fraction of the incident light. This requires use of dyes with very large absorption coefficients or photoelectrodes with very large effective areas.

In sensitized configurations, as opposed to semiconductor contact devices, the primary light absorber is generally not a good conductor, although much work is being carried out on organic semiconductors (15). In a semiconductor charge separation is affected by an electrical potential gradient created in the space charge region, whereas that at a photosensitized electrode must be effected by a chemical potential gradient featuring thermodynamically favourable coupling of the photoexcited dye to separate donor and acceptor species. Once a dye molecule is in the excited state, energy may be dissipated in a number of ways as illustrated in Figure 1.4. The electron is initially in a singlet excited state from where it can deactivate to the ground state by fluorescence or by radiationless relaxation, it can intersystem cross to a triplet state where it can deactivate by phosphorescence or again by a radiationless relaxation process. Should coupling to another molecule be sufficiently strong electron transfer from either the singlet or triplet states would be possible.

An energetic scheme for photoinitiated electron transfer in a dye sensitized photoanodic semiconductor wet cell is illustrated in Figure 1.5. The sensitizing molecules absorb visible light. The excited state of the dye must be higher in energy than the conduction band of the semiconductor, so that upon population of the dye's excited state electron transfer to the semiconductor's conduction band is thermody-

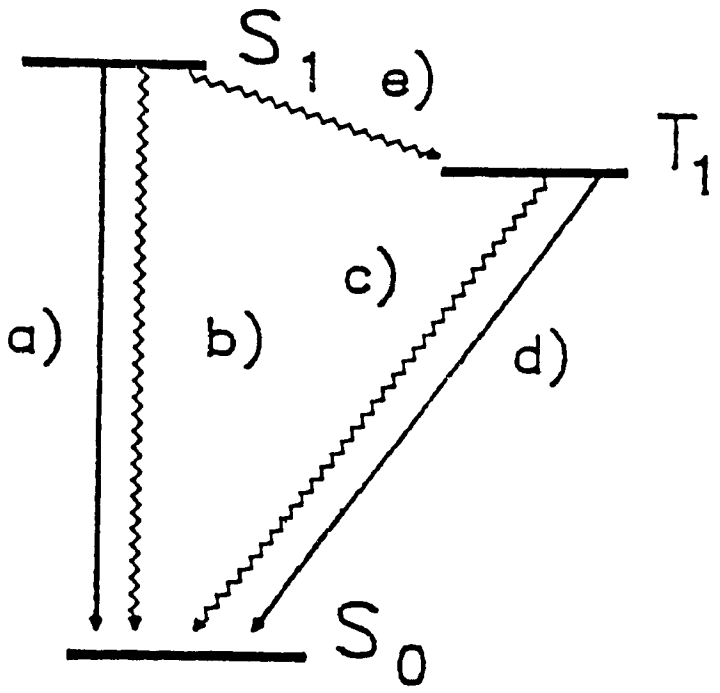

Figure 1.4 Diagram showing photophysical deactivation pathways of a photoexcited molecule. An electron in the lowest energy singlet excited state (S_1) can relax directly to the ground state (S_0) by (a) fluorescing; (b) vibrationally relaxing. From a triplet state (T_1) an electron can relax by (c) vibrational relaxation or (d) phosphorescence. (e) Intersystem crossing is the process by which an electron moves from a singlet to a triplet state by spin flipping.

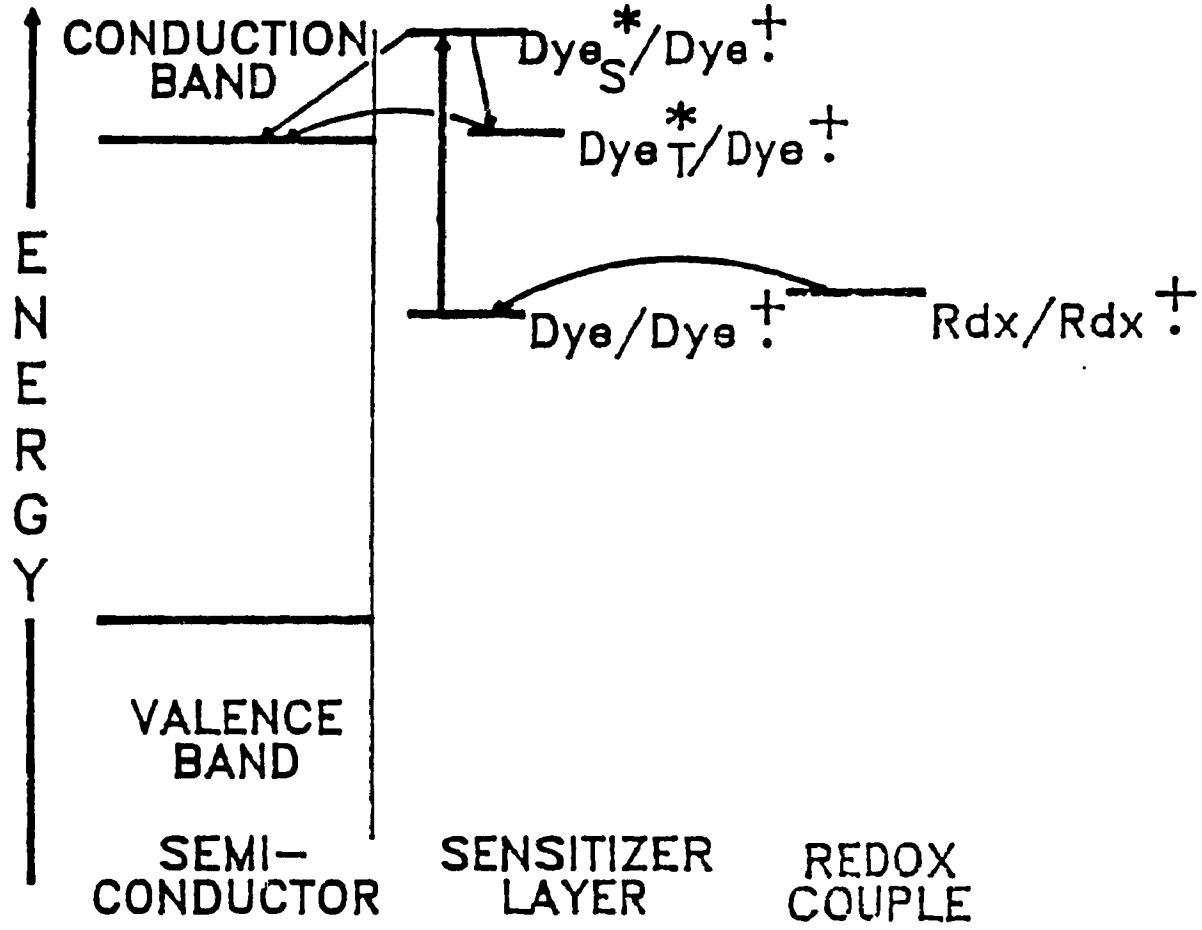

Figure 1.5 Photoelectrochemical scheme for a sensitized electrode. A dye molecule absorbs light and an electron populates a singlet or triplet excited state (Dye_s^* or Dye_t^*) from where transfer to the semiconductor electrode's conduction band is thermodynamically probable. The thus oxidized dye may be reduced by a solution redox species (Rdx), which itself may be reduced at a counter electrode in solution (not shown).

namically feasible. The reduced member of a solution redox couple of appropriate energy can then reduce the oxidized dye molecules to their initial ground state charge. The oxidized member of the redox couple can then diffuse to the counter electrode where it can be reduced, thus completing the faradaic portion of the circuit. There is no overall change in any of the reactants, so the system should be able to turn over many many times.

1.3 Modified electrodes

Immobilizing a chemically, optically, or electrochemically active molecule on the surface of an electrode may be thought of as an effort to efficiently couple the species of interest to an electron source or sink. The immobilized species should display chemical or electrochemical reactivities and optical properties similar to those of the unimmobilized species in order to predict the behaviour of such electrode systems. This is often the case and offers a great advantage when formulating the energetics of modified electrode surfaces. Such electrodes have seen application development over the last ten years in: 1) corrosion protection and photoactivation of photovoltaic or fuel producing electrodes (16,17), photoelectrolytic splitting of water (18); 2) substrate selective electroanalytical sensors (preconcentration analysis); 3) controlled release of chemically active reagents; 4) enzyme immobilization or biosensors (19); 5) electrochromism (20); 6) molecular based electronic devices (21); 7) reference electrode systems; 8) basic studies of electron transfer within surface films (22).

For photosensitization monolayer modification permits very efficient coupling of modifier to the electrode, but even the best photosensitizers have insufficient extinction coefficients to absorb a very large fraction of incident light as a monolayer. Multilayer films of photosensitizing molecules often show poor conductivity and hence charge produced at layers distant from the surface of the electrode would be unable to reach the electrode. Outer layers would simply attenuate the intensity of the light impinging upon molecules capable of transferring electrons to the electrode, those being immediately adjacent to the electrode. A better strategy is to incorporate the photosensitizer into a conductive matrix which allows coupling of the equivalent of many monolayers to the electrode surface. Polymers have seen the most application as electrode modifying matrices, these offering the advantage of greater stability than monolayers.

Polymers prepared from ionizable monomers are termed polyelectrolytes. Polyelectrolytes can be redox polymers, where an electroactive moiety forms part of the backbone of the polymer, ionically conductive and electronically conductive polymers. These coatings should already contain or be able to retain active species within the film, that is, they should possess favourable ion exchange partition coefficients for the species of interest. Polyelectrolytes used as electrode coatings should possess the following properties: 1) strong irreversible binding to the electrode surface; 2) good ion exchange capacities for ionic photochemically and electrochemically active species; 3) retention of these species within the film; 4) rapid charge propagation (electronic and ionic); 5) and chemical and mechanical stability.

Films can be immobilized covalently (e.g. by silanization of metal oxide surfaces) or, more simply by film deposition in which some combination of chemisorptive effects and low solubility in the contacting solution produces anchoring. Deposition may be accomplished by either casting a preformed polymer from solution (the film being insoluble in the studied electrolyte), chemically or electrochemically generating the polymer in situ from its monomers (the film itself must be electroactive to grow films much more than a few monolayers thick as with for example polypyrrole or polythiophene (23,24), electrodeposition where a certain redox state of the polymer has significantly less solubility than another (25), or chemically or electrochemically assisted crosslinking.

Efficiently coupling the photosensitizer to a conductive polymer can be accomplished in a number of ways: 1) coordinating a ligating dye molecule to a potential ligand which forms part of conducting polymer (6); 2) ion exchanging an ionic photosensitizer molecule as a counterion in an ion exchange polymeric film (8,9); 3) incorporating a dye molecule as part of a monomer which can be polymerized (26).

In order to absorb a significant fraction of the radiant energy with dye molecules of high extinction coefficient a relatively thick modifying layer is required. In a photovoltaic scheme efficient coupling of the equivalent of many monolayers of dye molecules to the electrode surface for electron tranfer as well as to solution redox species for regeneration of the ground state chromophore is necessary. Optimum modifying matrices therefore feature good electronic as well as ionic conductivities.

1.4 Charge transport through polymer films

It is not so much the presence of photoelectrochemical, electrochemical and chemically active substances in polymeric films modifying the surface of electrodes, but the accessibility of these that is the most important factor in designing electrode coatings.

Charge can propagate through polymer films via electronic conduction through a delocalized electronic band structure of the polymer, physical diffusion of electro-active species and/or electron self exchange reactions between oxidized and reduced neighbours which can be fixed or mobile within the film (known as redox hopping). Charge propagation rates are also affected by the movement of polymer chains in order to accommodate the diffusion of species such as electroactive molecules, charge compensating ions and solvent molecules through the film or to bring redox centers bound to polymer chains in close contact for electron transfer. The overall rate is a combination of all the above. It has been shown that this overall rate obeys Fick's diffusion laws (ie. that it resembles a diffusion process) and can be described by an effective diffusion coefficient (D_{eff}) (27).

Diffusion coefficients can be evaluated by chronoamperometry or by evaluating scan rate dependencies. To evaluate the D_{eff} of the oxidized form of a species of interest using chronoamperometry, the potential of the working electrode is stepped from a region where the species is completely oxidized to one where it is completely reduced. Using a sufficiently large potential step (completely across the voltammetric wave) in a quiescent solution the concentrations of oxidation states are no longer

limited by the potential, that is, at extremes of potential concentrations of electroactive species are taken as zero. In this case and if electrode kinetics are not limiting, the concentration of the oxidized species will be nearly zero at the electrode surface. This will set up a concentration gradient and the measured current will be totally controlled by mass transfer. This is termed semi-infinite diffusion. Similarly, in a polymeric matrix the oxidized species diffuse through the almost completely oxidized matrix that is formed initially adjacent to the electrode surface and the D_{eff} for the oxidized species is best estimated from a negative step and the D_{eff} for the reduced species from a positive potential step. The current decay versus time profile following a potential step may be fit to the Cottrell equation,

$$i(t) = \frac{nFAD_o^{1/2}C_o^*}{\pi^{1/2}t^{1/2}} \qquad (1.1)$$

where $i(t)$ is current in amperes as a function of time, n is the stoichiometric number of electrons transferred, F is Faraday's constant (96484.6 C/equiv), A is the working electrode area in cm^2, D_o is the diffusion coefficient of the oxidized species in cm^2/sec, C_o^* is the bulk concentration of the oxidized species in $mole/cm^3$, and t is time in seconds. A plot of $i(t)$ versus $t^{1/2}$ should be linear.

The validity of the Cottrell equation must take into account a number of limitations, both instrumental and experimental. At short times the Cottrell equation predicts very high currents. Measurement of this is often limited by the response of potentiostat or recording device. Also some charging current due to resistive elements will exist at short times. At longer times the likelihood that convection will disrupt

the diffusion layer becomes a difficulty. A practical time window for Cottrell measurements is between 2 and 40 seconds.

D_{eff} may also be evaluated by linear sweep voltammetry. In the case of an initially oxidized species, a negative potential scan started well anodic of the species' standard reduction potential E°' will show no faradaic current. As the electrode potential approaches and passes the species' E°' faradaic current will flow. The surface concentration of the oxidized species drops to zero creating a concentration gradient dependent upon the scan rate. Mass transfer and hence current reaches a limiting value known as the peak current (i_p). The voltammetric peak current for diffusing species is then proportional to $v^{1/2}$ and is given by the Randles-Sevcik equation,

$$i_p = (2.69 \times 10^5) n^{2/3} A D_o^{1/2} v^{1/2} C_o^* \qquad (1.2)$$

where v is the scan rate in volts/second for a reversible reaction

Both the above techniques can be used to evaluate charge transport through polymeric film modified electrodes. The ohmic resistance of modifying films can affect D_{eff} values, but application of larger potential steps in the case of chronoamperometry can overcome this problem. Chronoamperometry is the preferred of the two methods (28) since diffusion coefficients determined by this method are not affected by film ohmic resistance.

1.5 Candidates for photosensitizers

1.5.1 General considerations

There are four requirements for an effective sensitizer for use in photovoltaic schemes. Firstly, the species must have appreciable absorption in regions that correspond to the output of a particular light source. The light source of most interest is, of course the sun and its spectral distribution was given in Figure 1.3. Second, the species must be stable to excitation and a longlived excited state may be favourable if this increases the probability of electron transfer rather than deleterious thermal deactivation of the excited state. Generally a rigid structure limiting the electron transfer reorganization barrier energy and which does not contain chemically reactive groups is necessary. Third, the molecule should be stable in more than one oxidation state with reversible reaction between these. Fourth, the ground state and excited state energy levels must be such that thermodynamically favourable overlap exists between donor or acceptor levels of both electrode and solution species for rapid electron transfer as well as regeneration of the initial oxidation state of the sensitizer. Candidates should have a chromophoric core that is essentially planar and free from steric crowding effects which tend to twist the dye predisposing it to internal conversion or chemical reaction instead of sensitization by electron injection (29).

1.5.2 Maleonitriledithiolate complexes

The maleonitriledithiolate ligand is known to form four coordinate square planar complexes with many metal ions such as the d^8 metals Ni, Pt, Pd. Bis(maleo-

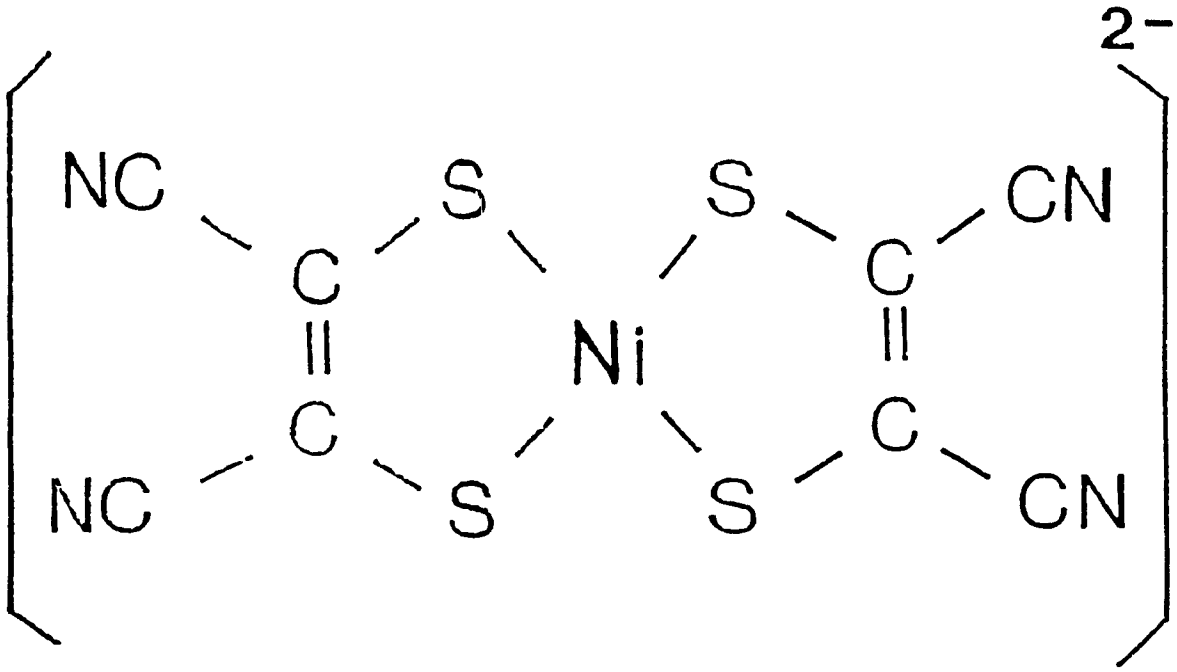

Figure 1.6 Structure of bis(maleonitriledithiolato)nickelate(II) ($Ni(mnt)_2^{2-}$)

nitriledithiolato)nickelate(II) is diagrammed in Figure 1.6. The net ionic charge of these complexes can range from 0 to 3-. The mono and dianions are stable and are easily isolated. The trianion and neutral species are not isolable, but have been established electrochemically and spectrally (30,31). Structural and electronic studies of these compounds have been reviewed (32; Chapter 1.2). There is significant delocalization of charge over the entire molecule. Although various bond distances have been found to change between the two stable oxidation states, the overall planar structure does not change appreciably. Resonance raman and low temperature absorption spectroscopy have established that the lowest energy intense bands of $Ni(mnt)_2$ correspond to metal to ligand charge transfer states (33). The similarity of the two stable oxidation states suggests that electron transfer could be facile. The $Ni(mnt)_2$ dye has been shown to be effective in electron transfer in polymer matrices (8,10).

1.6 Semiconductor particles

The majority of solid state photovoltaics are based on single crystal semiconductors. These, however are expensive to produce. Small particle semiconductors can offer a number of theoretical advantages: 1) high extinction coefficients; 2) relatively low cost; 3) dispersions have high surface areas, therefore are more efficient light harvesters; 4) they can now be prepared to very small sizes (34,35) which minimizes interference due to scattered light. Typical lifetimes of electron hole pairs in semiconductors is often orders of magnitude shorter than those of organic sensitizers. The

smaller the particle the greater the likelihood that the electron can get to the surface and escape before recombination occurs. As particle size decreases, however, the semi-continua that characterize the conduction and valence bands give way to quantized energy levels. This has been shown to push threshold absorption for the semiconductor to higher energies (36). Quantum yields for charge separations of colloidal semiconductors are low due to fast undesirable electron hole recombination. Some of the difficulties have been overcome by incorporation into polymer films, vycor glasses, clays, organized surfactant aggregates (37).

Preparing size controlled semiconductor particles has recently become a topic of concern particularly in light of the interesting properties of Q-sized particles (34-36,38-41). The use of structured reaction media can produce arrested precipitation improving size control and stability. Zeolites, ionomers, porous glass, vesicle and micelle media and gels have been utilized (40 and references cited therein) to effect size control. The interest in this preparation method is not to produce Q-sized particles, but to produce a size controlled particle for incorporation into our ion exchange polymer blend films.

Chapter 2

Experimental

2.1 Materials

All chemicals were of reagent grade supplied by the Concordia Chemistry and Biochemistry Department (CCB) and were used without further purification unless otherwise stated. Water was distilled in glass or double deionized supplied by CCB. Bis(maleonitriledithiolato)nickelate(II) ($Ni(mnt)_2$) tetraethylammonium perchlorate salt was prepared by literature methods (81) and was the kind gift of D.A. Biro and E. Lindsay.

2.1.1 Synthesis of poly(xylylviologen) bromide

Following the procedure of Factor and Heinsohn (44) poly(xylylviologen) bromide ($PXV\text{-}Br_2$) was prepared by dissolving 2.64 g (10.0 millimole) 4,4' bipyridyl (Fluka, > 99%) and 1.56 g (10 millimole) α,α'dibromo-(p)-xylene (Aldrich, 98%) in 75 ml acetonitrile (Caledon HPLC grade) in an erlenmeyer flask with ground glass neck. Once dissolved the flask was sealed and its contents stirred in the dark for 24 hours. During the course of the condensation polymerization the bright yellow polymer precipitated out of acetonitrile and was simply filtered, washed with acetonitrile and dried. Reported yields are over 85% (44), those found in this lab were over 70%. The average polymer so produced is known to contain 8 or 9 repeat units giving an average molecular weight of roughly 3500 g/mol (25,44). Elemental analysis (Guelph Chemical Labs) gave values (%C, 47.5; %H, 3.6; %N, 6.6; %Br, 36.8) very close to expected stoichiometry for %H and %N. Calculated values were

%C, 51.45; %H, 3.81; %N, 6.67; %Br, 38.07. The structure of this polymer is pictured in Figure 2.1a. Br deviated from expectation by a relatively small amount. This could be due to a limited amount of association of the polymer chains which would cause exclusion of the Br counterions. Carbon deviated substantially from expected stoichiometry, but poor accuracy of carbon readings has been noted in the past from this type of analysis (45).

PXV-Cl_2 was prepared by first preparing a perchlorate salt from concentrated aqueous PXV-Br_2 and NH_4ClO_4 solutions. The precipitate was filtered, washed with water and dissolved in acetonitrile to which was added an acetontrile solution of terta-n-propyl ammonium chloride (Alfa, 99%). The resulting precipitate was thoroughly washed and used as is.

2.1.2 Synthesis of quaternized ionic conductive polymer (QP)

The monomers for this synthesis were purified to remove polymerization inhibitors by passing the monomers through a 20 cm column of an ion exchange resin (De-hibit 100, PolySciences). 0.85 g (8.2 mmole) of styrene (Aldrich, 99 + %) and 5 g (32.8 mmole) vinylbenzyl chloride (Eastman Kodak, p and m isomeric mixture) were passed through the column with about 75 ml benzene (Aldrich, 99%). To this solution was added 0.65 g (4 mmole) 2,2'-Azobis(2-methyl-propionitrile) (commonly, AIBN) (Eastman

Kodak) which had been recrystallized from ethanol. This solution was added to a triple neck flask connected to a condenser. The solution was flushed with prepurified

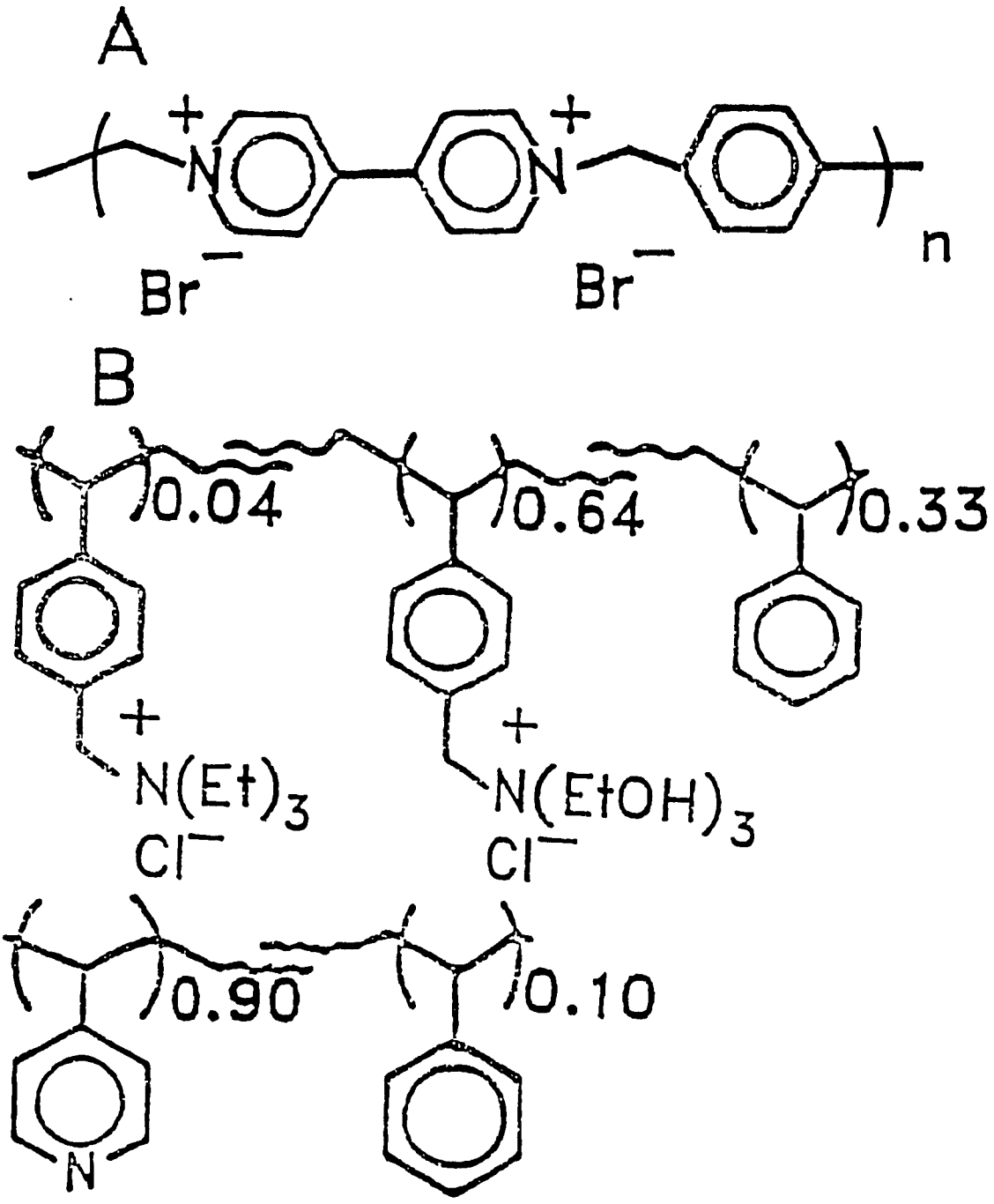

Figure 2.1 Structure of (a) poly(xylylviologen)bromide and (b) components of QP blend (quaternized random copolymer above and poly(4-vinylpyridine)-costyrene below).

nitrogen for 30 minutes, then heated to 60°C and refluxed under nitrogen for 24 hours. The intermediate copolymer was precipitated in methanol, filtered, washed and dried giving a yield of 6.3 g.

The chlorinated moieties were quaternized following the Menschutken reaction (42). The intermediate copolymer was redissolved in benzene to which was added a 5 fold molar excess of triethylamine (Aldrich, 99%) and refluxed at 65°C for 2 hours. A 5 fold molar excess of triethanolamine (Aldrich, 98%) was added, followed by 1 more hour of reflux. The solution turned cloudy then a yellow mass settled out of solution on the bottom of the flask. The supernatant was decanted off and the yellow mass was rinsed with benzene and decanted once more. The crude product was dissolved in a minimum amount of methanol then reprecipitated in cold 2-propanol. The precipitate settled out of solution, the supernatant was decanted off and the precipitate rinsed with 2-propanol. The gelatinous mass was then lyophilized and crushed to give a light pale yellow powder of yield 2.88 g.

The structure of the resulting polymer determined from the nitrogen and chlorine ratio (%C, 62.40; %H, 8.78; %N, 4.38; %Cl, 10.72; Guelph Chemical Labs) is as shown in Figure 2.1a. Expected carbon and hydrogen values calculated from reported nitrogen content were %C, 69.73; %H, 8.80. The proportions of monomers (styrene, 33%; triethylamine methylstyrene chloride, 4%; triethanolamine methylstyrene chloride, 64%) are in doubt due to the inaccuracy of carbon content by this analysis. A single sample measured on two separate occasions gave carbon readings of 59.7 and 62.4%. The product was tested to determine whether the ammonium

moieties were quaternized by titration for chloride ions by Fajan's method (43). The degree of quaternization was determined to be between 53 and 61% of the total monomer concentration for replicate determinations. The lack of precision is due to the lack of a sharp end point for the titration and limited availability of sample, but this confirms the cationic nature of the polyelectrolyte.

2.1.3 Synthesis of carboxylate capped CdS particles

2.1.3.1 Preparation of p-mercaptobenzoic acid

The benzoic acid is prepared from a procedure by Campaigne and Meyer (46). 5 g (36.5 mmole) p-aminobenzoic acid (Aldrich), 7.5 ml concentrated HCl and 10 ml H_2O were added to a beaker and cooled in a ice bath. When the temperature had fallen to < 5°C, 2.5 g (30 mmole) of sodium nitrite ($NaNO_2$, ACP Chemicals) in 10 ml H_2O was added dropwise to the solution maintaining the temperature below 5°C, giving a clear solution of the diazonium salt. 37.5 ml of a 1.0 M solution of Na_2S (Fluka Chemie, AG), sulfur (Fluka Chemie AG), and NaOH (0.0375 moles each) was cooled in an ice bath and the cold diazonium solution was added slowly while maintaining a temperature below 5°C, giving an intense orange coloured precipitate. The solution was warmed slowly, evolving nitrogen gas producing the sulfur bridged 4,4'-dithiobisbenzoic acid. The solution was made acidic to litmus paper with HCl, filtered by suction. The solid was dissolved in warm 10% aqueous sodium carbonate, filtered of impurities, reacidified with HCl, collected and dried in air giving a yield of 5.2 g (16.8 mmole) for a yield of 92%.

The crude disulfide as well as about 2 g of fine zinc powder (activated with a few ml HCl) were suspended in 40 ml glacial acetic acid. This was heated to reflux and stirred vigorously under a steady stream of prepurified nitrogen for 6 hours. Extra small portions of Zn powder were added periodically to the reaction flask during this period. The pale yellow product was collected by filtration. It was rinsed with 100 ml of hot water and filtered again. To this product was added 50 ml H_2O and sufficient NaOH to make the solution basic to litmus paper. Filtering removed unreacted Zn as well as any insoluble impurities. Rendering the solution acidic with HCl precipitated the product. The solution was centrifuged at 10 000 rpm for ten minutes, the supernatant decanted off and the precipitate lyophilized. This was finally sublimed to yield a light colourless powder (of some odour!) whose melting point (213°C) corresponded reasonably closely to that published (216-7°C) (45) for p-mercaptobenzoic acid.

2.1.3.2 Surface derivatized CdS particles

The synthesis was loosely based upon a procedure used by Brus and coworkers (47) to derivatize the surface of II-VI semiconductor clusters. Adapting their work directly to our purposes proved problematic due to disparate solubilities between derivatizing moieties. The work of Lianos and Thomas (34) was also used as a guide in this synthesis. The semiconductor particles were prepared in reversed micelles which permit size control of the crystallites.

Standard 1.0 M aqueous solutions of $CdCl_2 \cdot 2H_2O$ (Fluka Chemie AG) and

$NaS_2 \cdot 9H_2O$ (Fluka Chemie AG) were prepared. The surfactant dioctyl sulfosuccinate, sodium salt (Aldrich, 99 %) (commercial abbreviation: AOT) was purified by dissolving in petroleum ether (Aldrich, bp: 35-60°C, pesticide-free), degassing with prepurified nitrogen, filtering off insoluble impurities and evaporating to dryness.

83.4 g (187 mmole) AOT was dissolved in 1300 ml heptane (Aldrich, 99%) in a 2 liter round bottom flask and degassed with prepurified nitrogen for 20 minutes. 5 ml H_2O was added and the solution stirred until homogeneous under a continuous flow of nitrogen. Setting the concentration ratio of water to AOT ($\omega = [H_2O]/[AOT]$) defines the size of the water pools within the micelles and therefore the upper size limit to which the crystallites can grow. 2.75 ml (2.75 mmole) of standard Cd^{2+} solution was added to the surfactant solution which was mixed until homogeneous. Then 2.5 ml (2.5 mmole) of standard Na_2S solution was added and stirred. The solution developed a yellow colour over time (whose spectrum corresponded to CdS). An additional 1.25 ml (1.25 mmole) standard Cd^{2+} was added, stirred till homogeneous, then 0.35 g of p-mercaptobenzoic acid in 17 ml H_2O (rendered soluble with a minimum amount of NaOH) was added. The final ω ratio was 12 for which size absorption in the visible is expected for the particles. Carboxylate capped semiconductor particles should be ejected by electrostatic repulsion from the reversed micelles since the micelles are negatively charged. The solution was centrifugated, the supernatant decanted and the acid capped CdS particles filtered and washed with heptane. The carboxylate form of the particles was obtained by suspending the particles in water and adjusting the pH to *ca.* 9 with NaOH and stirring for 2 hours.

The particles were then filtered washed with a minimum amount of water and dried. The product was analyzed by FTIR, electronic spectroscopies and its ionic nature was confirmed by a pH titration.

2.1.4 Preparation of modified electrodes

Modified electrodes were prepared by either deposition of preformed polymers by droplet evaporation and by *in situ* polymer electrodeposition. PXV was electrodeposited onto bare SnO_2 electrodes or through polymer films following the procedures of Creager and Fox (25) or Chang et al (48).

PXV was directly electrodeposited by cycling the working electrode from 0 to -1.0 V (versus Ag/AgCl) at 200 mV/s for up to 30 minutes in an aqueous 0.5 M solution of PXV-Cl_2 with 1.0 M KCl as background electrolyte. Creager and Fox reported that electrodeposition was most successful with Cl^- as PXV^{2+} counterion. The solution was degassed with prepurifed nitrogen for 10 minutes prior to the experiment.

A crosslinked poly(xylylviologen) modified electrode was fabricated by electrochemical crosslinking of PXV in the presence of glutaraldehyde and tris(hydroxymethyl)aminomethane (**Tris**). This procedure afforded more adherent films than simple electrodeposition since PXV^{2+} with bromide as counterion is freely soluble in water. Poly(xylylviologen) and glutaraldehyde (Sigma, Grade I, 25% aqueous soln) were dissolved in deaerated 50 mM Tris (Sigma, Primary standard grade)(pH 7); concentrations were 0.25% w/v and 0.75% v/v, respectively. Electrodes were prepared potentiostatically at -1.00 V versus SCE for sufficient time to pass between 50 and 80

mC/cm^2. A membrane thickness of *ca.* 0.1 μm was reported on glassy carbon when 71 mC/cm^2 was passed (48). Electrodes were rinsed with distilled water following deposition. PXV grown into QP blend films would appear purple in colour, but would quickly fade to colourless.

2.1.5 Preparation of casting solutions

Poly(4-vinylpyridine-co-styrene) (P4VP) (Aldrich, 10% styrene, Lot. no.'s BV 05036LT, JV 04877JV) was crushed and dried prior to use. A 2% w/v solution in methanol (Fischer, HPLC grade) was prepared by slowly adding 0.2 g P4VP to 10 ml of rapidly stirred methanol. This solution was stirred vigorously overnight. Undissolved portions of the copolymer were allowed to settle to the bottom of the flask and were not used in subsequent blending. These insoluble portions represent high molecular weight fractions of the copolymer.

PXV was dried before use. A 2% w/v solution in water was prepared by mixing 0.2 g of the freely water soluble PXV-Br_2 in 10 ml deionized water.

A 2% w/v methanolic solution of the QP ion-conducting random copolymer was prepared by dissolving 0.5 g in 25 ml methanol.

A 2:1 blend of QP and P4VP was prepared by slowly adding 2 ml of the 2% QP in methanol to a stirred 1 ml aliquot of 2% P4VP in methanol. Up to 20 mg of PXV-Br_2 could be incorporated into this casting solution by adding the dried solid and stirring till dissolved (*ca.* 30 minutes).

2.1.6 Incorporation of photoactive species into films

2.1.6.1 Dyes

Dye molecules were incorporated into films either as part of casting solutions or by ion exchanging them into predeposited films. Methanol is the solvent of choice for QP blends since it dissolves the hydrophobic P4VP-costyrene as well as the hydrophilic ion-conducting polymer. The maximum solubility of Ni-mnt_2 in methanol is in the order of 3×10^{-3} M. Incorporating $Ni(mnt)_2$ into the QP blended films was most effectively accomplished as part of the casting solution. Care must be exercised in preparing the Ni-mnt_2/P4VP/QP. Improperly prepared solutions show turbidity or formation of precipitate which gives a poorly behaved film. Best results are obtained by slowly adding about 1.5 ml of a concentrated methanol solution of Ni-mnt_2 to a stirred 1.0 ml solution of PVP. This solution is then placed on a stirrer/hotplate and reduced slowly down to about half the initial volume. This solution is then very slowly added (drop by drop) to a stirred 2.0 ml solution of the QP methanolic solution. Methanol has a low vapour pressure thus fairly concentrated solutions are needed to cast sufficiently thick polymeric films onto the SnO_2 substrates.

The dye was ion exchanged into precast films from concentrated acetonitrile or methanolic solutions of the $Ni(mnt)_2^{2-}$. Film coated electrodes were soaked in these solutions for 15 minutes to 24 hours. A problem with this method is that exchange is often not homogeneous. In the case of films containing PXV, ion exchange was the most effective method.

2.1.6.2 Semiconductor particles

There exists a number of recent examples of *in situ* preparation of CdS semiconductor particles within polymeric matrices (41,49). These have involved first incorporating the Cd^{2+} cation into the polymer by ion exchange then bubbling H_2S gas through the vessel. This has worked well with anionic polymeric films (49). The QP blend requires first incorporation of the sulfide. The QP blend was first soaked in *ca* 6 mM ammonium sulfide (Fisher certified) at pH 8.5 for 4 hours and carefully rinsed with distilled water. The electrode was then transferred to a 0.1 M solution of $Cd(NO_3)_2$ of pH 5.8 to soak for an additional 4 hours.

Preformed CdS particles, either commercially available (Aldrich, 99.999%) or capped particles whose preparation was described above were added to methanolic solutions of the QP blend and stirred for 15 minutes. The resulting suspension was quickly cast onto SnO_2 electrodes.

2.2 Methods

2.2.1 Electrodes

Optically transparent electrodes (OTE's), roughly 1 x 5 cm, were cut from sheets of heavily n-doped SnO_2 coated Pyrex glass (Swift Glass Co., Connecticut). They were soaked in sulfochromic acid cleaning solution for 20 minutes, rinsed with running tap water for 10 minutes, rinsed repeatedly with deionized water, then dried under a stream of prepurified nitrogen care being exercised not to contaminate the SnO_2 surface prior to film deposition. When not in use the electrodes were stored in

deionized water. The resistivity of these electrodes was between 55-70 Ω/cm. These electrodes were connected to electrochemical equipment with aluminum or nickel alligator clips and used in a conventional cell. Alternately, SnO_2-coated glass disks (O.H. Johns. Co.) of diameter 2.5 cm were mounted as an optical window to a teflon cell over a silicone seal, electrical contact being made with a brass or copper strip pressed against the outer edge of the SnO_2 OTE any film on the surface of the electrode being wiped clean prior to this. This afforded a window of 0.8 cm^2.

2.2.2 Electrochemistry

Experiments were carried out in electrochemical cells with wire or 0.5 cm^2 platinum as counter electrode and either saturated calomel (**SCE**) or saturated Ag/-AgCl as reference electrode in water and a silver electrode in non-aqueous solvents. The design of electrochemical cells used in this investigation are shown in Figures 2.2 for vertical electrode cells and 2.3 for horizontal electrode cells. Volumes of solutions used in the conventional cell were typically 30 ml, in the teflon cell about 8 ml and in the horizontal electrode cells as little as 3 ml to up to 15 ml. Cyclic voltammetry was carried out using a Metrohm E506 potentiostat coupled to a Metrohm E612 scanner. Hard copy of cyclic voltammograms were made on an X-Y recorder (Philips PM 8143). Current was recorded by incorporating an ammeter (Keithley 177, multimeter) in series with the counter electrode, outputting the ammeter reading to an X-t strip chart recorder (Servogor 210) as in Figure 2.4. All electrochemical polymerizations were effected with a galvanostat/potentiostat (EG&G Princeton Applied Research

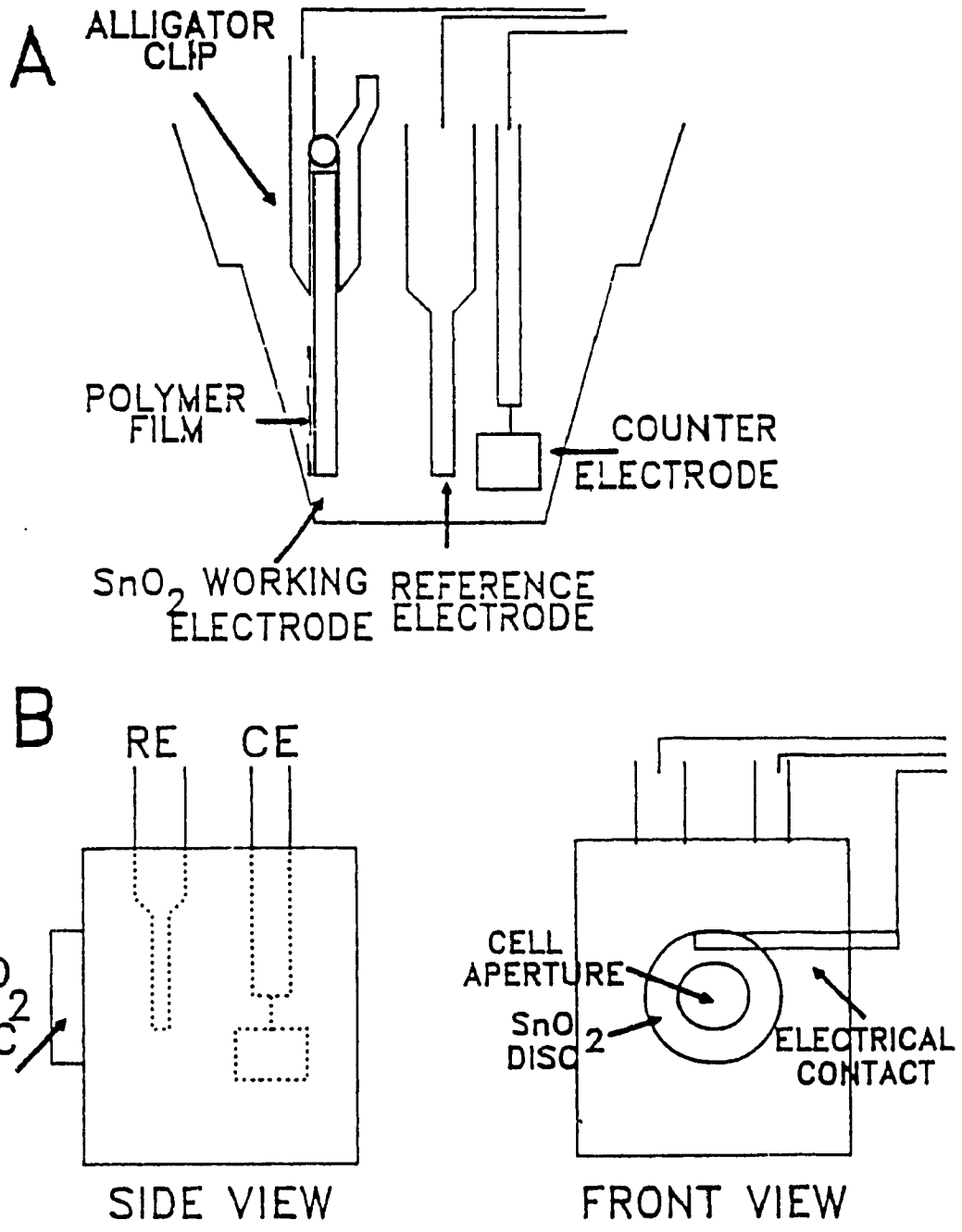

Figure 2.2 Schematic of photoelectrochemical cells where SnO_2 electrode is in a vertical position. (a) conventional cell; (b) SnO_2 disc as optical window.

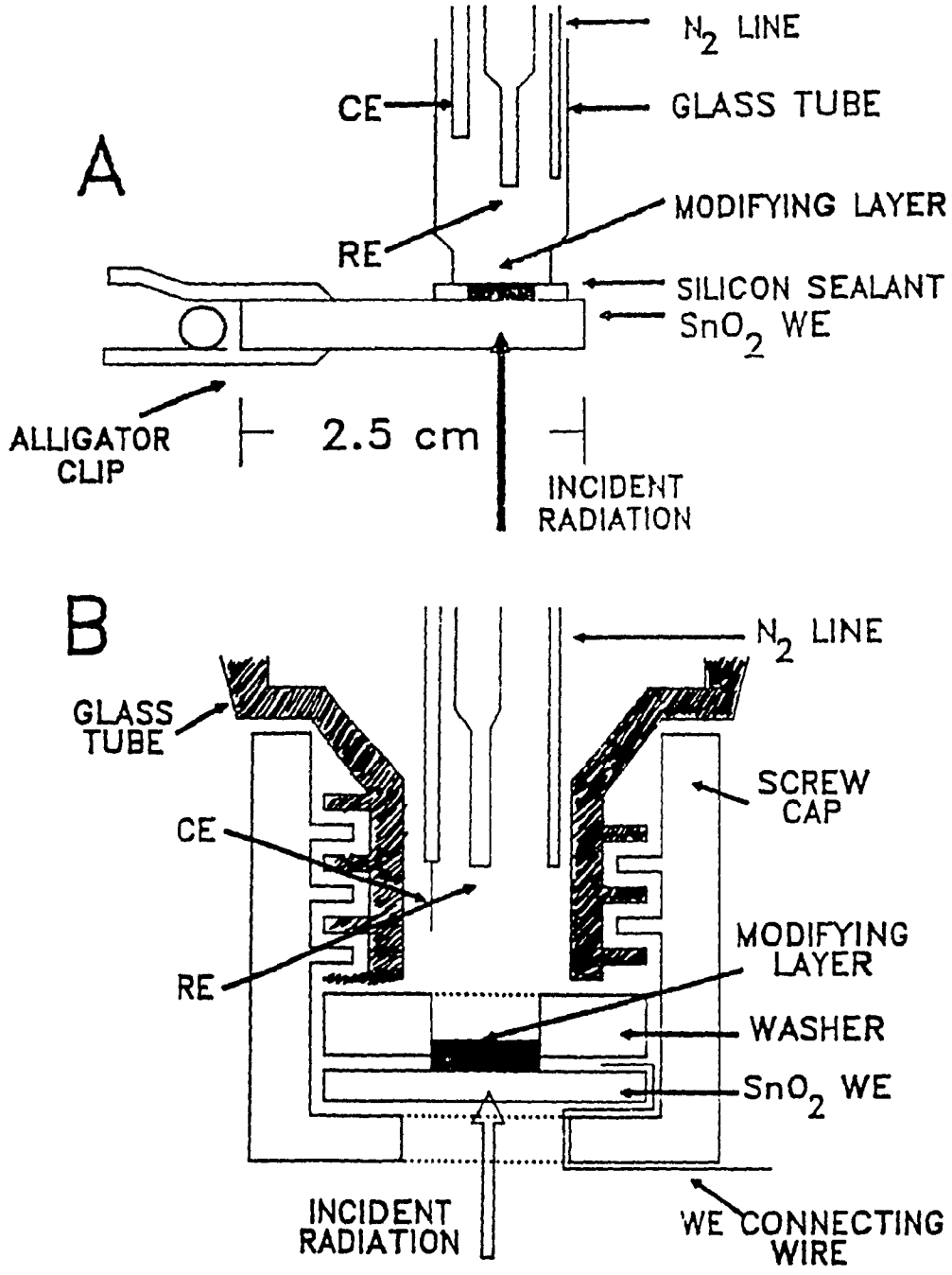

Figure 2.3 Schematic of photoelectrochemical cells where SnO_2 electrode is in a horizontal position. (a) small single-use cell; (b) screw-cap assembly cell.

Model 363) with the number of coulombs passed being recorded on a strip chart (Fischer Recordall Series 5000).

2.2.3 Photoelectrochemistry

A tungsten halogen lamp (EKN 300W Sylvania) coupled with a locally made power supply was used as an adjustable intensity light source. The beam was passed through a 5 cm water filter (made of glass), an ultraviolet (< 400 nm) cutoff filter and a collimating lens (made of glass) focussing only visible light filtered of UV and IR radiation as illustrated in Figure 2.5. OTE's, in an electrochemical cell were oriented at the focal point of the light beam and irradiation intensities at this point were adjusted to 100 mWatts/cm^2 using a Coherent 210 power meter. Short-circuit photocurrents (**SCPC**'s) and open circuit voltages ($\mathbf{V_{oc}}$) were measured across the OTE and Pt counter electrode with a multimeter (Kiethley model 177) coupled to a strip chart recorder. Dark currents for all experiments were allowed to stabilize (10-15 minutes). When solutions were stirred, magnetic stir bars and mechanical stirrers were used. Solutions were degassed by bubbling prepurified nitrogen through solutions for 5-10 minutes. Photocurrents in the absence of electrolyte were measured by clamping a leaf of gold foil to the film side of a modified SnO_2 OTE, this gold leaf being the counter electrode for SCPC measurements. During experiments, electrodes were cooled with a fan to reduce contributions from thermal currents. Single line photoexcitation was performed with a Coherent Innova 70 argon ion laser in single line mode. Line intensities were adjusted with a power meter.

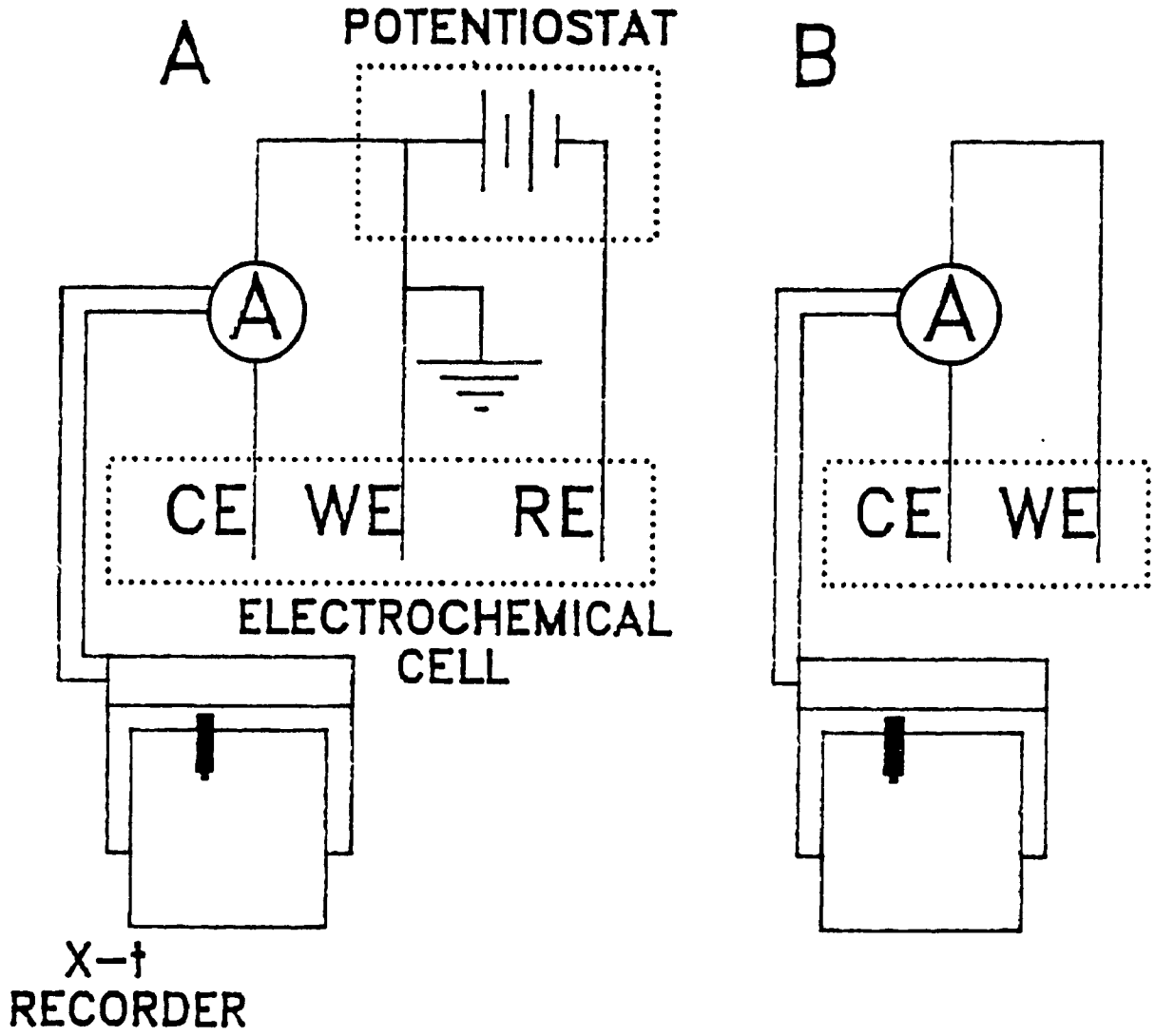

Figure 2.4 Schematic of electrochemical measurement setups. (a) electrochemical cell (CE = counter electrode, WE = working electrode (grounded), RE = reference electrode, A = ammeter); (b) setup for measure short-curcuit photocurrents.

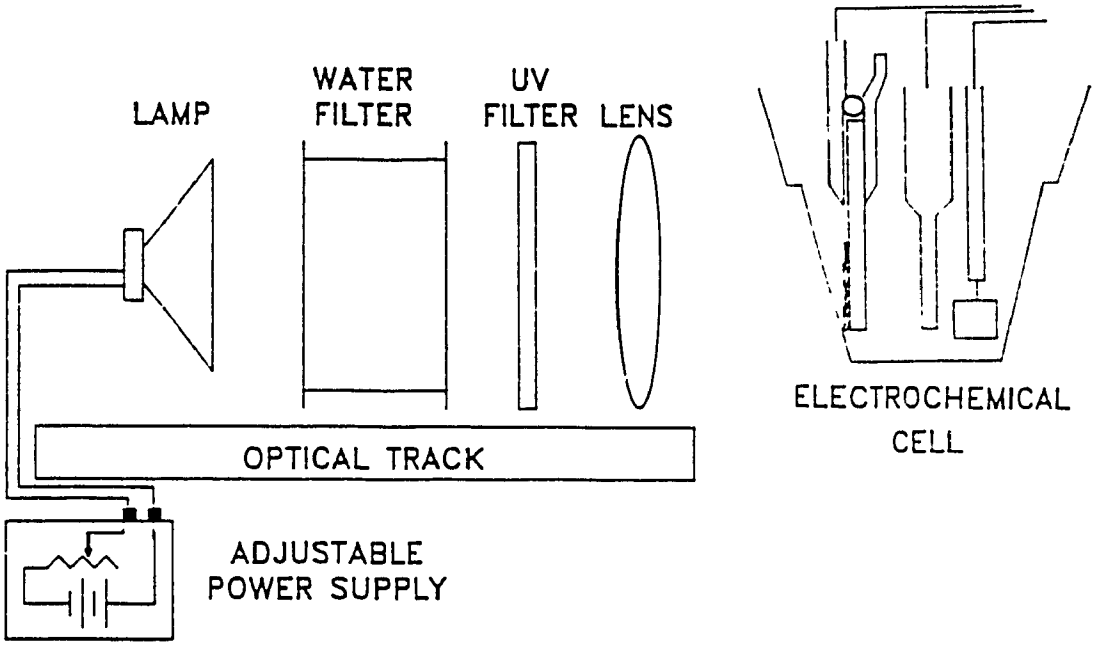

Figure 2.5 Schematic of photoelectrochemical setup. The beam from a tungsten/halogen lamp with an adjustable power supply is passed through water and UV (< 400 nm) filters and focussed onto a film coated SnO_2 electrode with a collimating lens.

2.2.4 Spectroscopy

Ultraviolet-visible spectra were obtained on an Hewlett Packard 8452A diode array spectrophotometer interfaced to an IBM/PC. Near Infrared spectra were measured on a Shimadzu UV-160. Spectra of solid films on the SnO_2 OTE's, blanked accordingly were recorded when scatter from the opaque films was not too great. In cases where scatter was a problem, films were dissolved into known quantities of either deionized water or dimethylformamide (Aldrich, Spectroscopic grade) and solution spectra obtained. Fluorescence was measured using a Perkin Elmer MPF-44. Infrared spectra were measured on a fourier transform infrared spectrometer (Bomem Michelson 102). The spectra of various polymers and blends were obtained as films cast upon an IRTRAN2 disc and those of solids as KBr pressed pellets. Background and samples were typically scanned 256 times and baseline corrected where necessary. Photoacoustic electronic spectroscopy was performed at l'Université de Québec à Trois Rivières by Claude Arbour. Resonance Raman experiments were performed at Universiteit van Amsterdam by Cooper Langford and Theo Snoeck.

Chapter 3

Results

3.1 Overview

The magnitude of short-circuit photocurrent (**SCPC**) in wet cell photovoltaic devices based upon polymer modified electrodes will depend ultimately upon the efficiency of charge separation at the primary excitation site, the transfer of the charge at solution/modifying film and electrode/modifying film interfaces and the transport processes within the film. The electronic charge transport process depends on the resistance of the film, the mobility of charge and the lifetime of the excited carrier.

The bis(maleonitriledithiolates) have features that make them good candidates for photosensitization such as absorption in the visible, multiple stable oxidation states, as well as an ability to form ion pair salts. Wet junction photovoltaic cells can only hope to reach the efficiency of solid state devices in a form that permits coupling of a great number of light absorbers to the electrode surface. This can be accomplished by arranging the absorbers in a conductive matrix supported on the electrode. Supporting both the electronic and faradaic processes present in wet junction photovoltaics requires that the electronic conductor be interspersed in a medium of high ionic conductivity. A necessity is, of course, to place the light absorbers at the interface between regions that feature these types of conduction.

An ionically conductive polymer blend developed by Montgomery and Anson (50) demonstrated much promise for our purposes because of internal ionic mobilities within an order of magnitude of solution values and an ability to bind the anionic chromophore $Ni(mnt)_2^{2-}$. The limiting factor in this system, however, was the poor

electronic conductivity characterized by the electronic traps within the matrix. This research has been directed to improvement of electronic conduction within a good ion conducting matrix. Intrachain electronic conductivity generally relies upon conjugation of unsaturated moieties (71). Interchain conductivity requires overlap of these polymer chains which depends either on a high degree of orientation between neighbouring chains or on a close packed polymeric structure. The latter is the easier strategy to improve electronic conductivity but will hardly lead to high ion mobility. Of greater practical utility is to deposit electronic conductors through the solvent channels of an ion conducting polymer film.

This section outlines the attempts made at incorporating conductors which can function as acceptor species for light absorbers, into good ion conducting matrices. A conductor explored previously (51,52) which demonstrated promise in this direction was polypyrrole which could be electropolymerized through the solvent channels of the ion conducting QP blend. A drawback was that the anionic chromophore would not dope the polymer which, should it have done so, would have directly coupled the light absorber to an electronic conductor. Poly(xylylviologen) is a cationic "redox self exchange" conductor. Attempts at incorporating this conductor into films of the QP blend are described. Another strategy to couple absorber and conductor is to intersperse a high concentration of small sized narrow bandgap semiconductor particles within the film which function as both primary light absorber and conductor.

3.2 $Ni(mnt)_2$/QP blend modified electrodes

A point of departure for this project was to reprepare the system already reported by Biro (51; Chapter 4) and from there apply a number of strategies to improve conductivity through the ion conducting polymer film modified electrodes.

3.2.1 Spectroscopy

Figure 3.1 shows the electronic spectrum of a $Ni(mnt)_2$/QP blend modified electrode. Distinct peaks appear at 484, 386, 318 and 286 nm corresponding to the stronger absorbing bands reported in published spectra for salts of this metal complex (53). Closer inspection revealed all reported peaks (Table 3.1). A shift in the

Table 3.1: Electronic absorption of $Ni(mnt)_2$/QP blend on $Sn()_2$.

Observed Peaks (nm)	Reported Peaks* (nm)	Relative Observed Intensity (arb. u.)	Reported Extinction Coefficient* ($M^{-1}cm^{-1}$)	Assignment*
-	855		30	(x^2-y^2 -> xy)
576	579	0.045	570	(xz -> xy)
518sh	519	0.105	1,250	(x^2-y^2 -> Lπ*)
484	476	0.241	3,800	(xz -> Lπ*)
386	378	0.493	6,600	(Lπ -> xy)
318	319	1.629	30,000	(Lπ -> Lπ*)
286	270	1.399	50,000	(Lσ -> xy)

* From (53).

$Ni(mnt)_2$ (Md -> Lπ*) absorption from its solution value of 472 to 484 nm is noted. It is proposed that this is due to interaction with the polymer. Relative peak inten

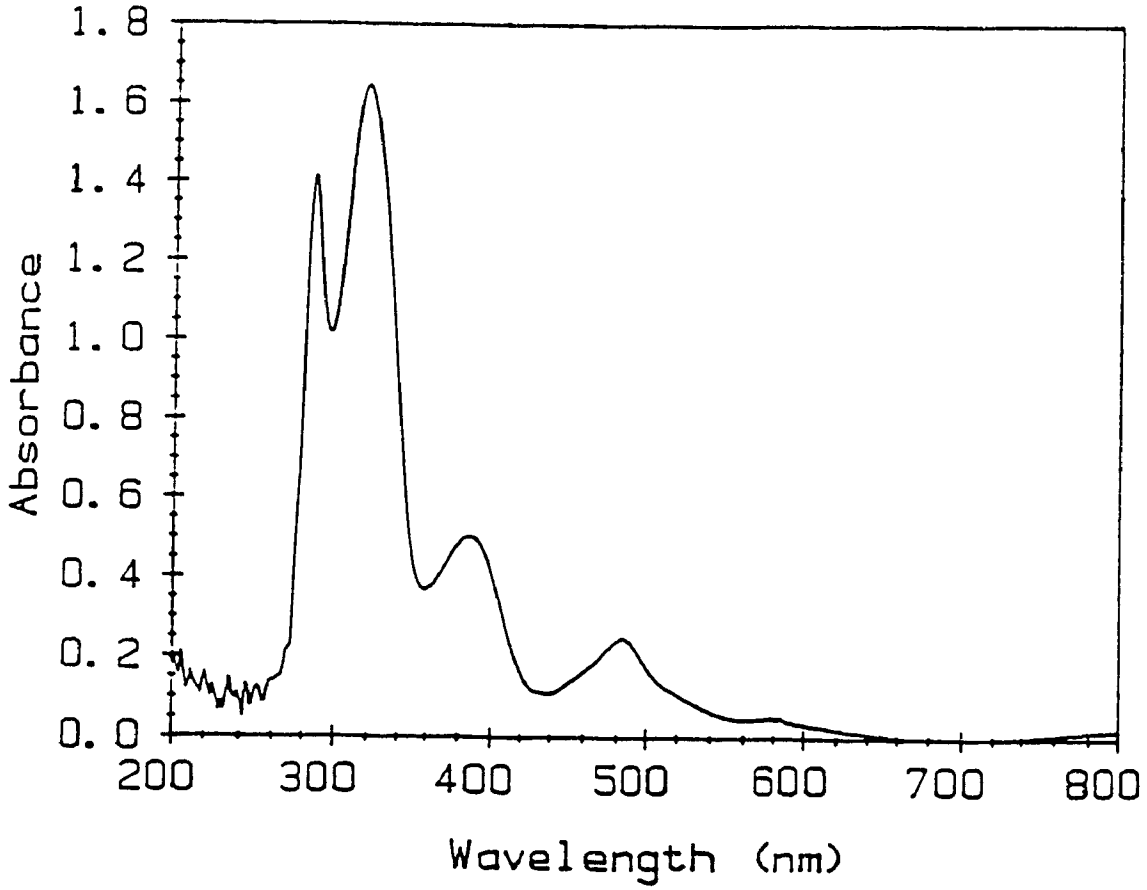

Figure 3.1 Electronic absorption spectrum of $Ni(mnt)_2$/QP blend as a film on SnO_2.

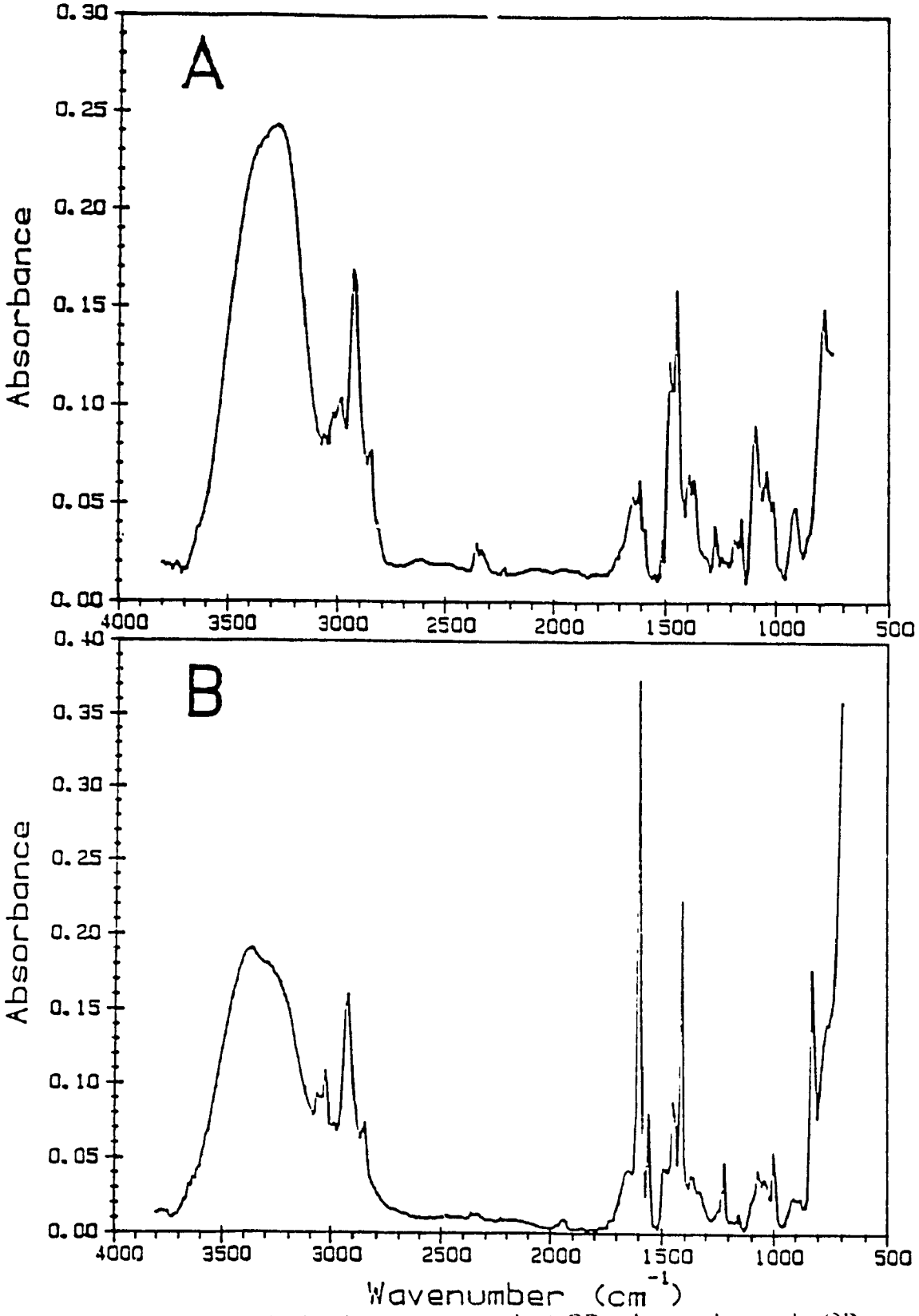

Figure 3.2 FTIR absorbance spectra of (a) QP polymer alone; (b) QP blended with P4VP on IRTRAN disc.

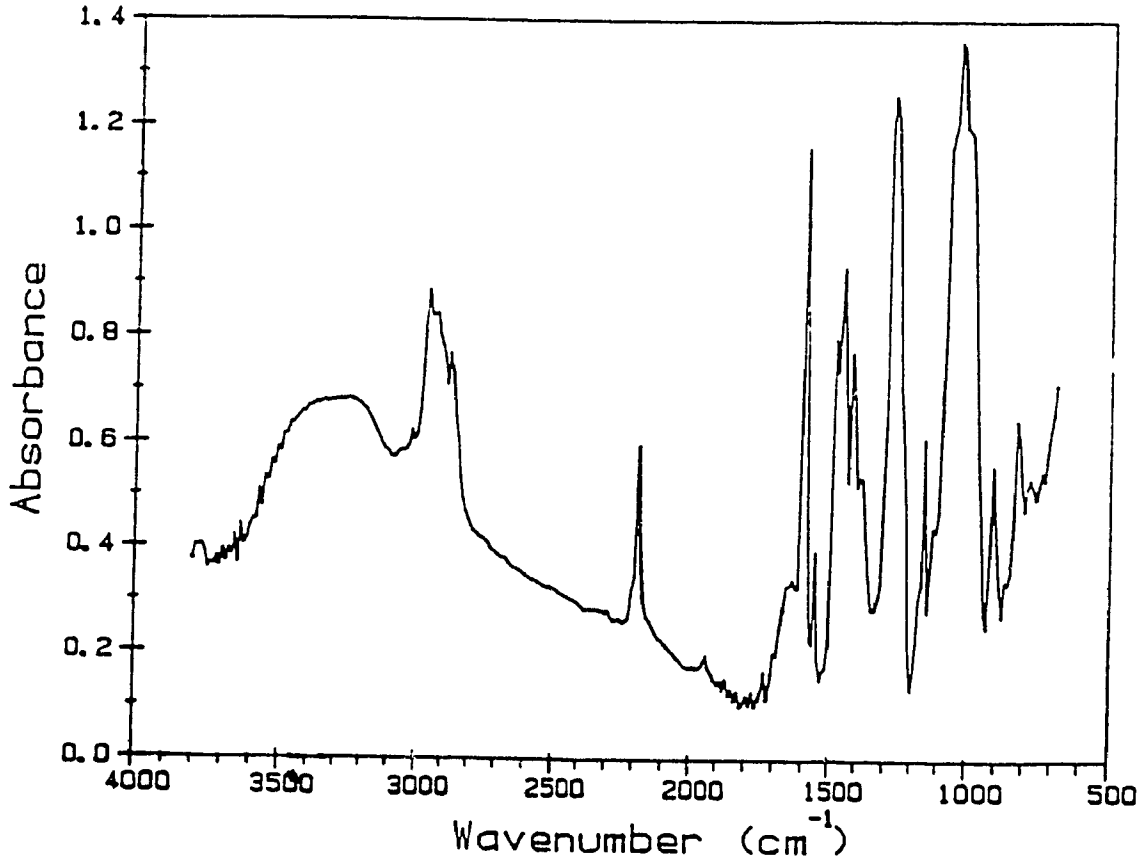

Figure 3.3 FTIR absorbance spectrum of $Ni(mnt)_2$/QP blend on IRTRAN disc.

sities corresponded to reported extinction coefficients for the dye, except for that at 286 nm which is due to interference from the SnO_2 electrode.

Figure 3.2a shows the FTIR spectrum of a thin film of the QP alone cast upon an IRTRAN disc. Peak positions and assignments are listed in Table 3.2. Peaks for the tertiary amine are difficult to assign but could conceivably contribute in the 1100 to 1000 cm^{-1} region (54). Figure 3.2b shows the infrared spectrum of the QP blend and peak positions and assignments are listed in Table 3.3. The spectrum appears to be dominated by absorption associated with the P4VP. The characteristic para-substituted pyridine ring stretching vibrations between 1600 and 1400 cm^{-1} result from the complete interaction of the C=C and C=N vibrations and are therefore difficult to isolate. The peaks in the region above 3050 cm^{-1} could be blurred by moisture during the experiment since polymer blends which include pyridine are known to be very hygroscopic (55). Peaks due to styrene are weak, largely masked by the stronger pyridine vibrations (54).

Upon incorporation of $Ni(mnt)_2^{2-}$ into the blend (see Figure 3.3) new peaks arise which closely match published IR spectra of the compound (56)(see Table 3.4). A number of peaks, e.g. at 2187, 1270 and 1022 cm^{-1}, showed significant enhancement not attributable simply to the sum of the constituents. The weak peak at 2187 cm^{-1} is assigned as a quaternized ammonium and the 1022 cm^{-1} peak as a (C-O) stretch of the quaternized triethanolamine of the copolymer indicating that these vibrations of the blend are enhanced upon incorporation of $Ni(mnt)_2^{2-}$. This suggests that the incorporated anion assumes a position as an ion pair on the quaternary ammonium sites in the

film. There are no changes to the pyridine ring vibrations and very little else to suggest that coordination of the anionic complex to the pyridine is significant.

Table 3.2: Features in IR spectrum of QP on IRTRAN disc.

Observed peaks cm^{-1}	Assignment
834m	(C-H) out-of-plane deformation
1049m	(C-OH) stretch (characteristic)
1100m, 1155w	(C-O) stretch
1218w, 1352sh	$(C-H)_{ring}$ bend
1450m, 1495m, 1600m	$(C=C)_{aromatic}$ stretch
2850m, 2920s, 2984m	$(C-H)_{aliphatic}$ stretch
3018m	$(C-H)_{aromatic}$ stretch
3347s	(O-H) stretch

Table 3.3: Features in IR spectrum of QP blend on IRTRAN disc.

Observed peaks cm^{-1}	Assignment
821m	(C-H) out-of-plane deformation
996m	Heterocyclic ring breathing
1219m, 1068m	$(C-H)_{ring}$ in-plane deformation
1414m, 1500w, 1555w, 1597s	$(C=C)_{aromatic}$ stretch characteristic of substituted pyridine
1450m	$(C=C)_{aromatic}$ stretch
1650w	$(C=N)_{aromatic}$ stretch
2852m	$(C-H)_{aliphatic}$ stretch symmetric
2927s	$(C-H)_{aliphatic}$ stretch asymmetric
3022m	$(C-H)_{aromatic}$ stretch
3268sh	(-H···N) + (-H···O) bonding stretch
3347s	(O-H) + (N-H) stretch

Table 3.4: New IR features upon incorporation of $Ni(mnt)_2^{-2}$ into blend on IRTRAN disc.

Observed peaks cm^{-1}	Assignment
1032s	(C=S) stretch
1109w	(C-CN) out-of-plane bend
1147m	(C-S) + (C-C) stretch
1478m	(C=C) stretch
2190m, 2214sh	(C≡N) stretch

Raman spectroscopy probes characteristic vibrations of molecules. The scatter from a sample irradiated with a strong monochromatic beam of light provides a spectrum that gives many of the same features as IR spectroscopy. Resonance Raman (**rR**) involves irradiating into an electronic absorption band of the species being studied, this can offer insights into the primary excitation step. Comparing on-resonance with off-resonance spectra can characterize the excited state of a particular species. Irradiation into the Md -> Lπ* of the $Ni(mnt)_2$ saw little change in Raman line intensities between salts of $Ni(mnt)_2^2$ and samples in P4VP in which charge transfer is expected to take place. A small change of resonance enhancement for a metal-sulfur bond vibration was reported perhaps indicative of the axial ligation of the pyridyl moiety to the Ni metal center of the complex (57).

3.2.2 Electrochemistry

Figure 3.4 shows the cyclic voltammetric behaviour of $Ni(mnt)_2$/QP blend films having thicknesses of *ca.* 10 ± 3 μm. The QP blend would not ion exchange the

anionic dye of this study well, therefore the dye was incorporated into solutions of the QP blend prior to casting onto electrodes. All films were thoroughly deoxygenated by bubbling with prepurified nitrogen and allowed to stabilize before voltammograms were recorded at 100 mV/s. Figure 3.4a shows an $Ni(mnt)_2$/QP blend film behaviour in 1.0 M KCl. A well defined cathodic peak assignable to the irreversible pyridine to pyridine radical anion reduction is observed at -0.65 V (vs Ag/AgCl). What could be the anodic peak of this reaction is seen as a broad peak at -0.35 V. The pyridinium radical is known to dimerize rendering the peaks irreversible (58). The $Ni(mnt)_2^{2-/-1}$ is observed as an unsymmetric pair of peaks at 0.19 and 0.28 V, the cathodic peak being barely discernible.

Current greatly increased upon transfer of the electrode to a 2.0 mM $Fe(CN)_6^{3-/4-}$/0.10 M KCl solution as seen in Figure 3.4b. Strong $Fe(CN)_6^{3-/4-}$ peaks are observed at 0.34 and 0.025 V indicating that the couple readily penetrates the film. The scan rate dependence is shown in the inset of Figure 3.5 and is linear for square root of scan rate consistent with diffusion limited behaviour. Voltammetric data for $Fe(CN)_6^{3-/4-}$ is included in Table 3.5. Peak separations were from 128 - 318 mV for scan rates between 10 and 100 mV/s.

Apparent diffusion coefficients for $Fe(CN)_6^{3-/4-}$ can characterize ionic mobility through the polymer film (59). D_{eff}'s were evaluated by chronoamperometry by fitting the current decay of a potential step to the Cottrell equation and from scan rate dependence with the Randles-Sevcik equation. For chronoamperometry, electrodes that had attained stable $Fe(CN)_6^{3-/4-}$ peaks in the redox solution were rinsed with

distilled water and transferred to supporting electrolyte. Electrodes were allowed to stabilize 10 minutes and a potential step from +0.6 to -0.6 was applied for $Fe(CN)_6^{3-}$ and a step from 0.0 to +0.9 V for $Fe(CN)_6^{4-}$. The resulting transient current response was monitored and plotted vs $t^{-1/2}$. The slope of the linear portion of the data at short times was used to calculate diffusion coefficients using the Cottrell equation (equation 1.1). D_{eff}'s were $6 \pm 3 \times 10^{-7}$ cm^2/s, the D_{eff} for $Fe(CN)_6^{4-}$ generally being slightly smaller than that for $Fe(CN)_6^{3-}$ due to the larger electrostatic attraction between $Fe(CN)_6^{4-}$ and quaternized ammonium moieties of the QP blend film. Film thicknesses were evaluated with a hand-held micrometer on dry films which could introduce error since hydrophilic polymeric films are expected to swell in aqueous solution. Concentrations of the electro-active anions within the film were evaluated directly before and directly after the chronoamperometric experiment by measuring charge passed for the species at slow scan rate at a limit where charge becomes proportional to moles of electro-active species (this was at 10 mV/s). D_{eff}'s for $Fe(CN)_6^{3-}$ in 0.1 M KCl on bare SnO_2 were evaluated as $5 \pm 2 \times 10^{-6}$ cm^2/s close to that reported, $0.763(5) \times 10^{-5}$ cm^2/s for the ferricyanide ion in 0.1 M KCl (60).

D_{eff}'s determined by scan rate dependence were typically over an order of magnitude smaller than those determined by chronoamperometry ($4 \pm 1 \times 10^{-8}$ cm^2/s) The chronoamperometric values are expected to be a more accurate reflection of the actual D_{eff} since they are less affected by film resistance than are those evaluated by scan rate dependence (28). The fact that there is a significant difference between D_{eff}'s evaluated by these two methods suggests that the films are fairly resistive.

The ionic nature of the QP blend film is responsible for the ability of the film to incorporate the $Fe(CN)_6^{3-/4-}$ redox couple. Figure 3.6 demonstrates the different levels of incorporation of $Fe(CN)_6^{3-/4-}$ at two pH's, one where the pyridine moieties are likely to be protonated (ie. pH 3.3) and one where the pyridine moieties are more likely not to be (ie. pH 9.6). It is to be noted that the quaternized ammoniums will remain cationic over this range of pH. $Fe(CN)_6^{3-/4-}$ peak currents are significantly smaller when pyridine is not protonated. This, however as will be illustrated in the following section did not appreciably affect photocurrents. Cyclic voltammetry run in standard solutions of $Fe(CN)_6^{3-/4-}$, adjusted to pH 5.7 shows strong peak currents for $Fe(CN)_6^{3-/4-}$ through the film. The concentration of redox couple in one film evaluated by integrating the charge under the voltammetric peaks of the couple at slow scan rate was 3.9×10^{-8} moles while that of $Ni(mnt)_2$ evaluated spectrophotometrically by dissolving the polymeric film off the electrode into DMF, diluting to an accurate concentration and using known extinction coefficients was 1.7×10^{-7} moles. The concentration of the reduced form of the redox couple was found to be *ca.* 10% greater than the oxidized form in most films due perhaps, to its larger charge and the electrostatic attraction into the film. The film did not retain the anionic redox couple within the film over long periods. Montgomery and Anson described an analogous film (50) which could retain anionic electro-active species for extended periods. Figure 3.7 shows voltammograms of an electrode saturated with the $Fe(CN)_6^{3-/4-}$ couple scanned immediately after transfer into a solution containing only background electrolyte and then 1.5 hours later. Continuous cycling over a period of about 2 hours leads to

Table 3.5: Electrochemical data for $Ni(mnt)_2$/QP blend on an SnO_2 working electrode with Pt as counter and SCE as reference electrodes in 2.0 mM $Fe(CN)_6^{3/4-}$ in 0.1 M KCl.

$(V/s)^{1/2}$ x10^3	i_{pa} μA	i_{pc} μA	E_{pa} mV	E_{pc} mV	E_{pa}-E_{pc} mV	E_o mV
70.7	124.2	121.0	248.0	120.0	128.0	184.0
100.0	181.5	169.4	268.0	105.0	163.0	186.5
141.4	238.7	210.5	282.0	92.0	190.0	187.0
200.0	319.4	337.1	309.0	65.0	244.0	187.0
244.9	367.7	378.2	323.0	48.0	275.0	185.5
282.8	429.8	411.3	335.0	30.0	305.0	182.5
316.2	476.6	451.6	343.0	25.0	318.0	184.0

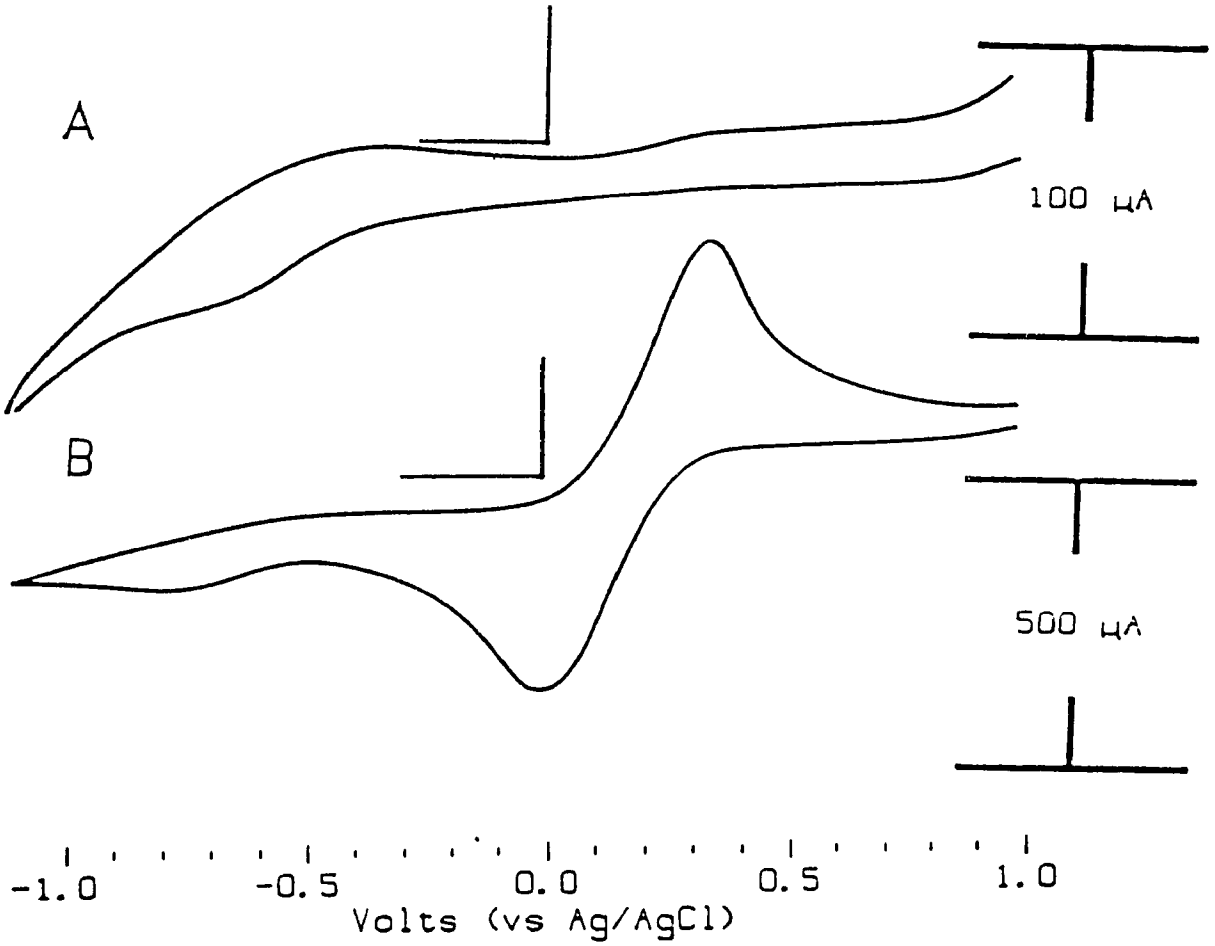

Figure 3.4 Cyclic voltammograms of $Ni(mnt)_2$/QP blend coated SnO_2 electrodes in (a) 1.0 M KCl and (b) in 2 mM $Fe(CN)_6^{3-/4-}$/0.1 M KCl at 100 mV/s starting at +0.9 V. (c) scan rate dependence for same electrode from 10 - 100 mV/s. Inset is i_p vs $(V/s)^{1/2}$ in 2 mM $Fe(CN)_6^{3-/4-}$/0.1 M KCl. Anodic currents are upwards.

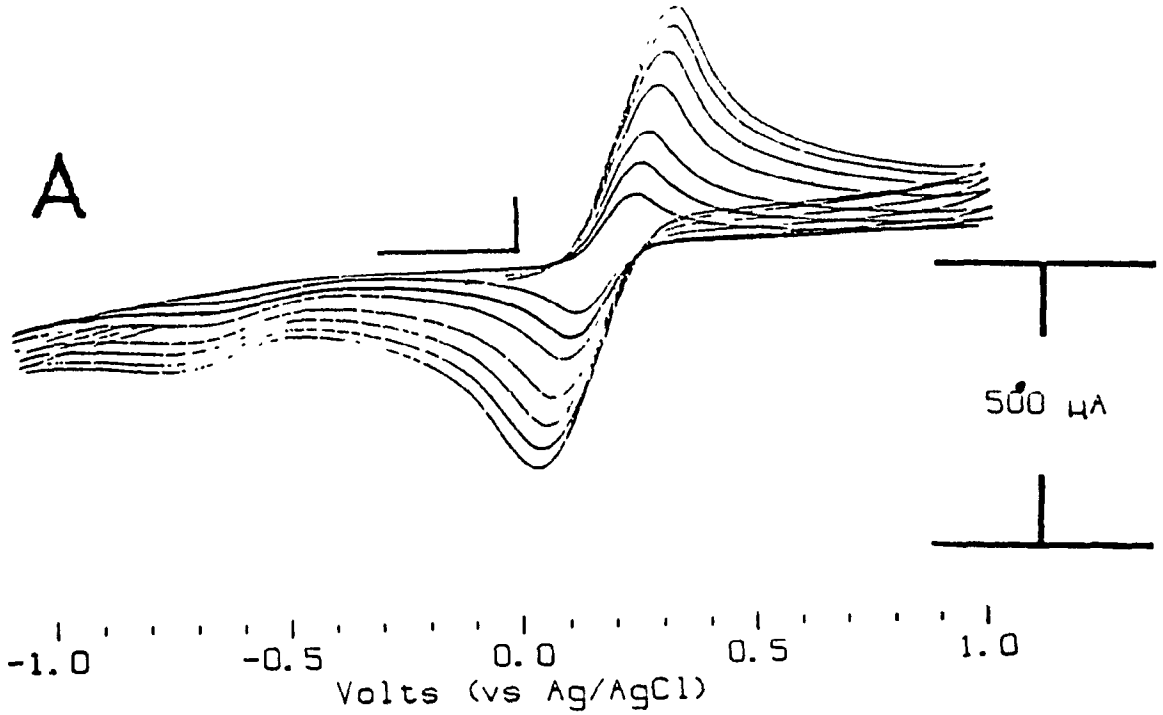

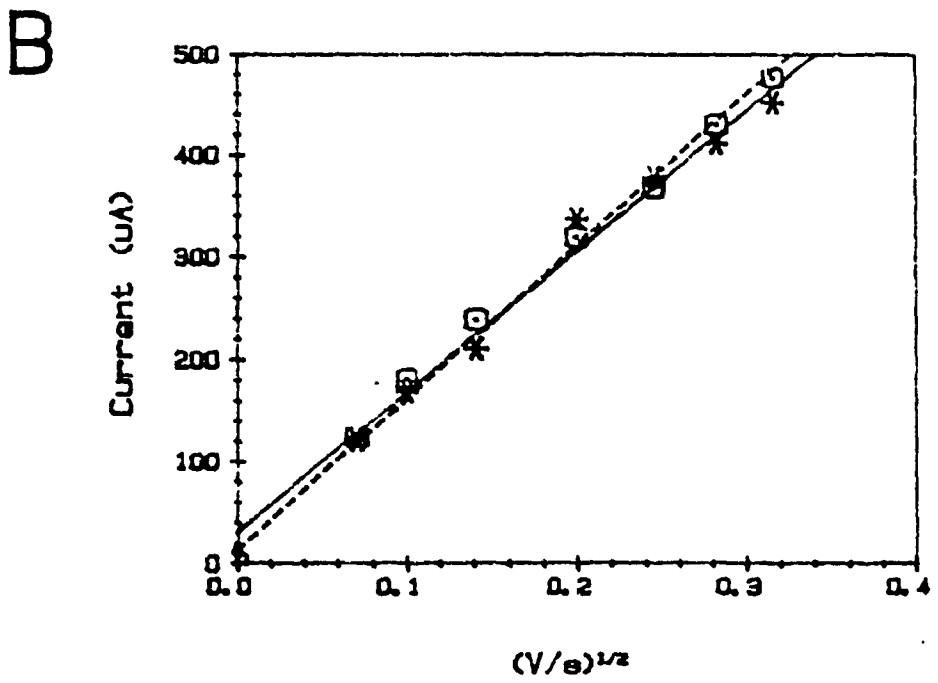

Figure 3.5 (a) Scan rate dependence for electrode of Figure 3.4 from 10 - 100 mV/s. (b) Peak current, i_p vs square root of scan rate $(V/s)^{1/2}$ in 2 mM $Fe(CN)_6^{3-/4-}$/0.1 M KCl. Anodic currents are upwards.

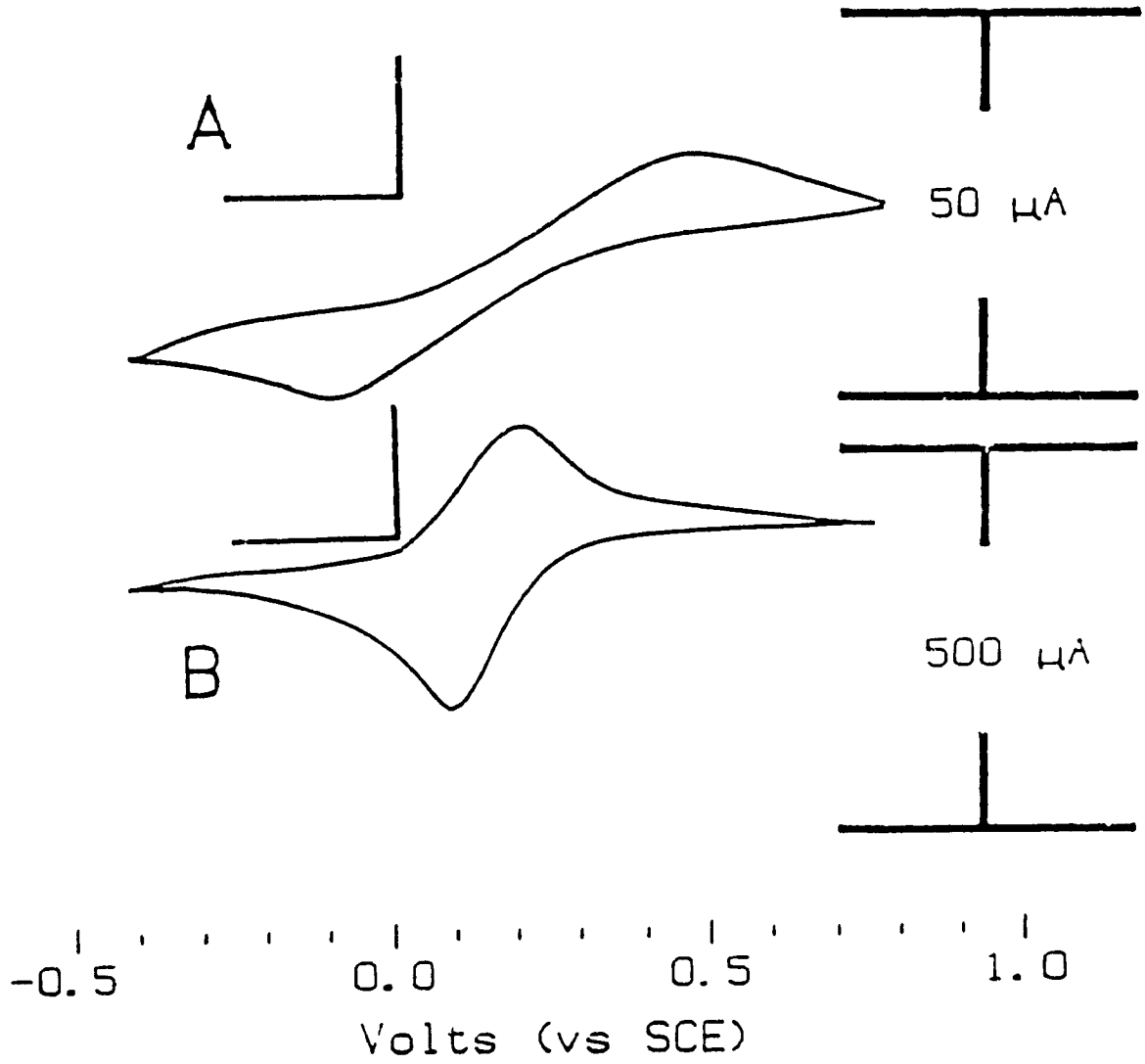

Figure 3.6 Cyclic voltammograms of $Ni(mnt)_2$/QP blend coated SnO_2 electrodes in 2 mM $Fe(CN)_6^{3-/4-}$/0.1 M KCl at pH (a) 9.6 and (b) 3.3. Scan rates are 100 mV/s starting at +0.8 V.

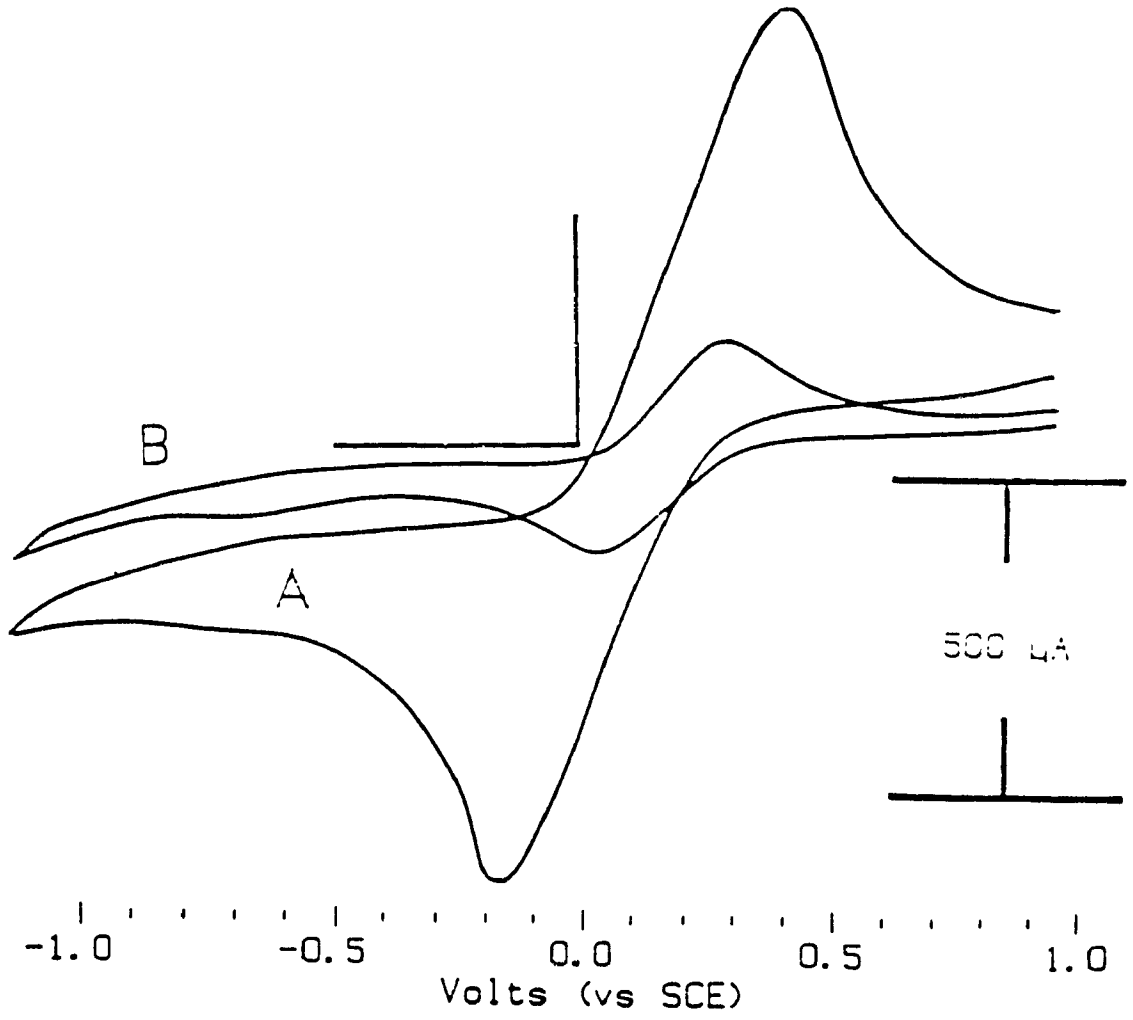

Figure 3.7 Cyclic voltammograms showing leaching of $Fe(CN)_6^{3/4}$ from Ni-(mnt)$_2$/QP blend coating (a) directly after transfer to supporting electrolyte; (b) after resting in supporting electrolyte for 1.5 hours. Scan rates are 100 mV/s and anodic currents are upwards.

complete loss of the couple from the film. Although retention of solution species within the film is not of primary importance to the application here, a substantial difference in electrode behaviour from that previously reported for this polymer blend (50, 51; Chapter 4.2) suggests a different morphology is present here.

3.2.3 Photoelectrochemistry

Upon stabilization of dark currents, SCPC's were measured at an illumination intensity of 100 mW/cm^2. In 1.0 M KCl currents were anodic and of between 0 and 50 nA/cm^2 and in 2.0 mM $Fe(CN)_6^{3-/4-}$/0.10 M KCl were between 250 and 320 nA/cm^2 (it should be noted that these values are about 1/10th of those previously reported for this system (51; Chapter 4.4)). A typical SCPC profile is shown in Figure 3.8a. This slow response to on- and off-switching is attributed to the filling of trap sites along the conduction path in the hydrophobic domains of the QP blend from chromophore to electrode. Once all sites are filled current reaches a maximum, but filling the traps takes time. The same behaviour is observed when the light source is switched off. Electrons in traps are thermally detrapped giving the slow photocurrent decay. On-switching rise time was typically between 3 - 8 minutes while off switching decay was generally twice as long. Photoelectrochemistry in 1.0 M KCl showed the same appearance for response as illustrated in Figure 3.8a. It was found that temporal response depended upon pH and hence on the protonation of P4VP, higher pH giving longer rise and decay times. pH is expected to directly affect the degree of protonation of P4VP (61), but photocurrents measured at varying pH of redox solution

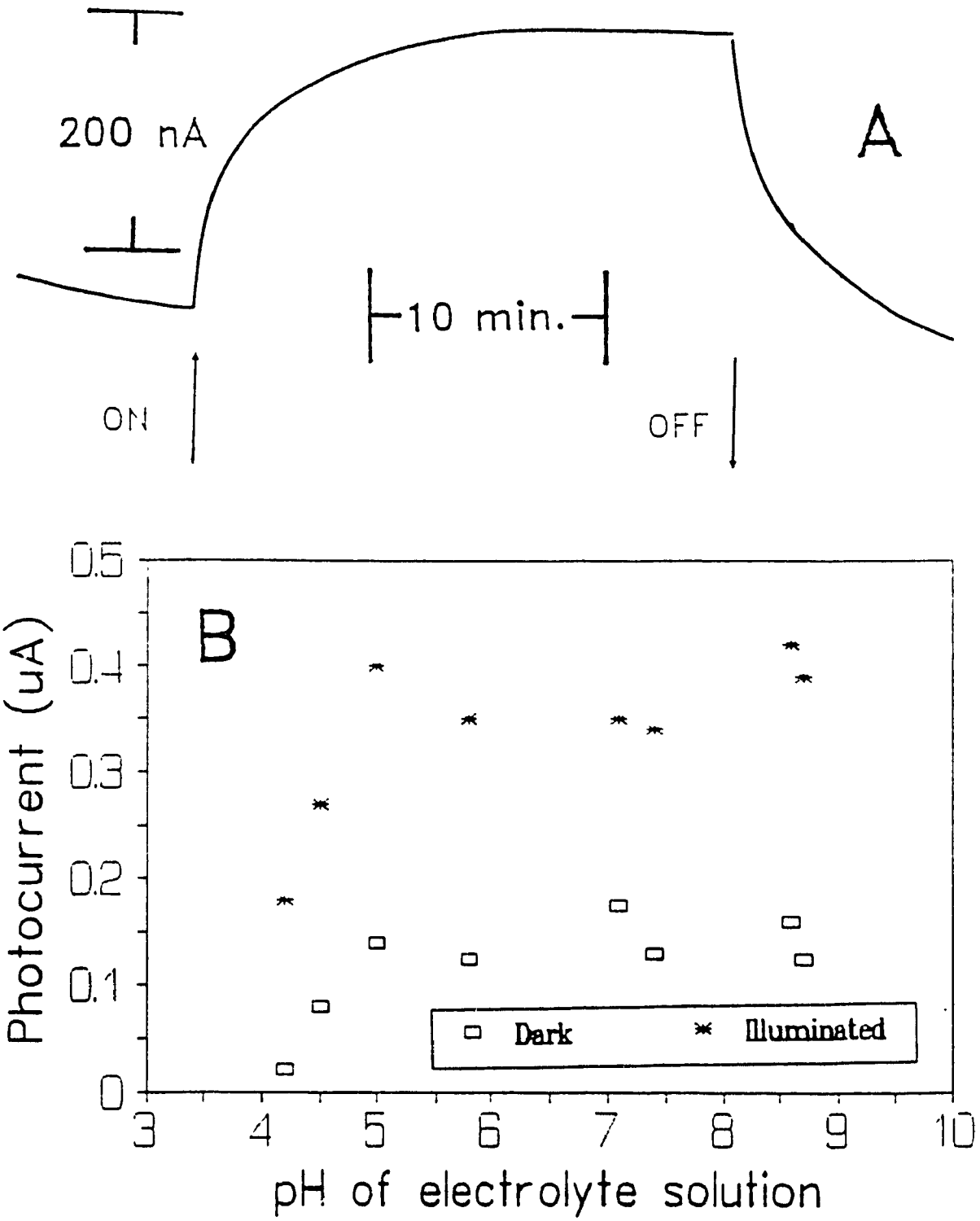

Figure 3.8 (a) short-circuit photocurrent vs time profile for $Ni(mnt)_2$/QP blend coated electrode in presence of 2 mM $Fe(CN)_6^{3-}$/0.1 M KCl at 100 mW/cm^2. (b) dark current and photocurrent vs pH of redox solution at 100 mW/cm^2.

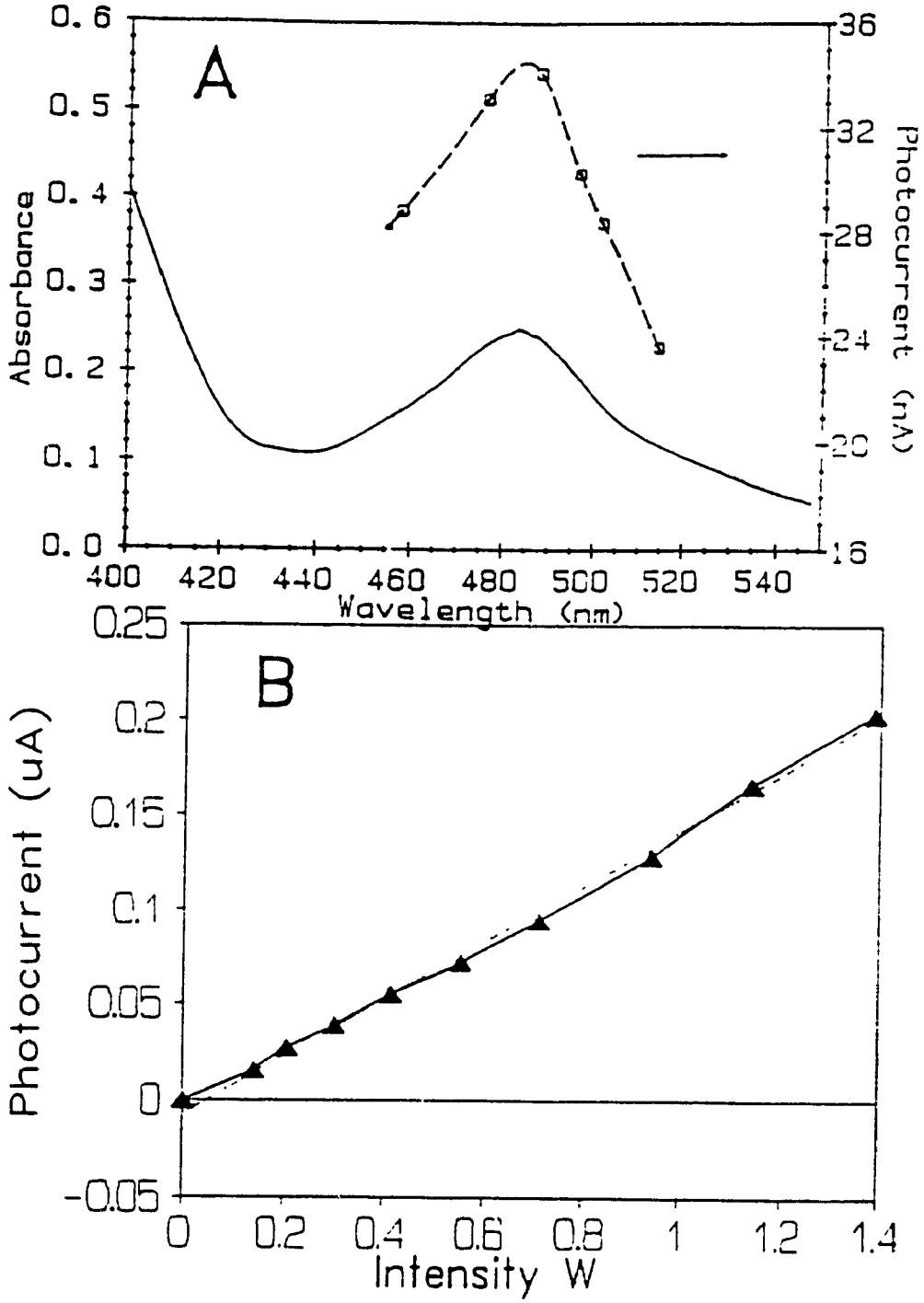

Figure 3.9 (a) absorbance vs wavelength (left scale) and short-circuit photocurrent vs wavelength (right scale) for a $Ni(mnt)_2$/QP blend electrode as dry cell with gold leaf as counter electrode. Illumination is from the visible lines of an argon ion laser adjusted to 50 mW per line. (b) photocurrent as a function of illumination intensity for same electrode under white light filtered of UV and IR.

revealed little dependence of photocurrent (Figure 3.8b) on whether the pyridinium moiety was protonated or not. At very low pH (*ca.* pH 3) dark currents started to become negative and decrease dramatically. Should electron transfer following initial photoexcitation from $Ni(mnt)_2$ to pyridine be the major charge separation step, SCPC should have shown a greater dependence upon the state of the pyridyl moiety.

Photocurrent appeared to be due to the chromophore since single line illumination from the visible lines of an argon ion laser gave SCPC's which corresponded to absorption of the $Ni(mnt)_2$ dye (Figure 3.9a). Dry cell photoelectrochemical experiments revealed that there exists electronic conduction within the film. A photocurrent versus illumination intensity plot (in Figure 3.9b) with irradiation into the main visible transition of the dye (Md -> Lπ*) had a very small degree of upward curvature. The dotted line shows the data calculated by linear regression demonstrating the weak curvature. Evidence presented here suggests the following scheme. Photoexcitation leads to transfer of an electron from the dye through a broad distribution of energy levels in the polymer to the SnO_2 electrode giving the oxidized dye $Ni(mnt)_2^+$. The oxidized dye oxidizes the solution redox couple $Fe(CN)_6^{4-}$ present in the film to $Fe(CN)_6^{3-}$ which can diffuse out of the film to the counter electrode to be reduced, thus sustaining the photovoltaic device. Photocurrent appears limited by poor efficiency of electron transfer to and conduction along the poorly conducting polymer. The need for a better electronic conductor is clearly the overall suggestion of these results.

3.3 $Ni(mnt)_2$/PXV film modified electrodes

Viologens (1,1'-disubstituted-4,4'-bipyridinium salts) are known as herbicides where they interfere in the photosynthetic centre and are often used as electron transfer agents in the photodecomposition of water. They are also photochromic and electrochromic materials. Viologens can readily form into polymers which can conjugate the photo- and electro-active bipyridyl moiety. It has been found that the photoreduction rate of polyviologens is much faster than that of the corresponding low molecular weight viologen (20). Formation into polymers also increases the separation between first ($PXV^{2+/1+}$) and second ($PXV^{1+/0}$) reduction potentials which may inhibit reduction to PXV^0 which in known to be irreversible. The propitious placement of PXV's first reduction potential relative to $Ni(mnt)_2$'s Md -> Lπ* absorption, its known redox self exchange mode of conduction and its tendency to form ion pair salts made PXV a promising candidate as electrode modifier with the $Ni(mnt)_2^{2-}$ dye.

3.3.1 Spectroscopy

PXV-Br_2 exhibited strong absorbance at 260 nm in good agreement with a published spectrum (44). $Ni(mnt)_2^{2-}$ was ion exchanged into the PXV film for the Br ion. A spectrum of a film dissolved into DMF is shown in Figure 3.10a. Distinct peaks for the PXV-$Ni(mnt)_2$ film were observed at 478, 388 and 384 nm which compare very closely in wavelength and intensity to reported spectra of $Ni(mnt)_2$ complexes (53). Reported $Ni(mnt)_2$ peaks of small intensity were not resolved. An observed peak at 274 nm is likely a solvent peak. Also noted was a small peak near

560 nm which may reflect absorption by the reduced form of viologen (62) indicating some ground state oxidation of the dye by the PXV.

Figure 3.10b shows the spectrum from 400 nm to the near infrared for PXV-$Ni(mnt)_2$. The principle visible region absorption is observed at 478 nm. A broad low intensity peak is noted for PXV-$Ni(mnt)_2$ near 890 nm which is observed in neither $Ni(mnt)_2^{2-}$ nor PXV^{2+} salts. This absorbance is assigned to PXV-$Ni(mnt)_2$ charge transfer.

Table 3.6: Electronic absorption of $Ni(mnt)_2$/PXV in DMF.

Observed Peaks (nm)	Reported Peaks* (nm)	Relative Observed Intensity (arb. u.)	Reported Extinction Coefficient* ($M^{-1}cm^{-1}$)	Assignment*
-	855		30	(x^2-y^2 -> xy)
-	579		570	(xz -> xy)
-	519		1,250	(x^2-y^2 -> Lπ*)
478	476	0.141	3,800	(xz -> Lπ*)
386	378	0.307	6,600	(Lπ -> xy)
318sh	319	1.200	30,000	(Lπ -> Lπ*)
560sh	555			PXV^{1+}

* from (53).

Fluorescence emission was undetectable in steady-state room temperature measurements of $Ni(mnt)_2^{2-}$. Upon incorporation into the polymer film irradiation at 478 nm (the main visible absorption of the chromophore) results in emission at 555 nm.

Figure 3.11a shows the FTIR spectrum of PXV-Br_2 cast as a film upon an IRTRAN disc. Peaks in this spectrum closely match a published vibrational analysis

of similar viologens (63,64) within 20 cm^{-1}. Peak positions and assignments are listed in Table 3.7. The $Ni(mnt)_2^{2-}$ anion was exchanged into the PXV film for the Br (Figure 3.11b). New peaks are listed in Table 3.8 and correspond to published IR data for the metal complex anion (56).

Table 3.7: Features in IR spectrum of PXV-Br on IRTRAN disc.

Observed peaks cm^{-1}	Assignment
1160, 1222, 1352	$(C\text{-}H)_{ring}$ bend
1448, 1501, 1600	$(C{=}C)_{ring}$ stretch (xylenyl)
1553	(N=C) stretch
1639	$(C\text{-}N^{+})$ + (C=N) stretches
Peaks at	
2850 to 3000	$(C\text{-}H)_{aliphatic}$ stretches
3111, 3039	$(C\text{-}H)_{ring}$ stretch

Table 3.8: New features in IR spectrum of PXV-$Ni(mnt)_2$ on IRTRAN disc.

Observed peaks cm^{-1}	Assignment
863	(C-S) stretch
1047	(C-S) + (C-C) stretch
1109	(C-CN) out-of-plane bend
1477	(C=C) stretch
2190, 2214	(C≡N) stretch

In contrast to the rR behaviour of P4VP in the presence of $Ni(mnt)_2^{2-}$, PXV^{2+} in the presence of $Ni(mnt)_2^{2-}$ shows enhancement of ring vibrations of the pyridinium moiety of the viologen (57). This suggests an electron transfer from $Ni(mnt)_2^{2-}$ to the

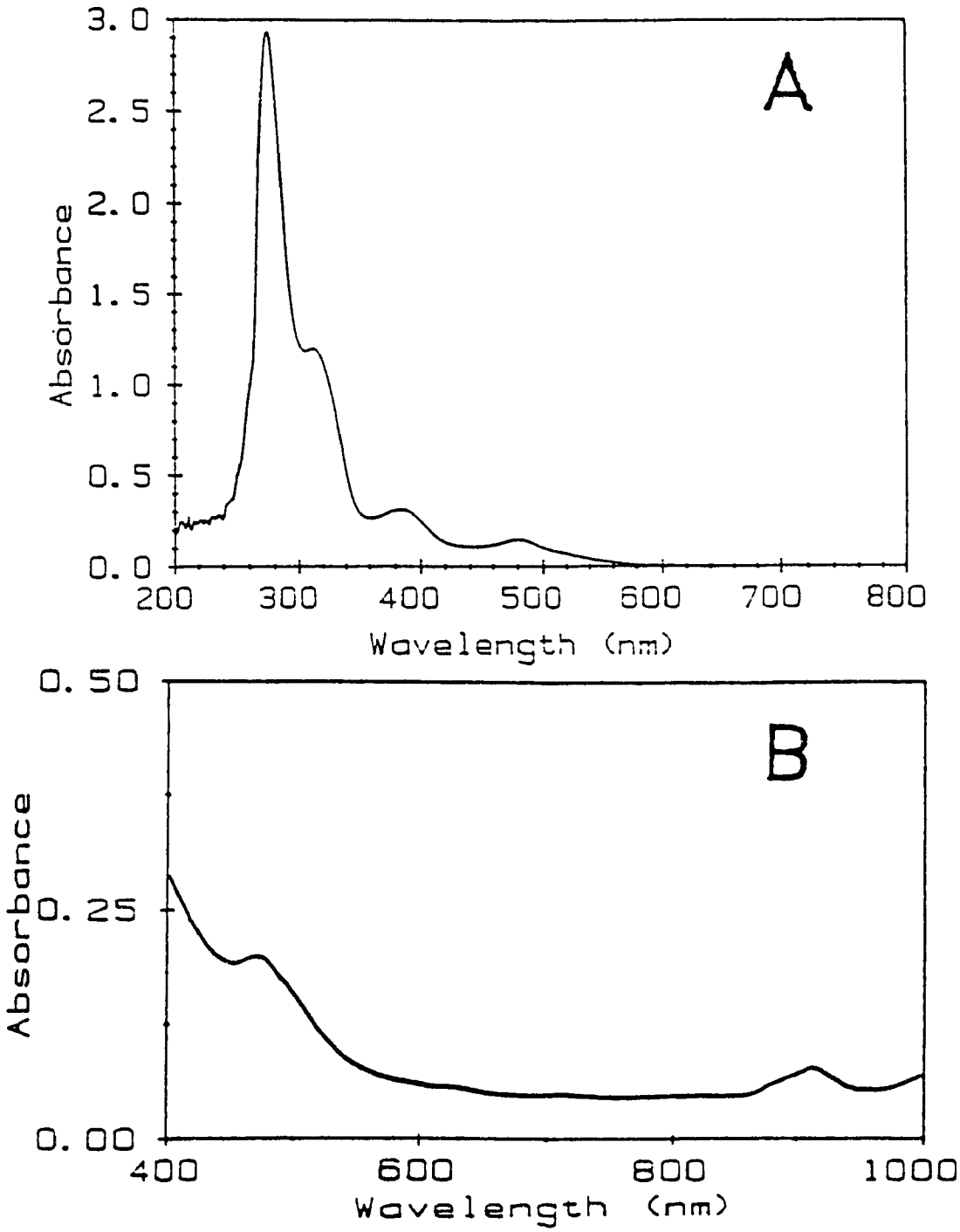

Figure 3.10 (a) electronic spectrum of PXV-Ni(mnt)$_2$ in DMF solution. (b) visible and near IR portion of spectrum of PXV-Ni(mnt)$_2$ in DMF.

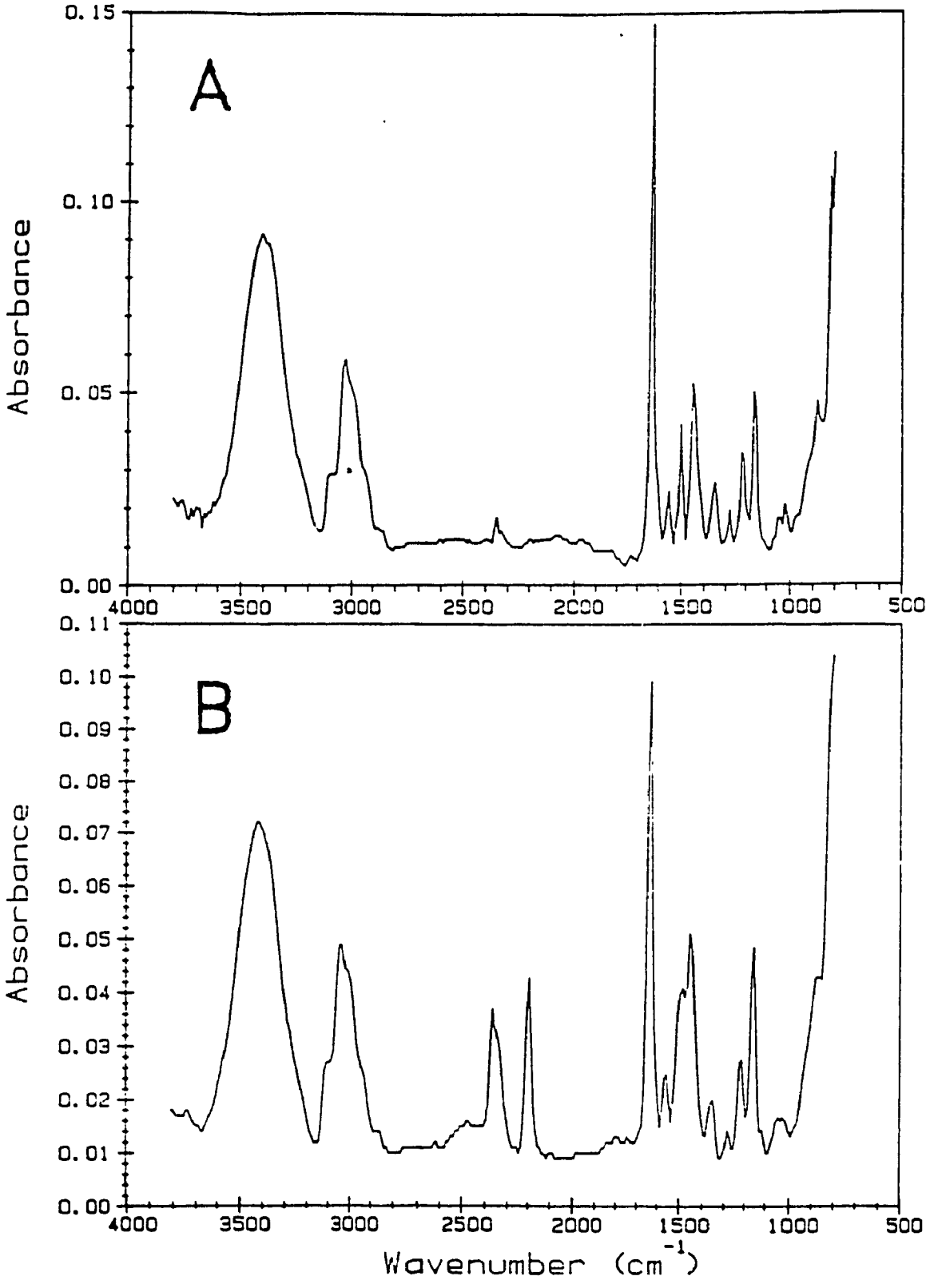

Figure 3.11 FTIR spectra of (a) PXV-Br_2 on an IRTRAN disc; (b) $Ni(mnt)_2$ ion exchanged into same film as (a) on IRTRAN disc.

PXV.

3.3.2 Electrochemistry

In the absence of a redox couple, cyclic voltammograms show small peaks for the $Ni(mnt)_2^{2-}$ one electron oxidation (Figure 3.12a). The waves were often very broad and appeared irreversible with ΔE_p = 0.30 V at 10 mV/sec. The observed $Ni(mnt)_2^{2-}$ potentials were consistent with literature values (53) which are between 0.23 and 0.3 V versus calomel in common organic solvents. Upon continuous cycling these peaks decrease in intensity. This decrease is found to be due not to leaching of the chromophore from the film since none was subsequently observed spectrophotometrically in the supporting electrolyte, but is attributed to a combination of crosslinking of the polymer and expulsion of counterions from the film. Scanning more cathodic of the first reduction wave of the polymer revealed the polymer's electrochromism. The film changed from a brown colour to a deep violet-blue at potentials less than -0.6 V (versus Ag/AgCl) indicating the presence of the viologen radical cation, but this colour developed only slowly. The films also returned to their initial colour slowly and at a potential more anodic than +0.4 V.

The viologen (4,4' bipyridyl) peaks on the negative sweep of the voltammogram are weak and are not well defined since they occur near the cathodic limit of the solvent. In some cases the second reduction peak of the viologen was not observed. It is well known that the cation radicals of polyviologens exist mainly in associated forms which are more stable than the monomeric species, and it is believed

that the stability of the former prevents the second reduction which is less reversible (20). The viologen dication to radical monocation reduction potential, observed at -0.45 V agreed with literature (44).

The second reduction of viologen is known to be irreversible (65). When the system was cycled more cathodic than this second reduction potential a decrease in all voltammetric peaks was observed due to loss of electro-activity of the polymer. This loss of electro-activity is attributed to crosslinking (66) and contraction of the polymer film as counterions are forced from the film into solution when the PXV^{2+} is reduced.

The ferri/ferrocyanide redox couple was readily incorporated into the films (Figure 3.12b). The $Fe(CN)_6^{3-/4-}$ couple showed a voltammetric wave at 0.27 V. The separation between the anodic and cathodic $Fe(CN)_6^{3-/4-}$ peaks (ΔE_p) was 200 to 400 mV for scan rates from 10 to 100 mV/sec. The redox couple readily penetrated the film, but loaded films subsequently placed into supporting electrolyte alone showed leaching of 75% of the $Fe(CN)_6^{3-/4-}$ into solution within 30 minutes as evinced by a decrease in the $Fe(CN)_6^{3-/4-}$ currents. The $Fe(CN)_6^{3-/4-}$ peaks largely masked the Ni-$(mnt)_2^{2-}$ peaks as the redox couple penetrated the film. Solutions showed no evidence of leaching of the chromophore upon incorporation of the redox couple.

The dependence of $Fe(CN)_6^{3-/4-}$ peak currents on the square root of scan rate was linear illustrating diffusion limited behaviour for the redox couple within the film. Voltammetric data for $Fe(CN)_6^{3-/4-}$ within the PXV-Ni$(mnt)_2$ film is tabulated in Table 3.9. The rate of charge transport through a polymer film can be described by effective diffusion coefficients which include electron hopping, ion migration and other aspects

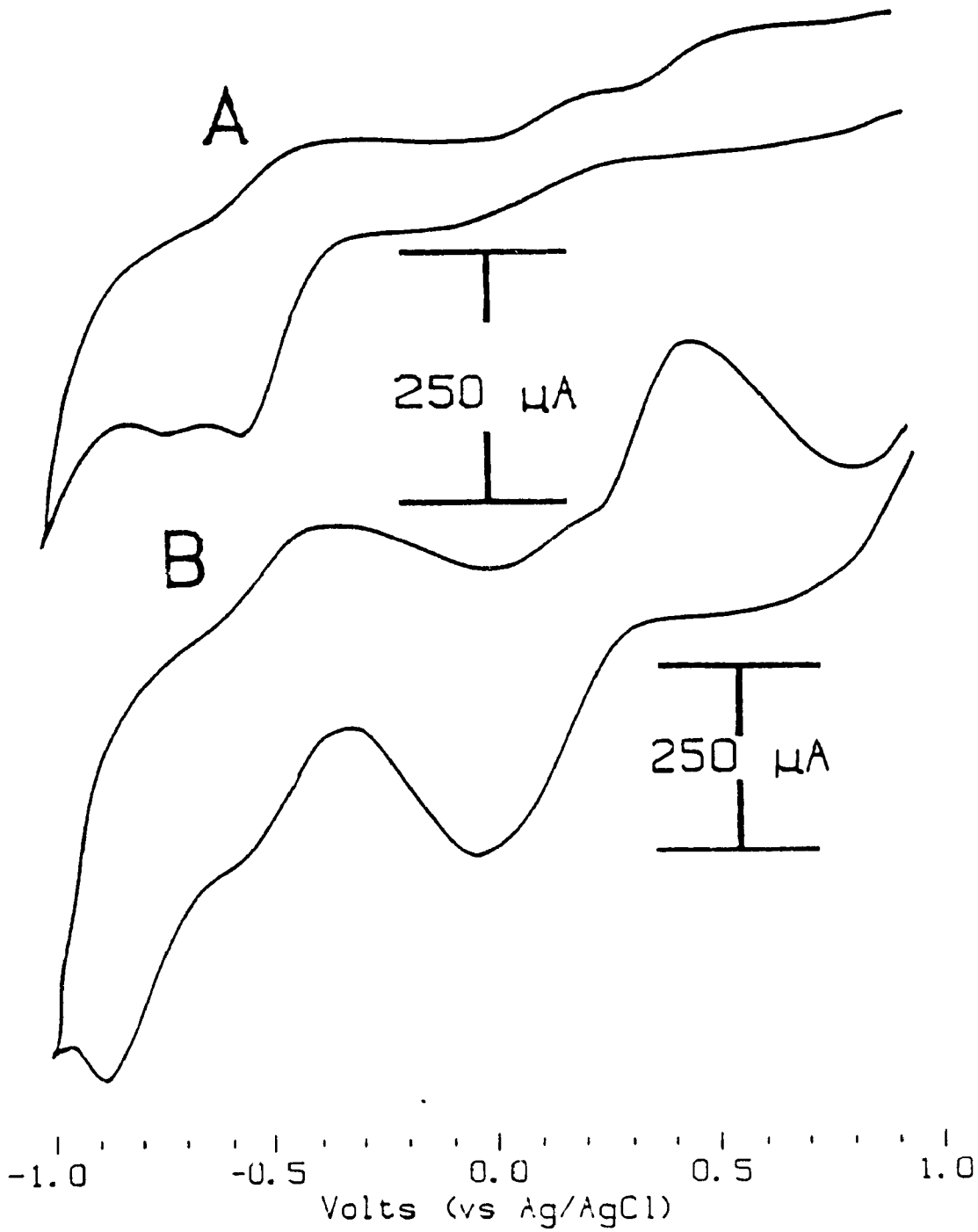

Figure 3.12 Cyclic voltammograms of PXV-Ni(mnt)$_2$ coated SnO_2 electrode in (a) 1.0 M KCl and (b) 2 mM $Fe(CN)_6^{3/4-}$/0.1 M KCl at a scan rate of 100 mV/s starting at +0.9 V.

Table 3.9: Electrochemical data for $Ni(mnt)_2$/PXV
on an SnO_2 working electrode with Pt as counter and Ag/AgCl as reference electrodes
in 2.0 mM $Fe(CN)_6^{3/4}$ in 0.1 M KCl.

$(V/s)^{1/2}$	i_{pa} µA	i_{pc} µA	E_{pa} V	E_{pc} V	E_{pa}-E_{pc} V	E_o V
0.10	177.42	274.19	0.50	-0.08	0.58	0.21
0.14	225.81	435.48	0.47	-0.06	0.53	0.21
0.20	338.71	612.90	0.46	-0.03	0.49	0.22
0.24	483.87	677.42	0.43	-0.01	0.44	0.21
0.28	612.90	806.45	0.38	0.02	0.36	0.20
0.32	677.42	887.10	0.34	0.07	0.27	0.21

of carrier mobilities (67). The coefficient from 3 films containing the $Fe(CN)_6^{3-/4-}$ couple evaluated chronoamperometrically was 5 ± 1 x 10^{-9} cm^2/sec for a potential step from 0.0 to +1.0 V and for 0.6 to -0.6 V.

3.3.3 Photoelectrochemistry

The photoelectrochemical behaviour of polymer films was studied in background electrolyte in the presence and absence of $Fe(CN)_6^{3-/4-}$ redox couple. The background current for all electrodes studied was non-zero (-20 to +20 nA) and all photocurrents were anodic. SCPC's in only background electrolyte were all very small (≈30 nA) for stirred solutions with intensities of 100 mWatts/cm^2 and the temporal response of the films showed trap-controlled behaviour (similar to Figure 3.8a). The magnitude of the SCPC's was 365 ± 25 nA/cm^2 for PXV-Ni(mnt)$_2$ electrodes in 2.0 mM $Fe(CN)_6^{3-/4-}$/0.10 M KCl. The film in the absence of the dye was evaluated by incorporating the electro-inactive ClO_4^- anion into the PXV film. SCPC's reached 50 ± 5 nA/cm^2 for electrodes not containing the dye most likely due to light absorption by the $Fe(CN)_6^{3-/4-}$ redox couple.

Photocurrent profiles for the polymer films studied are illustrated in Figure 3.13. New PXV-Ni(mnt)$_2$ films demonstrated prompt response to light on/light off switching reaching a steady state current in about 10 seconds (Figure 3.13a). After 1 hour of use, however (shorter in some cases), the films would start to show slight capacitive response to switching (Figure 3.13b). Crosslinking of the polymer and loss of ions from the film leading to compression of the film are probable causes.

There is spectroscopic evidence to indicate that charge transfer from the $Ni(mnt)_2$ dye to PXV viologen backbone occurs. The prompt temporal response shows that conduction along the polymer is comparatively efficient. D_{eff}'s for the $Fe(CN)_6^{3-4-}$ redox couple, however, are low.

3.4 $Ni(mnt)_2$/PXV gel modified electrodes

PXV-$Ni(mnt)_2$ electrode modifying layers described above are compact and poorly swollen films permitting limited ionic mobility. A strategy to increase ionic conductivity based upon work by Audebert et al (68) involves swelling a polymeric matrix with a hydrophobic polar solvent creating a "gel". They used high equivalent weight Nafion (a perfluorosulphonic membrane developed by Dupont) which would form gels having ionic conductivities close to solution values and mechanical properties resembling those of a solid. The modified layer is a separate phase from the bulk aqueous electrolyte. They obtained apparent diffusion coefficients for ferrocene only one order of magnitude lower than solution values. The structure of the Nafion gel was comprised of a lattice of polymer rods surrounded by gel solvent, the perfluoroalkyl chains inside the rods and the sulphonic groups outside, solvated by solvent. The solvent channels were sufficiently large to offer little impedance to ionic diffusion.

Attempts to form gels with PXV met with limited success. Solubility of the PXV polymer in solvents miscible with the tributylphosphate (**tbp**) was generally small therefore thicknesses of prepared modifying layers was small, estimated at less

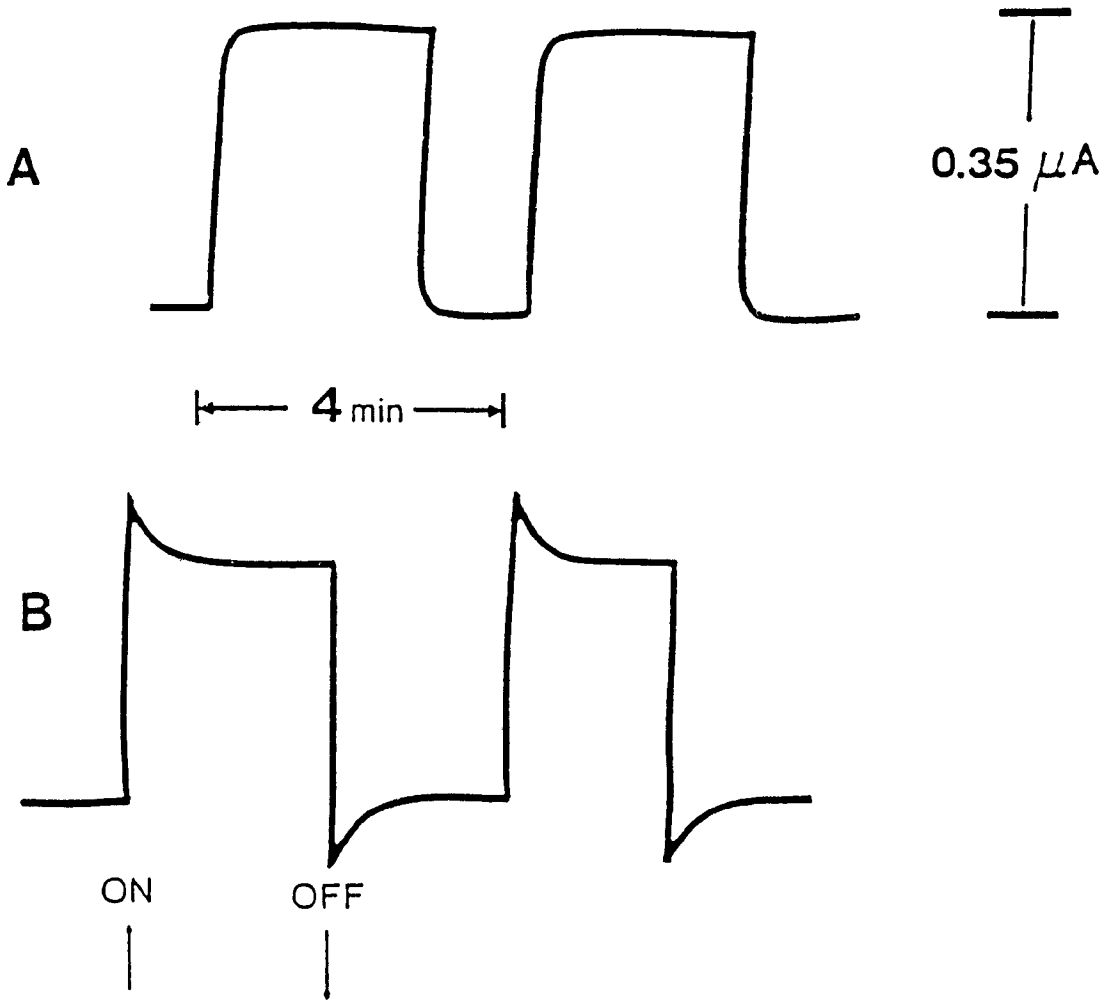

Figure 3.13 Short-circuit photocurrent profiles for PXV-Ni(mnt)$_2$ coated onto SnO_2: (a) new electrode; (b) old electrode.

than 1 μm. At such thicknesses the ability to form a solid network interspersed with large solvent channels seems unlikely, and these gels would not adhere well to SnO_2 electrodes. Two types of gel electrodes were distinguished, one where the swelling solvent, tbp ended up evaporating off and one where it remained. The former is not considered a gel, but simply a film from an alternative casting procedure.

3.4.1 Electrochemistry

The gelling solvent, tbp showed no voltammetric peaks in the potential window studied. Figure 3.14a shows a cyclic voltammogram typical of $Ni(mnt)_2$-PXV-tbp gel modified electrodes in 1.0 M KCl. Film voltammograms would show very small peaks for the reversible $Ni(mnt)_2^{2-/1-}$ reaction, E_{pc} = 0.235 V and E_{pa} = 0.29 V (Ag/-AgCl) at 100 mV/s. PXV peaks are not distinct at E_{pc} *ca.* -0.48 and E_{pa} *ca.* -0.36. Figure 3.14b is a voltammogram in 2 mM $Fe(CN)_6^{3-/4-}$/0.1 M KCl. $Fe(CN)_6^{3-/4-}$ peaks were E_{pc} = 0.093 V and E_{pa} = 0.395 V, PXV peaks shifted slightly cathodic to E_{pc} = -0.57 and E_{pa} = -0.38. Peaks attributable to the viologen's first reduction $PXV^{2+/1+}$ corresponded to those expected for the viologen (44). The second reduction was not observed in the potential window studied. The redox couple peak currents were much larger for film electrodes (as in Figure 3.14c), but would decrease over time for some electrodes suggesting collapse of a swollen polymer structure. $Fe(CN)_6^{3-/4-}$ would not be retained by either the films or the gels when subsequently placed into background electrolyte. This indicated that the $Fe(CN)_6^{3-/4-}$ did not penetrate into the tbp phase of gel electrodes well while the much larger couple peak currents and rapid loss (within

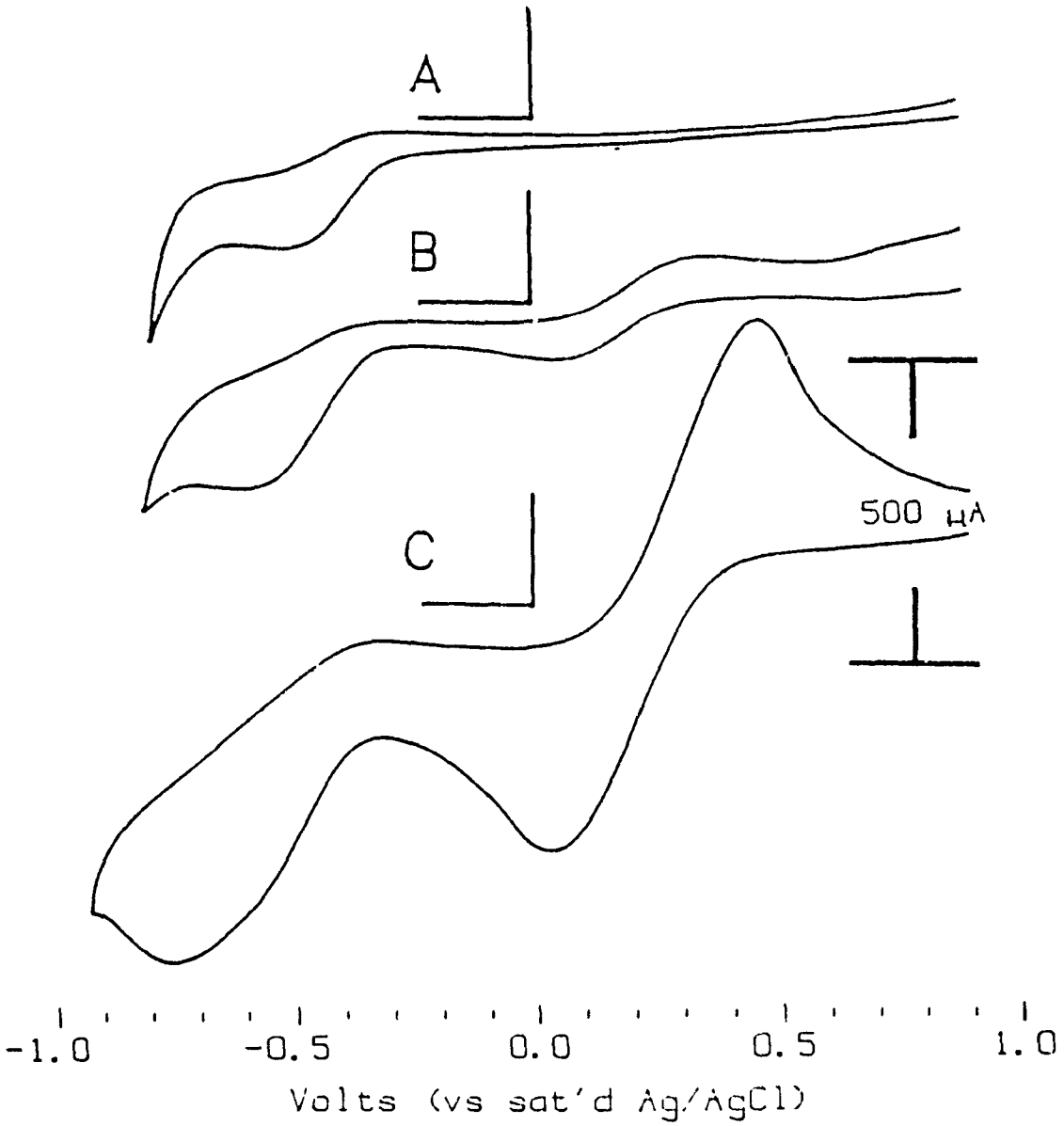

Figure 3.14 Cyclic voltammograms of $Ni(mnt)_2$/PXV gel in (a) 1.0 M KCl; (b) 2 mM $Fe(CN)_6^{3/4}$/0.1 M KCl. (c) an electrode of low tbp concentration in 2 mM $Fe(CN)_6^{3/4}$/0.1 M KCl. All scan rates were 100 mV/s starting at +0.9 V and anodic currents are upwards. All voltammograms are on the 500 µA scale.

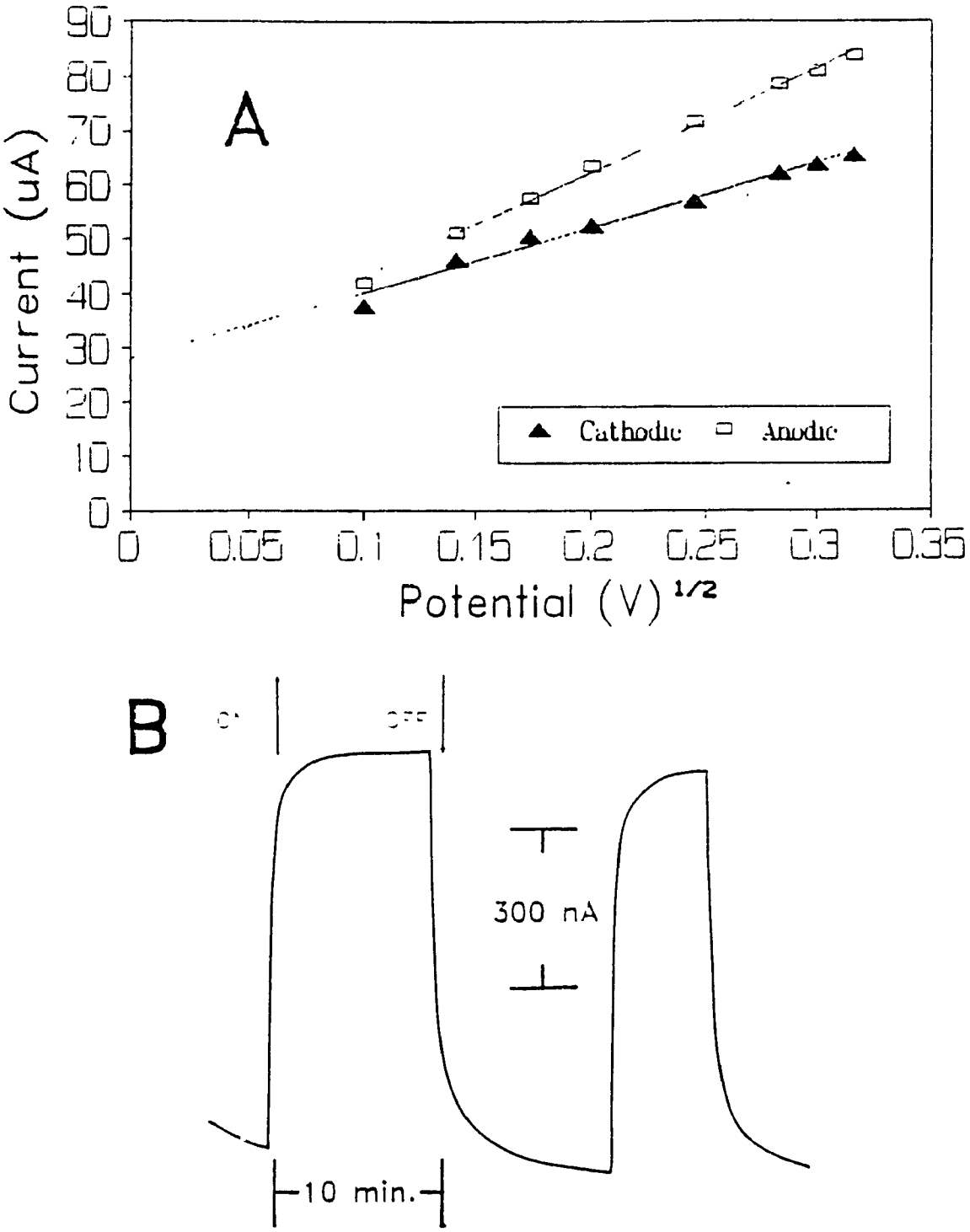

Figure 3.15 (a) scan rate dependence of $Ni(mnt)_2$/PXV gel in 2 mM $Fe(CN)_6^{3-/4-}$/0.1 M KCl. Scan rates are from 10 - 100 mV/s. (b) short-circuit photocurrent profile gel electrode in 2 mM $Fe(CN)_6^{3-/4-}$/0.1 M KCl under 100 mW/cm^2 visible illumination.

Table 3.10: Electrochemical data for $Ni(mnt)_2$/PXV gel on an SnO_2 working electrode with Pt as counter and Ag/AgCl as reference electrodes in 2.0 mM $Fe(CN)_6^{3-/4-}$ in 0.1 M KCl.

$(V/s)^{1/2}$	i_{pa} μA	i_{pc} μA	E_{pa} V	E_{pc} V	E_{pa}-E_{pc} V	E_o V
0.100	42.2	37.7	0.290	0.072	0.227	0.181
0.141	51.3	46.6	0.301	0.059	0.242	0.180
0.173	57.7	50.9	0.311	0.056	0.255	0.184
0.200	63.4	52.7	0.314	0.051	0.263	0.183
0.245	71.7	57.0	0.322	0.048	0.274	0.185
0.283	78.6	62.3	0.329	0.042	0.287	0.186
0.300	81.1	64.1	0.332	0.039	0.293	0.186
0.316	83.9	65.6	0.336	0.033	0.303	0.185

30 minutes) of $Fe(CN)_6^{3-/4-}$ from the film suggest that the films were not actually separate phases but a loose network of polymer chains permitting facile in/out flow of solution species. Regrettably, this loose structure, conducive to high ion mobility within the film was not stable and in most cases was found not to lead to overlap of the polymeric chains which is necessary for electronic conductivity within the film.

The scan rate dependence of the $Fe(CN)_6^{3-/4-}$ peak currents was linear for square root of scan rate and is shown in Figure 3.15a. D_{eff}'s for the solution redox couple were evaluated by chronoamperometry, but some error is expected since the films didn't retain the couple well. The concentrations of electro-active species were measured directly before and after the potential step experiment. For a series of 3 gel electrodes in a horizontal cell the D_{eff} for $Fe(CN)_6^{3-/4-}$ in films *ca.* 15 μm in thickness evaluated by chronoamperometry were *ca.* $3 \pm 1.5 \times 10^{-7}$ cm^2/s and by scan rate dependence $0.9 \pm 0.5 \times 10^{-7}$. For film electrodes D_{eff}'s were calculated as *ca.* 9×10 cm^2/s by chronoamperometry. Voltammetric data is tabulated in Table 3.10.

3.4.2 Photoelectrochemistry

Most tbp-cast film and gel electrodes showed small photocurrents of slow temporal response in contrast to the rapid response of conventional film electrodes of the PXV shown in the previous section. Electrodes would stabilize to below 0.1 $\mu A/cm^2$. In 1.0 M KCl SCPC's were anodic and *ca.* 80 nA. In 2.0 mM $Fe(CN)_6^{3-4-}$ /0.10 M KCl SCPC's were 210 ± 30 nA/cm^2 and temporal response to on- or off-switching was slow. For two chance film electrodes studied, SCPCs in 2.0 mM

$Fe(CN)_6^{3-/4-}$/0.10 M KCl were as high as 540 nA/cm^2 with similar temporal response (see Figure 3.15b). Dark currents were slightly higher than other electrodes and these currents decayed over about 45 minutes to values similar to the majority of electrodes studied, suggesting that the structure of these few electrodes was not stable, a solvent swollen structure ultimately collapsing and/or fortuitous electronic overlap of polymeric chains ultimately breaking down.

Limits of this system appear to be the poor incorporation of our solution redox couple into gel electrodes as well as the small concentrations of modifier possible using this polymer/dye. The potential of the strategy is illustrated by the high currents observed in a few cases, due presumably to a less compact polymer structure.

3.5 Composite electrodes based upon the $Ni(mnt)_2$/QP blend and PXV

The potential of PXV as a good conductor as well as its ability to form a charge transfer complex with $Ni(mnt)_2$ seen in Section 3.2 led to efforts to incorporate the PXV into a matrix featuring high ionic conductivity. A challenge is to obtain a sufficiently high concentration of conducting polymer in order to maintain a conducting polymeric wire to the electrode while not collapsing the solvent swollen structure of the host polymer blend by the crosslinking this polymer is known to undergo (65) and the hydrophobic repulsion of the $Ni(mnt)_2^{2-}$ exchanged PXV salt. Therefore, we wanted to grow conducting wires of PXV through the ionic conducting QP blend. It was incorporated either into the QP blend methanolic casting solutions or into preformed QP blend films by direct cathodic deposition as well as by codeposition

with glutaraldehyde.

3.5.1 PXV in QP blend films (incorporated into casting solutions)

The PXV polymer was dissolved into methanolic casting solutions of the QP blend. The films once ion exchanged with $Ni(mnt)_2^{2-}$ became very deeply coloured. These electrodes afforded the highest dye concentration of all composites of comparative thickness studied. Ion exchange was complete in as little as 5 minutes. The PXV^{2+} sites seem to lead to improved dye in-partitioning into composite films. All films studied were *ca.* 12 μm in thickness. Cyclic voltammetry in 1.0 M KCl is illustrated in Figure 3.16a. A cathodic peak attributable to the viologen center was noted at -0.42 V and anodic peaks at -0.34 V. A weaker one at -0.59 V which was seen to vary among films is attributed to the pyridinium reduction wave. The $Ni(mnt)_2^{2-}$ gave peaks at E_{pa} = 0.30 V and E_{pc} = 0.20 V. The amount of $Ni(mnt)_2^{2-}$ incorporated into the QP blend/PXV films would depend upon the quantity of PXV previously incorporated into the casting solution. This also greatly affected the degree of incorporation and reversibility of the $Fe(CN)_6^{3-/4-}$ couple as well as the electro-activity of the entire film. The difference between a high and low concentration of PXV to QP blend within the film in 2 mM $Fe(CN)_6^{3-/4-}$/0.1 M KCl is demonstrated in Figure 3.16b and c, respectively. In the presence of the $Fe(CN)_6^{3-/4-}$ for a low concentration of PXV to QP blend, peaks would appear at E_{pa} = 0.36 and E_{pc} = 0.075 V for the couple after extended cycling from +0.7 to -0.4 V (ie. around the $E^{o'}$ of the couple). Peaks for the $PXV^{2+ \rightarrow 1+}$ are found at E_{pc} = -0.46 V and E_{pa} = -0.27 V and for the $PXV^{1+ \rightarrow 0}$ at E_{pc}

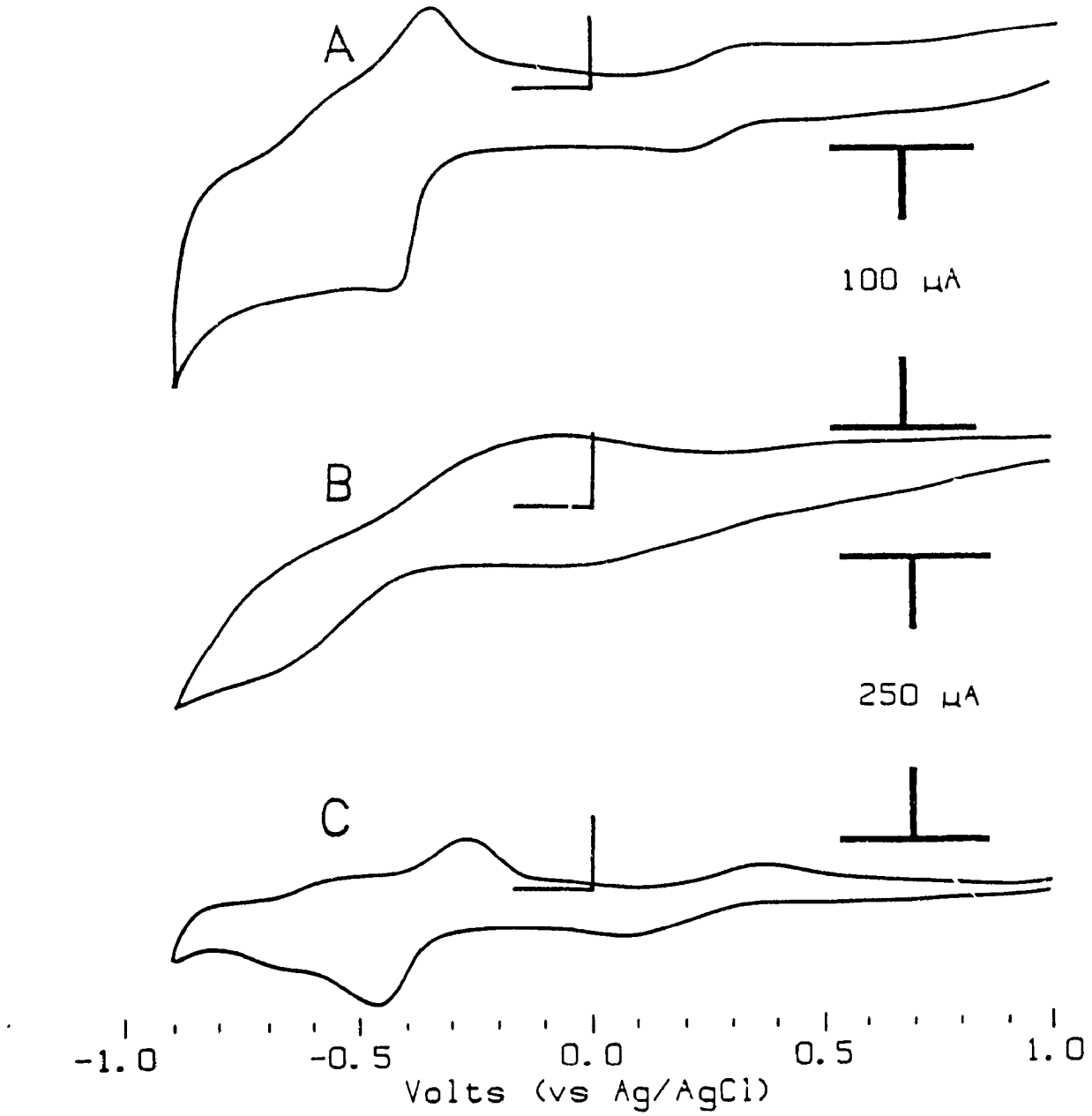

Figure 3.16 Cyclic voltammograms of $Ni(mnt)_2$/QP blend/PXV composite electrodes in (a) 1.0 M KCl and 2 mM $Fe(CN)_6^{3/4}$/0.1 M KCl for (b) high PXV concentration and (c) low PXV concentration. Scan rates are 100 mV/s starting at +1.0 V and anodic currents are upwards. Portions (b) and (c) are of the 250 µA scale.

= -0.67 V and E_{pa} = -0.60 V. When transferred back into supporting electrolyte, the $Fe(CN)_6^{3-/4}$ peaks would slowly, but ultimately disappear. Only a moderate concentration of $Fe(CN)_6^{3-/4-}$ seems to be incorporated into these films. D_{eff}'s could not be evaluated for these films due to the poor incorporation and irreversible nature of the redox couple within these films.

SCPC's in both 1.0 M KCl and in 2.0 mM $Fe(CN)_6^{3-/4-}$/0.10 M KCl were small. Background currents were significant at *ca.* 150 nA after stabilization for 2 hours. At 100 mW/cm^2 in degassed and stirred solutions SCPC's were 30 - 80 nA/cm^2 in either background electrolyte or redox solution and would generally decay to below 20 nA/cm^2. Response to light on/off switching was rapid (< 30 seconds).

The morphology of the QP blend that lends it its exceptional anion in-partitioning and ionic transporting properties appeared to break down with inclusion of PXV prior to film formation. The quaternary polymer aids in creating a network of interconnected hydrophobic P4VP interspersed with hydrophilic regions that lend the blend its ability to sustain high ionic mobilities (61). The PXV^{2+} appears to spoil this useful structure during its formation.

3.5.2 PXV in QP blend films (incorporated by cathodic cycling)

When PXV incorporation prior to film formation proved unsuccessful efforts to incorporate the PXV into preformed QP blend films were pursued. PXV was incorporated into films of the QP blend precast upon SnO_2 electrodes by electrodepositing the cationic polymer from aqueous solution. Creager and Fox described a method of

depositing PXV onto electrode surfaces such as gold, tin oxide and glassy carbon (25). Upon cycling a polymer blend coated electrode from 0 to -1.1 V (versus Ag/AgCl) in an aqueous solution of PXV-Cl_2 strong peaks grew in slowly, attributed to viologen. A purple colour developed suggestive of the viologen cation radical. After 30 minutes of deposition a strong cathodic peak is found at -0.76 V, a strong anodic peak at -0.485 V and another less intense anodic peak at -0.32 V as seen in Figure 3.17. These peaks do not correspond to reported peaks for this polymer (44). Scanning over the course of 4 hours shifted the cathodic peak initially at -0.76 V out of the potential window and the strong anodic peak initially observed at -0.485 decreased in intensity and shifted to -0.53 V. An explanation of the shift of the second PXV reduction to more negative potential is as follows. As PXV deposition proceeds the polymer builds up at the electrode surface. With a larger concentration of the viologen, association of PXV^+ radical cations can occur. This association is known to stabilize viologen (20) by preventing the second reduction which is more irreversible. Hence the shift of the $PXV^{1+ \rightarrow 2+}$ reduction reaction to more negative potential upon increased deposition of the polymer. A cyclic voltammogram of an electrode subsequently placed into background electrolyte following electrodeposition is shown in Figure 3.18a. E_{pc} at -0.41 and E_{pa} at -0.32 more closely match the $PXV^{2+ \rightarrow 1+}$ reduction reported (44). Scanning past the second reduction generally caused rapid decomposition of film currents.

$Ni(mnt)_2^{2}$ was either incorporated into the film before deposition of the PXV or was ion exchanged into the composite film afterwards. $Ni(mnt)_2$ did not show any electrochemical activity in either case. Cyclic voltammograms of a $Ni(mnt)_2$/QP

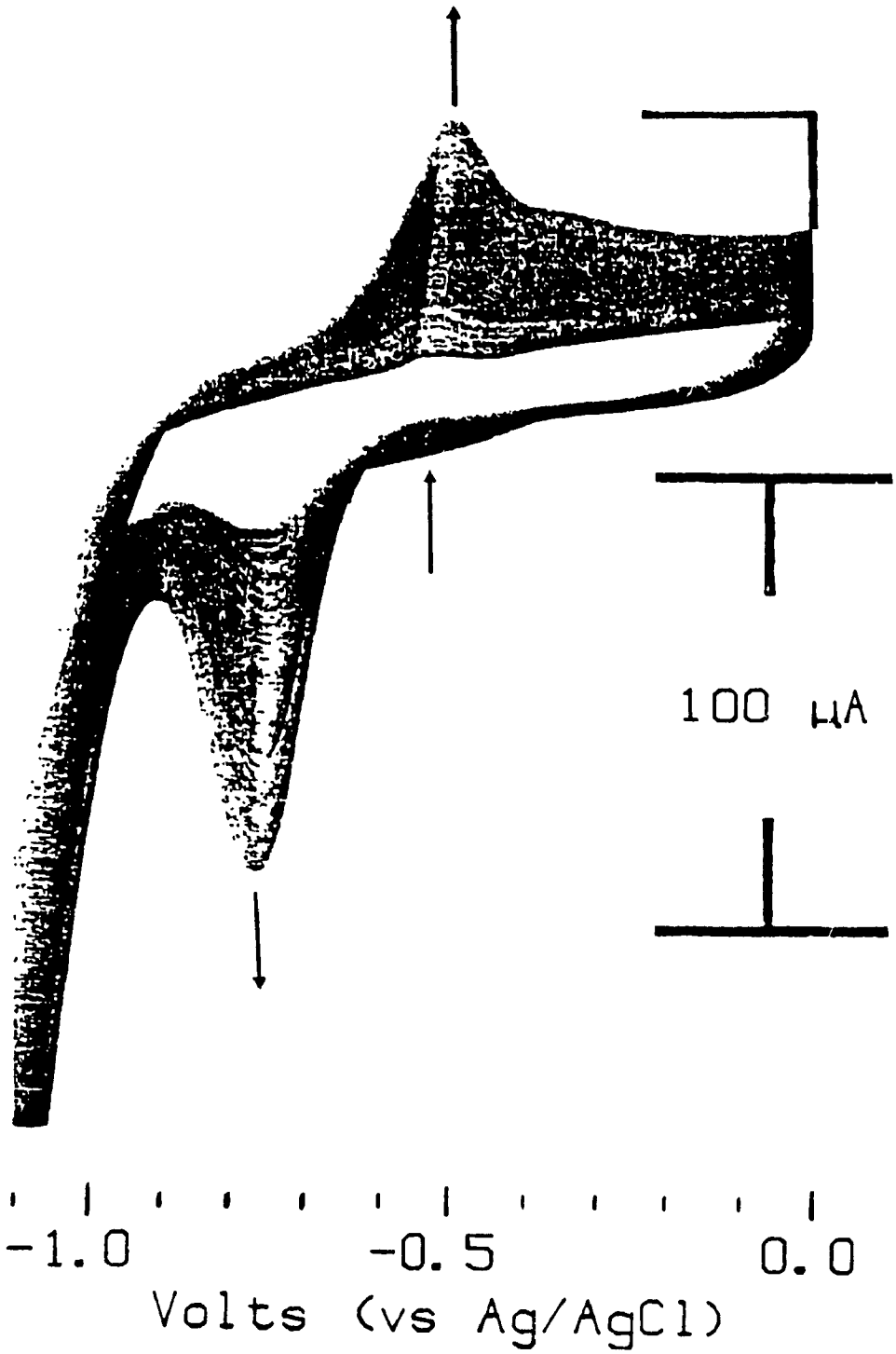

Figure 3.17 Continuous cyclic voltammogram at 200 mV/s over 1 hour demonstrating the growth of PXV peaks within a $Ni(mnt)_2$/QP blend coated SnO_2 electrode starting at 0 V to -1.1 V. Anodic current is upwards.

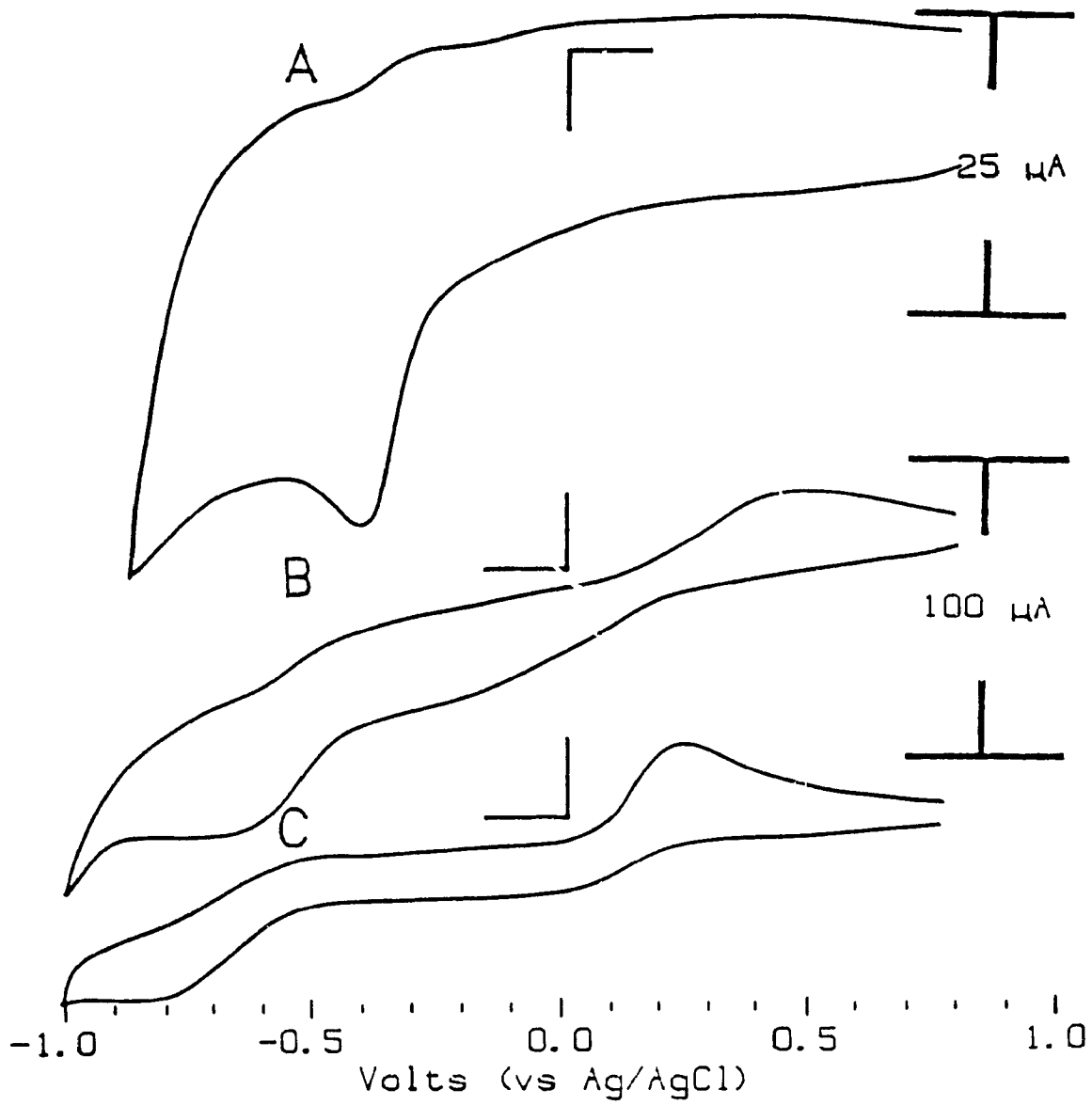

Figure 3.18 Cyclic voltammograms of $Ni(mnt)_2$/QP blend/PXV composite electrodes in (a) 1.0 M KCl and in 2 mM $Fe(CN)_6^{3-/4-}$/0.1 M KCl (b) directly after transfer into the redox solution and (c) after continuous cycling for 1 hour. Starting potential was +0.8 V and anodic current is upwards. The 100 μA scale corresponds to (b) and (c).

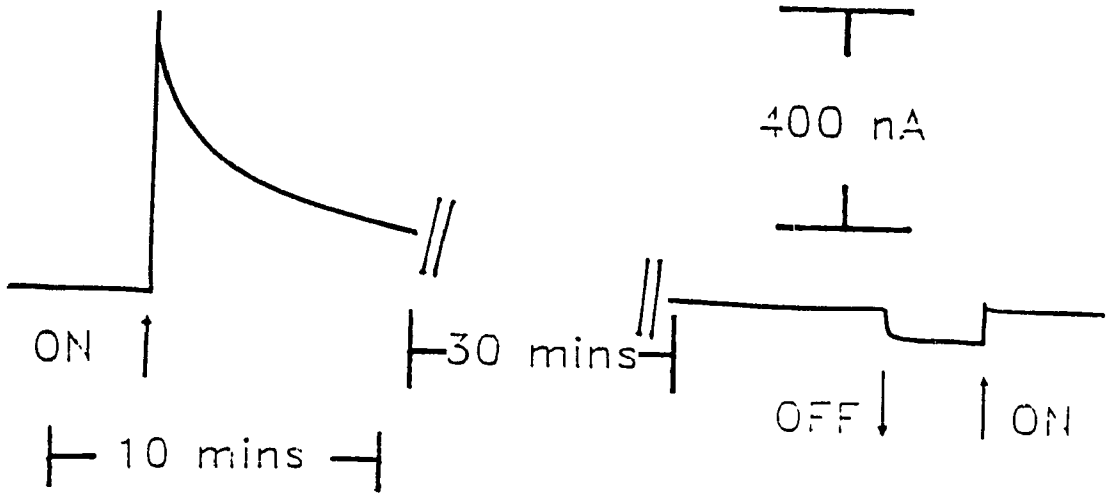

Figure 3.19 Short-circuit photocurrent profile of a $Ni(mnt)_2$/QP blend coated SnO_2 electrode into which PXV was cathodically electrodeposited. This shows response to initial on switching of light source as well as response observed *ca.* 40 minutes later. Photocurrents were anodic.

blend/PXV film in 2.0 mM $Fe(CN)_6^{3-/4-}$/0.10 M KCl are shown in Figure 3.18b and 3.18c. The $Fe(CN)_6^{3-/4-}$ couple no longer has symmetric peaks. Figure 3.18b shows the first scan in redox solution and Figure 3.18c a scan recorded 1 hour later after continuous cycling. The cathodic peak was not well defined at E_{pc} = 0.07 V, while the anodic peak was at 0.29 V and the peak separation decreased after extended cycling. Clear PXV peaks were quickly lost from the voltammogram in $Fe(CN)_6^{3-/4-}$. The film did not permit a large in-partitioning of the $Fe(CN)_6^{3-/4-}$ redox couple. A plot of peak currents versus square root of scan rate for the $Fe(CN)_6^{3-/4-}$ couple was linear, thus indicating that movement of the couple within the film is diffusion limited. D_{eff}'s evaluated by chronoamperometry and scan rate dependencies were up to an order of magnitude smaller than that for the neat QP blend in section 3.2. These values are in doubt, however, due to the poor retention of $Fe(CN)_6^{3-/4-}$ by saturated electrodes subsequently transferred to background electrolyte for chronoamperometric experiments.

Greater success was achieved with films that already contained the Ni(mnt)$_2$ dye before PXV deposition. Ion exchanging the dye from acetonitrile would often give low concentrations within the film, since the amount of PXV retained was probably small. SCPC's for films of *ca.* 12 μm thicknesses were *ca.* 20 nA/cm^2 in only background electrolyte. In 2.0 mM $Fe(CN)_6^{3-/4-}$/0.10 M KCl a relatively large capacitive spike of up to 610 nA/cm^2 was observed the first time the light source was switched on. This ultimately decayed over the course of 40 minutes to a steady 85 ± 20 nA/cm^2 (Figure 3.19). Subsequent switching on did not give the large capacitive spike observed at first, but did give a sharp response.

It appears that PXV chains do grow or collect at the surface of the SnO_2 electrode through films of the QP blend. The slow, steady growth of the electro-active polymer's reduction peaks, it was hoped would be an indication that the polymer was extending through the solvent swollen channels of the host polymer away from the electrode surface. The well defined PXV voltammetric peaks were not preserved upon transfer of electrodes to redox solution. Response to switching was rapid in these films, indicating that electronic conduction was most likely mediated by the PXV polymer. Unfortunately, the extended structure of the PXV within the QP blend matrix seems to collapse shortly into the experiment.

3.5.3 PXV in QP blend films (incorporated by cathodic crosslinking)

A problem with the previous method of depositing PXV within the QP blend film was the apparent loss of PXV activity within the film. The deposition method involves the precipitation of the PXV^0 form of the polymer at the electrode surface. When the polymer attains its cationic form, however, it will likely dissolve back into the solution. A method of controlled crosslinking of the viologen polymer with glutaraldehyde and tris(hydroxymethyl)aminomethane (**Tris**) should produce more permanent PXV structures within the QP blend film. The Tris functions to stabilize the glutaraldehyde. Chang et al (48) reported that the reduced form of the viologen would react with free aldehyde groups of the hydroxymethylamine stabilized glutaraldehyde giving an insoluble crosslinked PXV membrane.

QP blend membranes were typically *ca.* 12 μm thick. Controlled potential

deposition at -1.1 V (vs SCE) for *ca.* 40 minutes would pass between 50 and 80 mC/cm^2. Similar results were obtained at -0.8 V, but at a slower rate. The films would appear purple corresponding to the PXV^{1+} cation radical. Once deposition was stopped and the electrodes rinsed, the purple colour would fade generally over the course of 2 - 10 minutes. For a few electrodes of very high deposited PXV concentration, the purple colour faded only after more than 2 days!

Two separate electrode preparation procedures could be distinguished giving very different types of behaviour. First (**first type**) was electrodepositing the PXV into a QP blend without dye and subsequently ion exchanging $Ni(mnt)_2^{2-}$ into the film. These electrode showed better ion exchange for $Ni(mnt)_2$ than the neat PQ blend ones. The anionic dye is likely to coordinate itself to the cationic sites of the PXV^{2+} redox polymer and in fact films containing the PXV^{2+} ion exchanged much more $Ni(mnt)_2^{2-}$ than did the neat QP blend film. Second (**second type**) was electrodepositing the PXV into QP blend films that already contained the dye.

The first type of electrode gave a cyclic voltammogram in background electrolyte at 100 mV/s as shown in Figure 3.20a (note scale). $Ni(mnt)_2$ showed peaks at E_{pc} = 0.17 V and E_{pa} = 0.32 V (vs Ag/AgCl). $PXV^{2+ \rightarrow 1+}$ reduction appeared at E_{pc} = -0.40 V and E_{pa} = -0.325 V. The pyridinium to pyridyl radical reduction should be observed in these films, thus the peak at -0.615 V was assigned as this reduction. A peak attributable to the pyridyl moiety appears at E_{pc} = -0.56 V and perhaps E_{pa} ≈ -0.15 V, though it was weak and broad. A rather surprising fact is that this type of electrode when placed into 2.0 mM $Fe(CN)_6^{3-/4-}$/0.1 M KCl did not show any electro

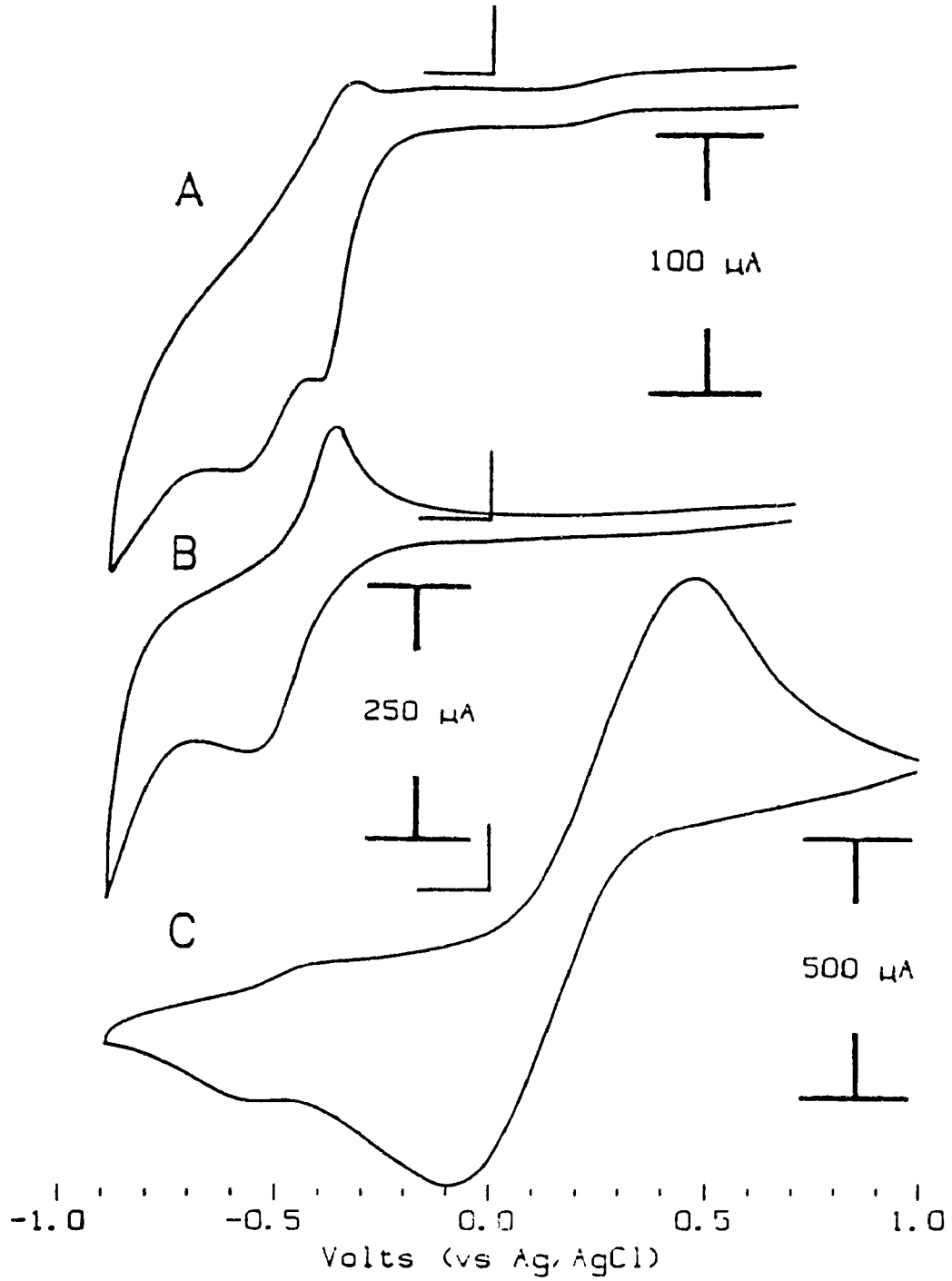

Figure 3.20 Cyclic voltammograms of $Ni(mnt)_2$/QP blend/PXV composite coated SnO_2 electrodes deposited via cathodic crosslinking with gluataraldehyde in (a) 1.0 M KCl and in 2 mM $Fe(CN)_6^{3-/4-}$/0.1 M KCl (b) for the second type of composite electrode (where $Ni(mnt)_2^{2-}$ was ion exchanged subsequent to PXV deposition) and (c) for the first type of electrode where $Ni(mnt)_2$ was incorporated into films prior to PXV deposition.

chemistry attributable to the redox couple.

A cyclic voltammogram of the second type of electrode in 1.0 M KCl is shown in Figure 3.20b. The $Ni(mnt)_2$ was not electro-active in this film. Well defined peaks were observed at -0.56 and -0.37 V (vs Ag/AgCl). A peak attributable to the pyridyl moiety appears at E_{pc} = -0.56 V. The anodic peak at -0.37 V was assigned as the viologen first reduction, the cathodic peak being just barely perceptible as a shoulder on the pyridinium reduction wave at *ca.* -0.40 V. In 2 mM $Fe(CN)_6^{3-,4-}$/0.1 M KCl (Figure 3.20c) strong peaks for the couple appeared at E_{pc} at -0.09 V and E_{pa} at +0.47 V. The peak separation, ΔE_p = 0.56 V at 100mV/s, was somewhat larger than in most films studied. In contrast to direct electrodeposition, described in the previous section, which did not show distinct PXV reduction peaks in $Fe(CN)_6^{3-/4-}$, peaks for the PXV reductions were observed after prolonged experimentation when PXV was deposited with the crosslinking agent. Peak current for $Fe(CN)_6^{3-/4-}$ was linear versus square root of scan rate, thus charge transport by the redox couple can be described by an effective diffusion coefficient. D_{eff}'s for the PXV incorporated films evaluated by potential step were 9 - 12 x 10^{-8} cm^2/s and by scan rate dependence 2 - 6 x 10^{-8} cm^2/s, which is within an order of magnitude of the neat QP blend film values.

The first type of electrode showed very small SCPC's in degassed stirred solutions. In 1.0 M KCl SCPC's were negligible and in 2.0 mM $Fe(CN)_6^{-4}$/0.10 M KCl were *ca.* 30 nA/cm^2 and response to light switching was capacitive, similar to that previously illustrated in Figure 3.13b. For the second type of electrode SCPC's were similar in appearance and magnitude, if a bit smaller than those obtained for Ni-

$(mnt)_2$/QP blend electrodes seen previously in section 3.2.

The incorporation of the PXV via crosslinking with glutaraldehyde did indeed lead to more permanent retention of the redox polymer within the QP blend films. The first type of electrode demonstrated good ion exchange for the $Ni(mnt)_2^{2-}$ dye and showed its voltammetric peaks, in contrast to the neat QP blend polymer. It did not, however, show any voltammetric peaks for the solution redox couple and all peaks were weaker than the second type, though the amount of PXV incorporated into the QP blend was the same (as estimated from charge passed during electrodeposition). The second type did not show voltammetric peaks for the dye, but showed very strong peaks for the redox couple and gave SCPC's similar to films without the PXV. Two scenarios present themselves: 1) for the first type of electrode crosslinked PXV grows at the surface of the SnO_2 electrode in the solvent channels of the QP blend. The method of immobilization, however creates a resistive coating at the electrode surface The crosslinking occurs at the fully reduced 4,4'-bipyridyl sites which by all indications impedes conduction along the backbone of the polymer. Conduction in this polymer occurs via redox self exchange between the 2+ and 1+ oxidation states of these same moieties of the polymer. Use of the viologen sites to bind the polymer, not surprisingly affected polymer conduction. When the dye was ion exchanged into the film, it preferentially coordinated to the PXV^{2+} sites, but this was a resistive mass at the surface of the electrode. The photoelectrochemistry for this is dictated by the state of the PXV at the surface of the electrode which is likely to be nonconducting. 2) For the second type the crosslinked polymer again grows at the surface of the SnO_2

electrode, but the dye, resident near the hydrophobic domains of the QP blend polymer does not particularly want to venture into the water swollen hydrophilic domains to coordinate onto the PXV^{2+}, and instead remains immobilized in the QP blend. In this case the photoelectrochemistry of the film is likely to be dictated by $Ni(mnt)_2$/QP blend film's characteristics and not by that of the PXV. So, the problem of PXV retention noted in direct electrodeposition in section 3.5.2 was solved with this procedure, but the mode of immobilization has itself presented a problem, deactivation of the conduction pathway within the polymer.

3.6 Semiconductor particles

In light of our efforts to improve electronic conduction from primary light absorber to electrode while at the same time maintaining the high ionic conductivity necessary to sustain faradaic processes, CdS semiconductor particles have been incorporated into the QP blend modified electrodes. Attempts were made to synthesize them *in situ* and to incorporate preformed derivatized particles into the polymer film. It was hoped that this strategy would create an electrode of high effective area coupling both electronic conduction through overlap of adjacent semiconductor particles and ionic conduction through the solvent swollen channels of the QP blended copolymer while at the same time passivating the particles against corrosion.

3.6.1 In situ formation of CdS particles within QP blend film

Semiconductor particles formed within the QP blend film were simply prepared

by soaking precast electrode films alternately in solutions of ammonium sulfide and then cadmium sulfate. Films were severely altered by this procedure. Films would not show any evident colour change.

Electronic spectra of these electrodes were marred by scatter. All showed visible decomposition in 2 mM $Fe(CN)_6^{3/4}$/0.1 M KCl solution. Films would crack and peel away from the surface of the SnO_2 electrode and generally being found to be unusable after about an hour in solution. Thus very little electrochemistry was recorded for these electrodes. Photoelectrochemistry was run in a polysulfide solution. 1.0 M each of sodium hydroxide, sodium sulfide and sulfur. A majority of electrodes were unusable, but a few electrodes showed response to light as in Figure 3.21. Dark currents were usually large and cathodic. With illumination with 100mW/cm^2 SCPC reached as high as 10 μA/cm^2 in polysufide solution and a photovoltage of 38 mV, but there was always a very large dark current and electrodes would decompose very quickly.

3.6.2 Surface derivatized CdS particles

The approach of capping size controlled CdS particles has two possible advantages over nonfunctionalized particles. The cap could impede decomposition and the ionic functionality may be expected to place a high concentration of the particles at the interface of hydrophobic and hydrophilic domains of the QP blend polymer of this study. Electrode films into which preformed semiconductor particles were incorporated did not give absorption due to the particles because of scatter. A photo-

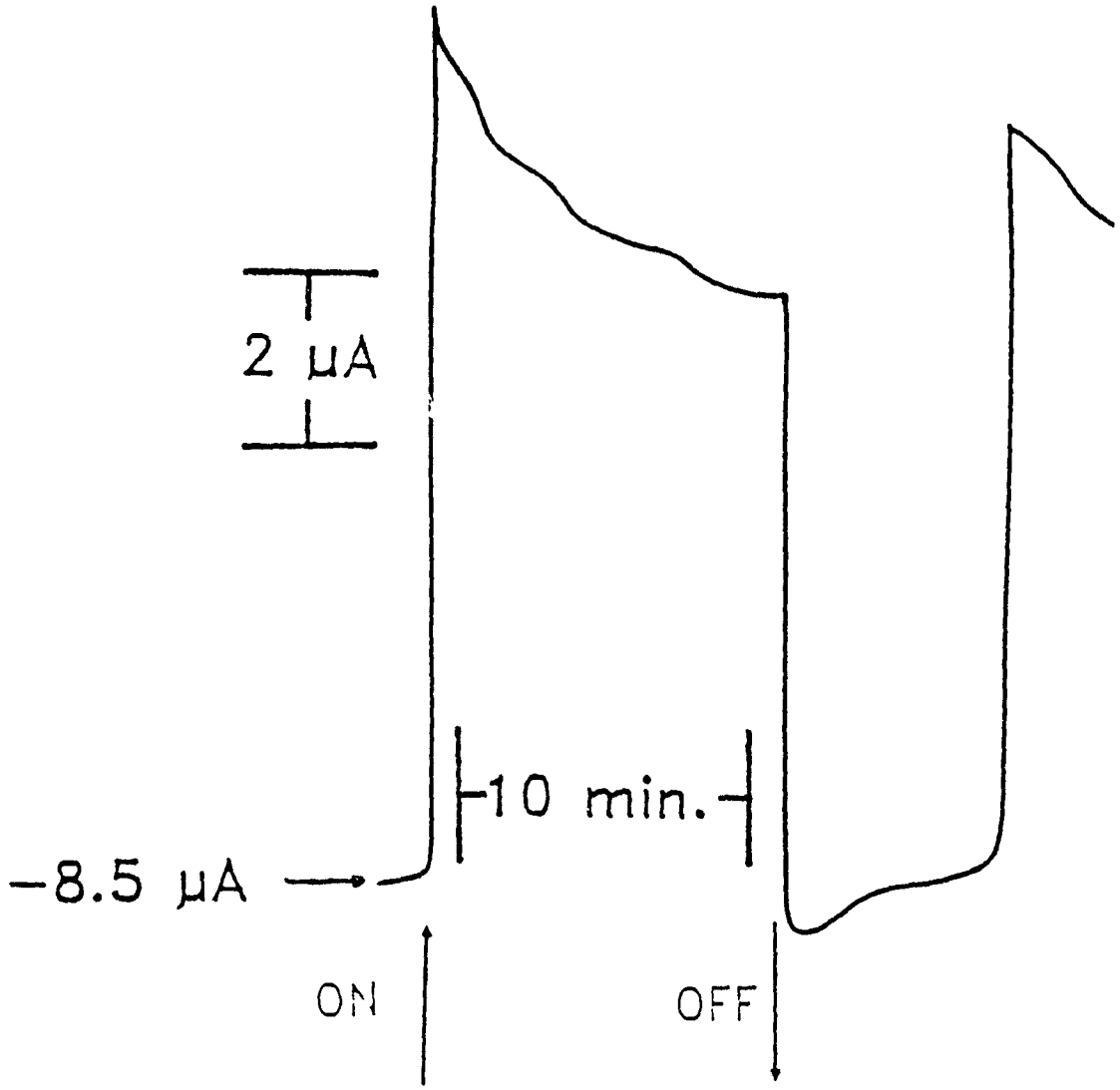

Figure 3.21 Short-circuit photocurrent profile for QP blend electrode in which CdS semiconductor particles were prepared *in situ*.

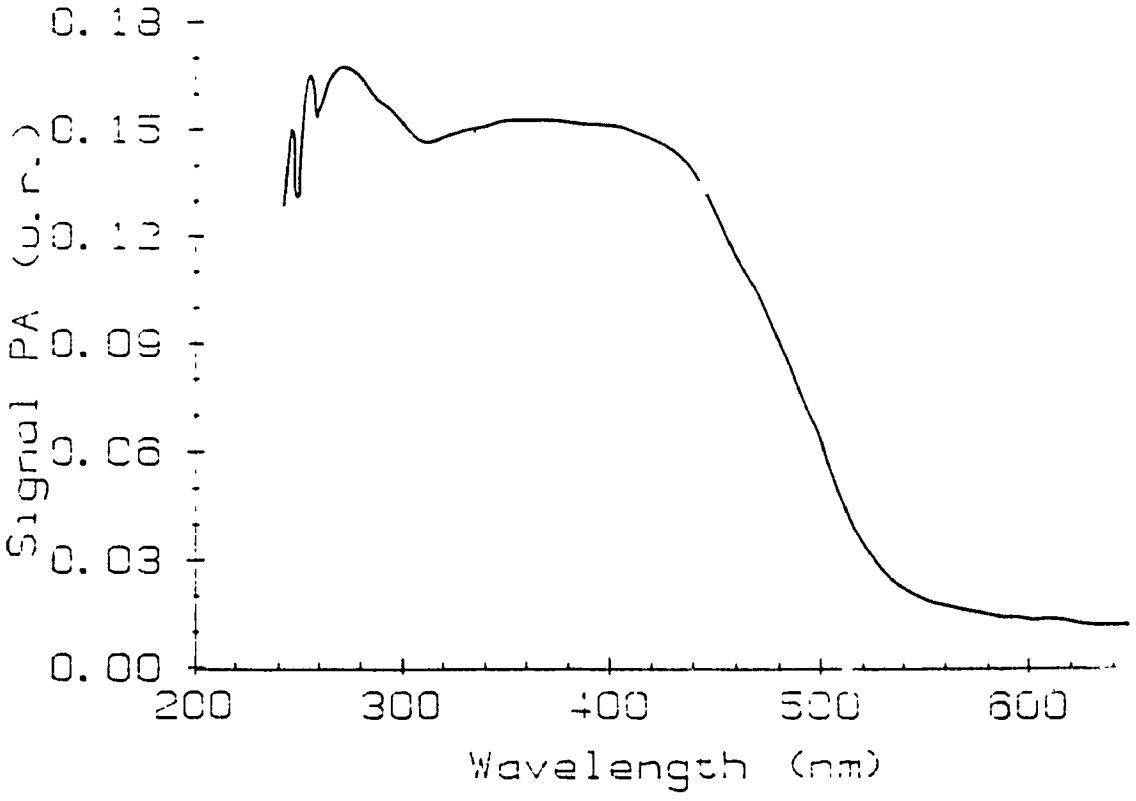

Figure 3.22 Photoacoustic electronic absorption spectrum of surface derivatized CdS semiconductor particles as a KBr pellet.

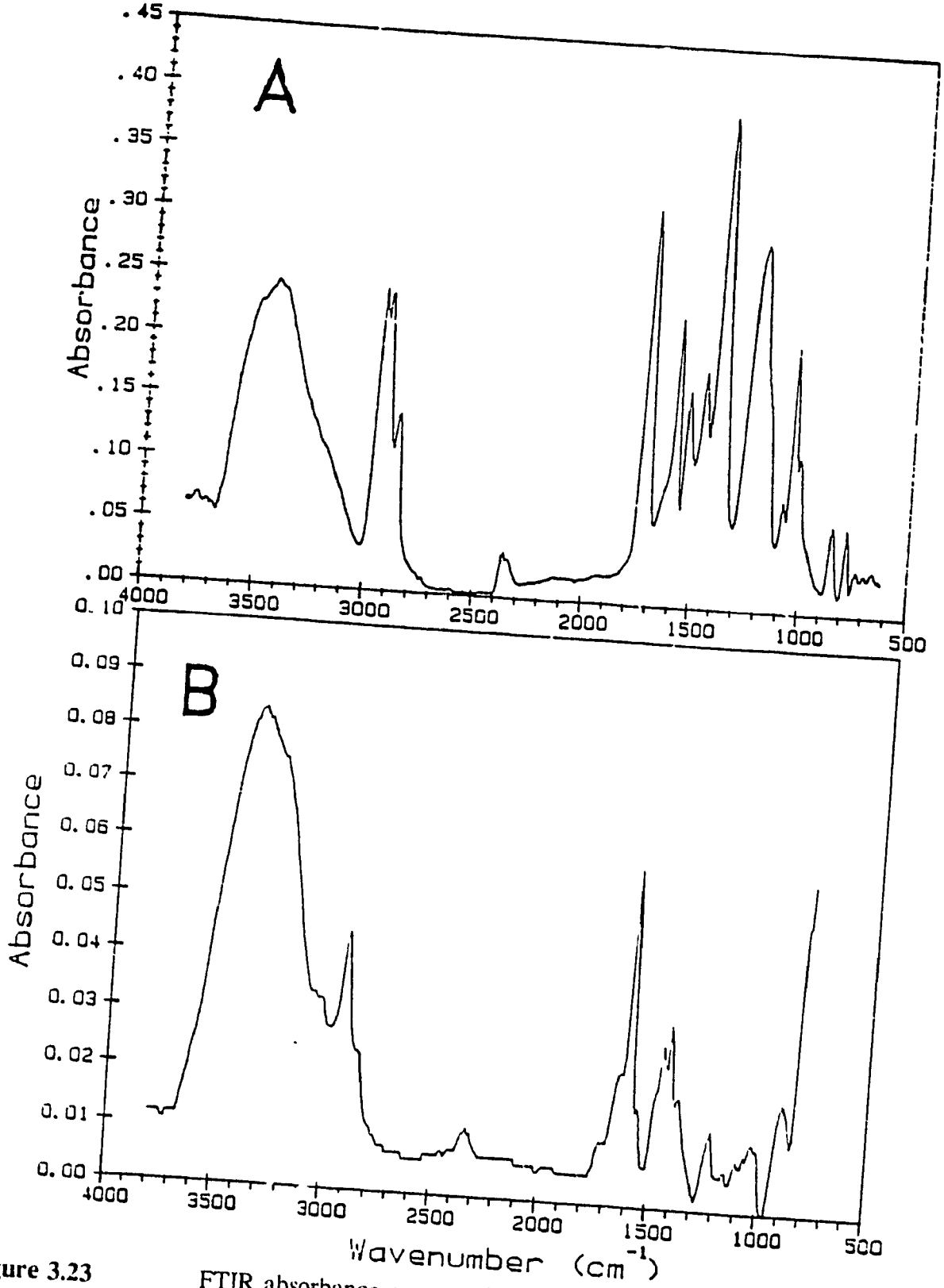

Figure 3.23 FTIR absorbance spectra of (a) capped CdS particles as KBr pellet and (b) capped particles within QP blend film on IRTRAN disc.

acoustic electronic spectrum of the capped particles as a KBr pellet shown in Figure 3.22 demonstrates the band edge of the particles. The onset of absorption is at *ca.* 520 nm indicative of nonquantum sized particles. Also noted is a shoulder at *ca.* attributable to absorption of the QP blend. The lack of sharp band edge absorption could mean that there exists a wide distribution of particle sizes in spite of our efforts to control size.

CdS does not show absorption in the IR, but the benzoic acid based "cap" should. The FTIR spectrum of the capped particles as a KBr pellet is shown in Figure 3.23a. The particles were washed with a basic solution (either KOH or NaOH) of pH of approximately 8 and dried. Particles treated with strong acid displayed no evidence of the cap, suggesting that acid could cleave the CdS-ϕ-CO_2^- bondand/or remove the surfactant fromt eh particle surface. Peaks attributable to aromatic (C=C) skeletal stretching in the 1600 - 1450 cm^{-1} region deviate somewhat from accepted values (see Table 3.10). The capped particles may exist in both a carboxylate ion and acid form as is seen from the fact that both the symmetric (O-C-O) as well as the (C=O) stretches are present in the spectrum with appreciable intensity (see Table 3.10). The presence of strong aliphatic (C-H) stretch vibrations below 3000 cm^{-1} and the lack of aromatic (C-H) stretch vibrations suggests a low degree of derivatization with the desired thiobenzoic acid cap. A possibility is that the surfactant used in the preparation of the capped particles remains on the surface of the particles. Spectral features such as a (-CH_2-) bend at 1462cm^{-1} as well as the peaks at 1230, 1053 cm^{-1} assignable to a (S=O) stretch, perhaps ambiguously since these stretches can overlap with the

(C=O) vibrations.

The particles were suspended in the QP blend and cast upon an IRTRAN disc to obtain an FTIR spectrum (Figure 3.23b). All features of the QP blend are present and peaks for the strongest of the capped particle peaks are weak, but discernible at 1725 cm^{-1} (C=O), as a shoulder at 1227 cm^{-1} and at 1046 cm^{-1} (C-O). The strong asymmetric (O-C-O) stretch is likely hidden by the much stronger polymer absorption in this region. The only perceptible change in the spectrum of the polymer is an increase in intensity in the H-bonding region. This is likely due to lab humidity, but could suggest that H-bonding could play a significant role in the binding of the particles to the polymer matrix. There is little unequivocal spectroscopic evidence to identify if and where the particles are coordinating themselves within the QP blend.

Table 3.10: Assignable features in IR spectrum of capped CdS particles

Observed peaks - cm^{-1}	Assignment
1053s, 1230s	(C-O) or (S=O) stretches
1404s	(O-C-O) symmetric stretch (carboxylate)
1462m	$(-CH_2-)$ bend
1596s, 1535m	$(C=C)_{aromatic}$ skeletal stretch
1733s	(C=O) stretch
2867m, 2974s, 2957s	(C-H) stretch

Figure 3.24a shows the electrochemistry of capped CdS particles within a QP blend film. The only feature in the voltammogram is the irreversible pyridinium to pyridinium radical at -0.61 V (vs SCE). A faint shoulder at *ca.* 0.30 V could be

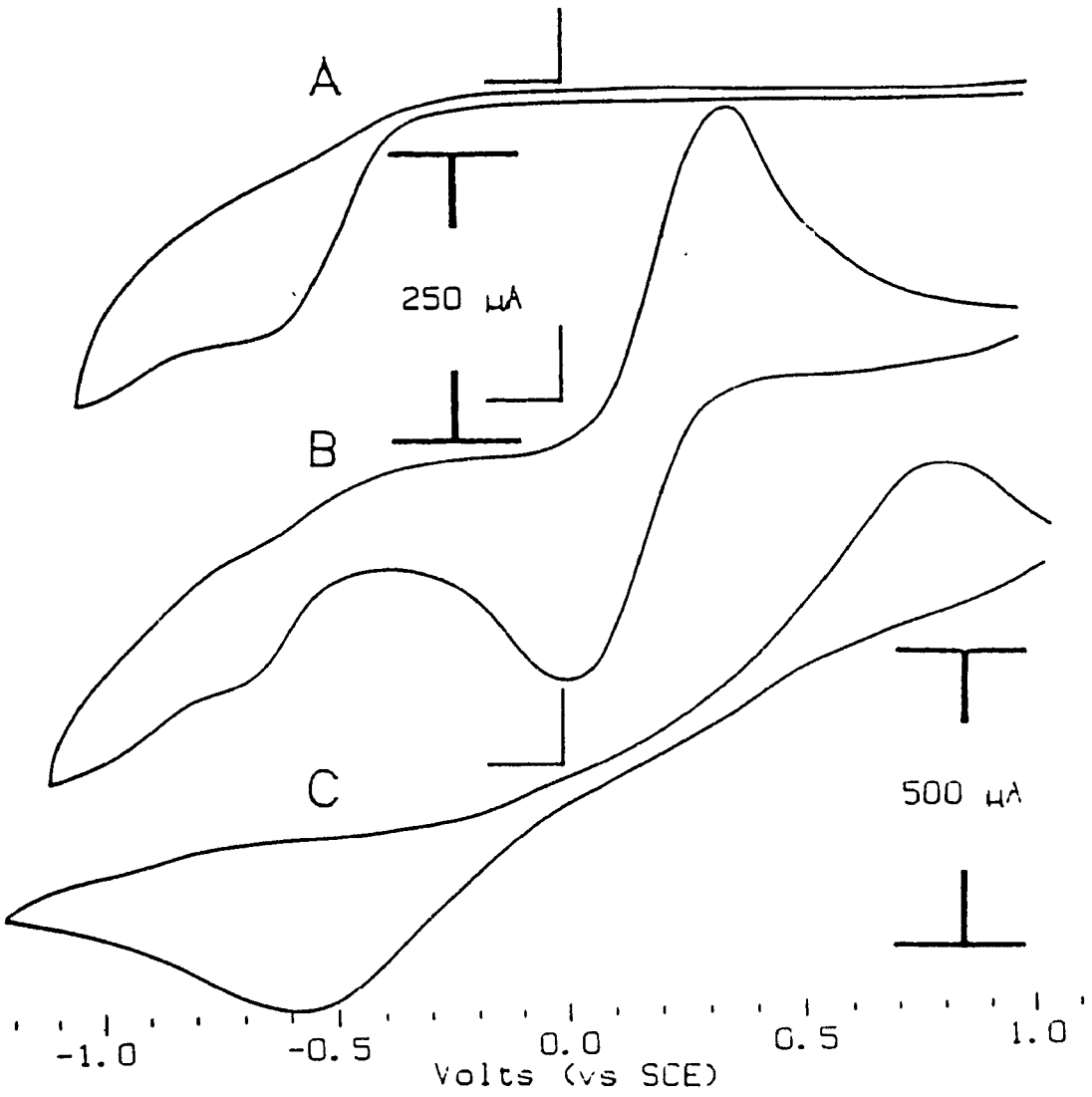

Figure 3.24 Cyclic voltammograms of capped CdS particles within QP blend films in (a) 1.0 M KCl and in 2 mM $Fe(CN)_6^{3-/4-}$/0.1 M KCl for (b) most electrodes studied and (c) for a minority of electrodes. (a) and (b) are on the 250 µA scale and (c) on the 500 µA scale

attributed to its anodic sister peak. Peaks due to $Fe(CN)_6^{3-}$ and $Fe(CN)_6^{4-}$ grew in when electrochemistry was run in redox solution. In a few cases the ΔE_p for $Fe(CN)_6^{3-/4-}$ was very large (as high as 1.4 V at 100 mV/s) for what appeared to be the voltammetric peaks of the redox couple (Figure 3.24c). The E°' for the couple appeared at 0.12 V (vs SCE). This behaviour would not persist, as continued cycling would shift the $Fe(CN)_6^{3-/4-}$ peaks to positions similar to the majority of electrodes studied. Most voltammograms in $Fe(CN)_6^{3-/4-}$, however, had well behaved peaks as in Figure 3.24b. E_{pc} = 0.02 V and E_{pa} = 0.37 V (vs SCE). All of these electrode coatings would crack and the colour of the particles would fade from an intense orange to faint yellow after a short time in solution and even colourless after extended time in solution. For the most part particles could not be fully contained within the modifying film, particles visibly protruding through the surface of film. This made impossible film thickness determinations. The majority of electrochemical behaviour for these electrodes is presumed to be due to diffusion of the redox couple through pinholes and cracks in the films as well as interaction of particles that protrude through the film/solution interface. With these facts in mind, calculation of diffusion coefficients for the redox couple within the film would probably not reflect actual ion transport within the film.

The surface of these capped particles are anionic whether they had been modified with thiobenzoic acid or whether the surfactant used in their preparation was present (which consists of sulfonate groups). Therefore, it is likely that reduction of the particles by the $Fe(CN)_6^{4-}$ (necessary in a photoanodic scheme) would be impeded by electrostatic repulsion of the like charged redox couple and semiconductor surface

modifiers. Replacement of ferri/ferrocyanide by couples of smaller charge of similar formal potential such as 0.1 M hydroquinone/0.1 M KCl or 0.2 mM ferrocene acetic acid/0.1 M phosphate buffer did not improve the system.

Figure 3.25 shows dark and visible illuminated currents of a capped CdS/QP blend electrode vs applied potential. The potential at which currents switch from positive to negative can give an estimate (although somewhat unreliable) of the conduction band edge of the semiconductor (69). The conduction band was placed at *ca.* 0.23 V (vs Ag/AgCl). Open-circuit voltages measured for these electrodes were between 10 and 50 mV and photovoltages, that is the voltage change upon electrode illumination (for 100 mW/cm^2) was between 0.7 and 5 mV.

SCPC's varied widely among films for 100 mW/cm^2 illumination. Commercially available CdS particles were incorporated into QP blend films. In 1.0 M KCl dark currents were very s w to stabilize and usually relatively large at 0.4 - 0.8 μA/cm^2. Initial light on-switching saw a very large capacitive response of up to 3.5 μA/cm^2 which would, however, decrease on subsequent off/on cycles. Steady state currents following switching relaxed to *ca* 200 nA/cm^2 (Figure 3.26a). These electrodes, when later placed into 2.0 mM $Fe(CN)_6^{3-/4-}$/0.10 M KCl also saw stable, large dark currents which depended upon the age of the electrode. SCPC's also depended upon age. Freshly prepared electrodes gave up to 1.5 μA/cm^2 (this being about 1/10 of those previously found for this system in this lab (70)), but would decay over about 1 to 2 hours to a steady 0.4 - 0.5 μA/cm^2. An electrode that had been soaked in redox solution over night shorted to a platinum counter electrode gave a response as in

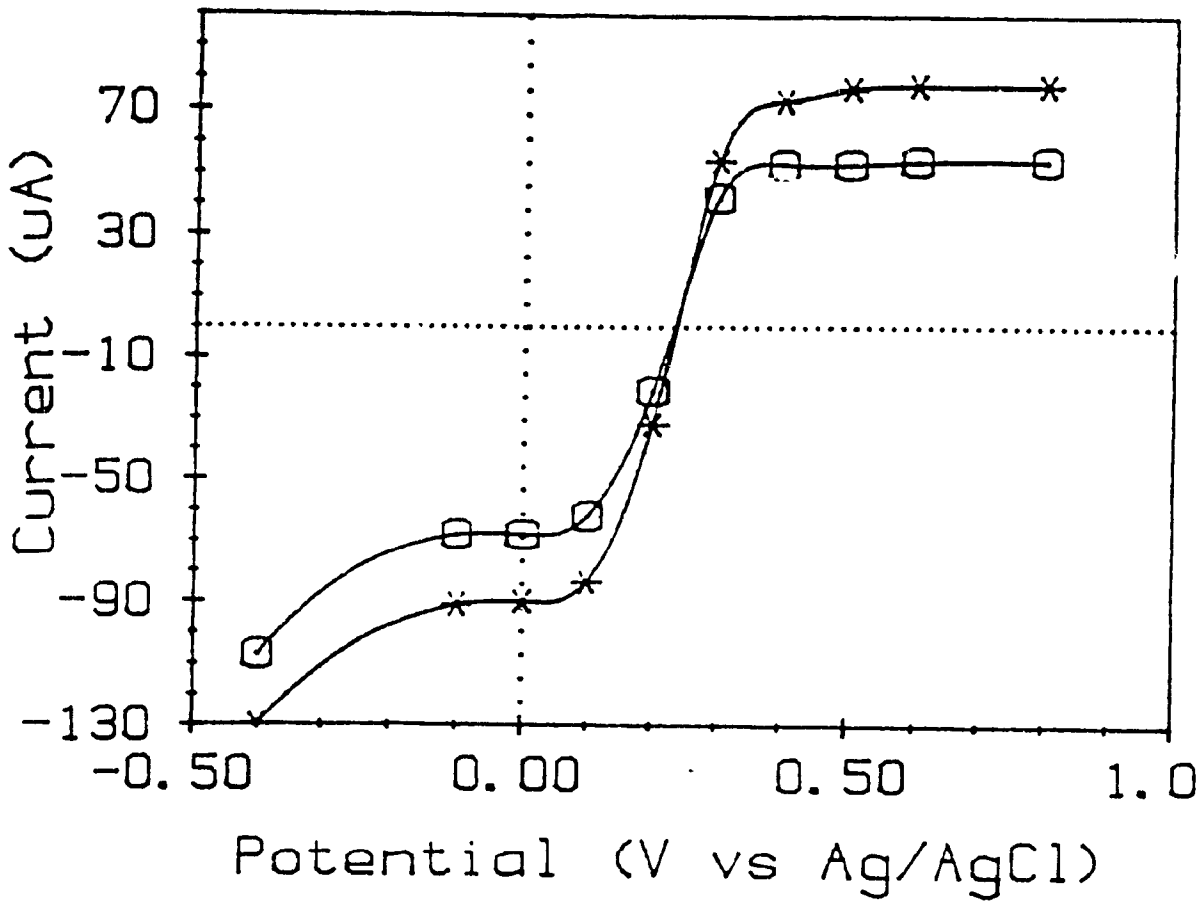

Figure 3.25 Dark (squares) and illuminated (stars) photocurrents for capped CdS particles within a QP blend film versus applied potential in 2 mM $Fe(CN)_6^{3-/4-}$/0.1 M KCl.

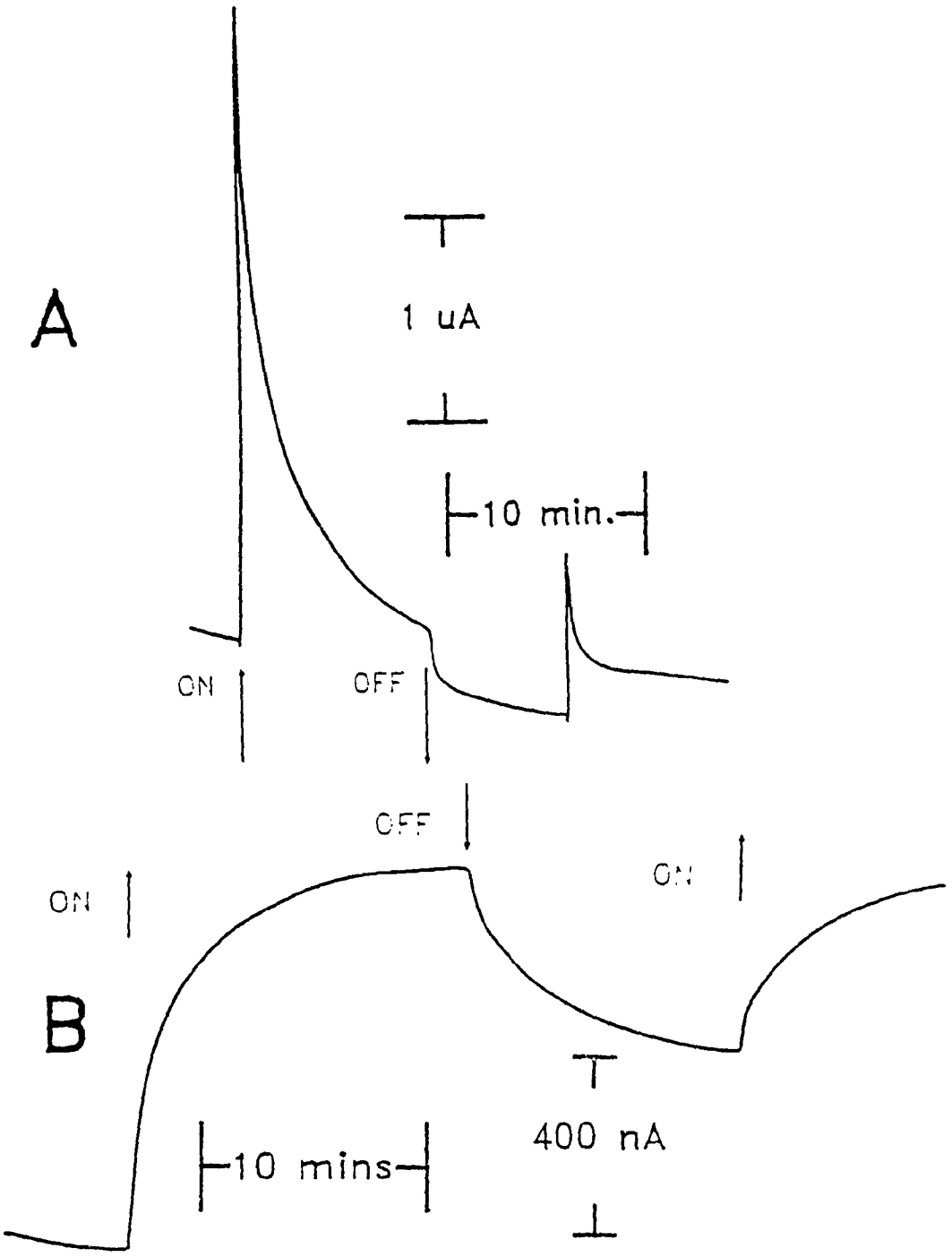

Figure 3.26 Short-circuit photocurrent profiles for capped CdS particles within QP blend film in (a) 1.0 M KCl and in (b) 2 mM $Fe(CN)_6^{3/4}$/0.1 M KCl. Photocurrent was anodic.

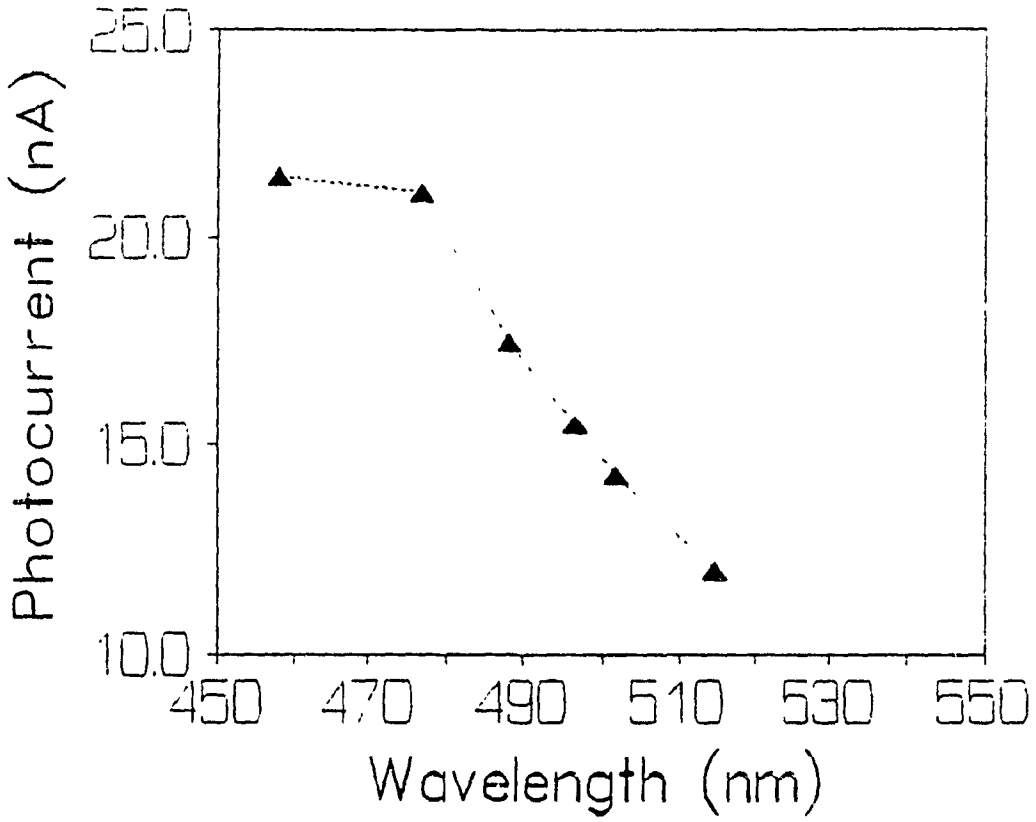

Figure 3.27 Photocurrent versus illumination wavelength for a capped CdS particle/QP blend composite electrode in a dry cell configuration. Illumination was from the visible lines of an argon ion laser adjusted to 50 mW/cm^2.

Figure 3.26b. Dark currents were relatively small, < 70 nA. The first light on-switching of the day saw a large response. Subsequent on and off cycles would not decay back to the original dark current, but to a new larger current as defined by the first off cycle (see Figure 3.26b).

Capped CdS particles gave much smaller dark currents than the uncapped commercially available particles. Dark currents ranged from -0.15 to -0.05 $\mu A/cm^2$ and were stable for days. Illumination gave anodic currents of between 150 and 700 nA/cm^2 depending on electrode age. Temporal response was trap controlled in appearance suggesting that conduction is mediated by the hydrophobic backbone of the QP blend polymer. Switching was very slow.

Figure 3.27 is a plot of photocurrent versus wavelength of illumination for a derivatized CdS particle/QP blend film in dry cell configuration using an argon ion laser in single line mode as radiation source adjusted to 50 mW per line. This illustrates that transduction of electromagnetic radiation is mediated by the CdS semiconductor particles. The photocurrent follows the band edge absorption of the CdS as illustrated in the particles' photoacoustic electronic spectrum in Figure 3.22.

Passivation of semiconductor particles has been effected by incorporation into conducting polymers (such as polypyrrole (41)). Unfortunately, the QP blend in our case is not a good conductor. Decomposition was evident from the large dark currents observed for most CdS/QP blend films. Within a 20 - 30 minute experiment electrode would show significant disintegration. The reactive holes of the semiconductor were obviously not being reduced by the intended solution redox species, but instead were

oxidizing itself or the surrounding QP blend decomposing the integrity of both. Surface derivatized particles showed smaller background current, but also smaller photocurrent than underivatized ones. The derivatized layer did not seem to help couple the particles to solution redox species.

Chapter 4

Discussion

4.1 Overview

The efficiency of wet junction photovoltaics can only reach that of conventional solid state devices in a form that couples the equivalent of a very high surface area of the light absorber to the surface of an electrode. A strategy followed over the course of this work was to integrate the absorber into polymer matrices. The light absorber represents the interface between electronic and faradaic processes, electron transfer toward the electrode and reduction of the thus oxidized absorber both having to occur here. It is therefore essential to couple the absorber to a medium of high electronic conductivity within a medium of high ionic mobility to support both "wet" and "dry" conduction.

4.2 Conductivity in polymers

Conduction in polymers strongly depends upon morphology. The greatest experimental conductivity observed thus far is for highly ordered polyacetylene (72) where charge flows along the oriented chain lengths of the highly conjugated polymer backbone. Polyacetylene shows increasing conductivity with degree of linearity of the polymer chains. Conductivity can be limited by: 1) the often circuitous tangle of polymer chains that exists in amorphous polymers, 2) interchain overlap which can vary depending on the degree to which the polymer is globular and 3) the presence of impurities or defects. This disorder gives rise to many localized states.

The presence of many localized states characterizes the energetics of amor-

phous polymers. In these solids intermolecular binding forces within polymers are weak and intermolecular electron transfer is dependent upon relatively weak Van der Waal bonds. In such a case the electronic structure of the material is more accurately described by individual charged polymeric chains (or molecular ions) than by bulk properties. Positive and negative molecular ion states are considered electron donors and acceptors and may be characterized by an ionization energy I_p and an electron affinity A_p for the polymer. Thermally induced disorder causes fluctuations in local dielectric polarization that has an effect on the energies of the molecular ions and hence the probability distribution of E_d and E_a states are best described by a Gaussian distribution (73).

A treatment of the electronic structure of insulating polymers developed by Duke and Fabish for ethylenic pendant polymers is known as the molecular ion model and has been described elsewhere (74-76). In their experiments they applied metals of different work function to the surface of insulating ethylenic homopolymers and measured contact potentials. Injection of charge into the polymer was assumed to be from the Fermi level of the contacting metal and charge is assumed to be injected into unique groups of polymeric states, thus an energy scale for donor and acceptor states of the polymer may be established. Electronic state densities that happen to be active in charge exchange experiments can be deduced from the dependence of the film potential generated in a given metal contact on polymer film thickness (77) equation 4.1,

$$\rho = \frac{2\varepsilon \Delta V}{b^2} \qquad (4.1)$$

where ρ is the bulk charge density, ΔV is the contact potential, b is the film thickness, and ε is the permittivity of the polymer. Thus, in such a way, the energy distribution of these polymers can be pictured. Electronic structural measurements have been carried out on poly(2-vinylpyridine) (**P2VP**) and poly(styrene) (77,78) which are similar to components of the polymer being investigated here. They also demonstrated that the energy distribution for copolymers or blends can be described by equation 4.2

$$N(E) = \sum X_i N_i(E) \qquad (4.2)$$

where X_i is the mole fraction of homopolymer "i" and N(E) is the energy density distribution (79). An approximated distribution of donor and acceptor states for the QP blend was developed by M.F. Lawrence and is shown in Figure 4.1 as calculated for this system by Crouch et al for this polymer blend (7). Electronic conduction in this polymer is assumed to be via the hydrophobic regions of the film whose constituent parts are P4VP and poly(styrene). The position of the centroid <E> will dictate the thermodynamic feasibility of charge injection from a photoexcited chromophore into the hydrophobic domains of the polymer. If the excited state dye is of sufficient reducing power and the ground state is of sufficient oxidizing power to be reduced by solution donors, the dye/QP blend can form the basis of a photoanode. The position of the centroid <E> was established in work carried out by Ordonez (80) on this same blend. A series of phthalocyanines with different metal centers of varying ground state, singlet and triplet excited state energy levels were prepared and incorporated into

the blend. It was found that only those complexes whose lowest energy excited triplet states were hig .er in energy than acceptor states within the polymer would show short-circuit photocurrent, while those whose excited state energies were below acceptor states showed none. This fact corroborates the placement of the <E> of the polymer blend in Figure 4.1.

The energetics of photo- and electro-active species in such systems can be established. The ground state energies of electro-active species can be estabilished from reduction potentials or from ionization potentials. The energetics of redox polymers are correlatable to the reduction potential of the redox species incorporated into the polymer chain. The time scale of photophysical processes are such that upon excitation to upper excited states, vibrational relaxation down to the lowest excited state will commonly be complete before any electron transfer events can occur. It is therefore assumed that all excited state reactivity will occur from the lowest excited states, either singlet or triplet. Once in the lowest excited state, deactivation of the excited electron can follow a number of routes as was described in Figure 1.4. Apart from the other deactivation routes described previously (in section 1.2.2) electron transfer can occur from either a singlet or tripet excited state. Flourescence and phosphorescence energies can give a good indication of the relative lowest singlet and triplet state energies to ground state energies, and hence can help place photo-active species on an energy scale. These excited states are the most likely to participate in photoinduced electron transfer. The relative energies of species investigated in this work are included in Figure 4.1.

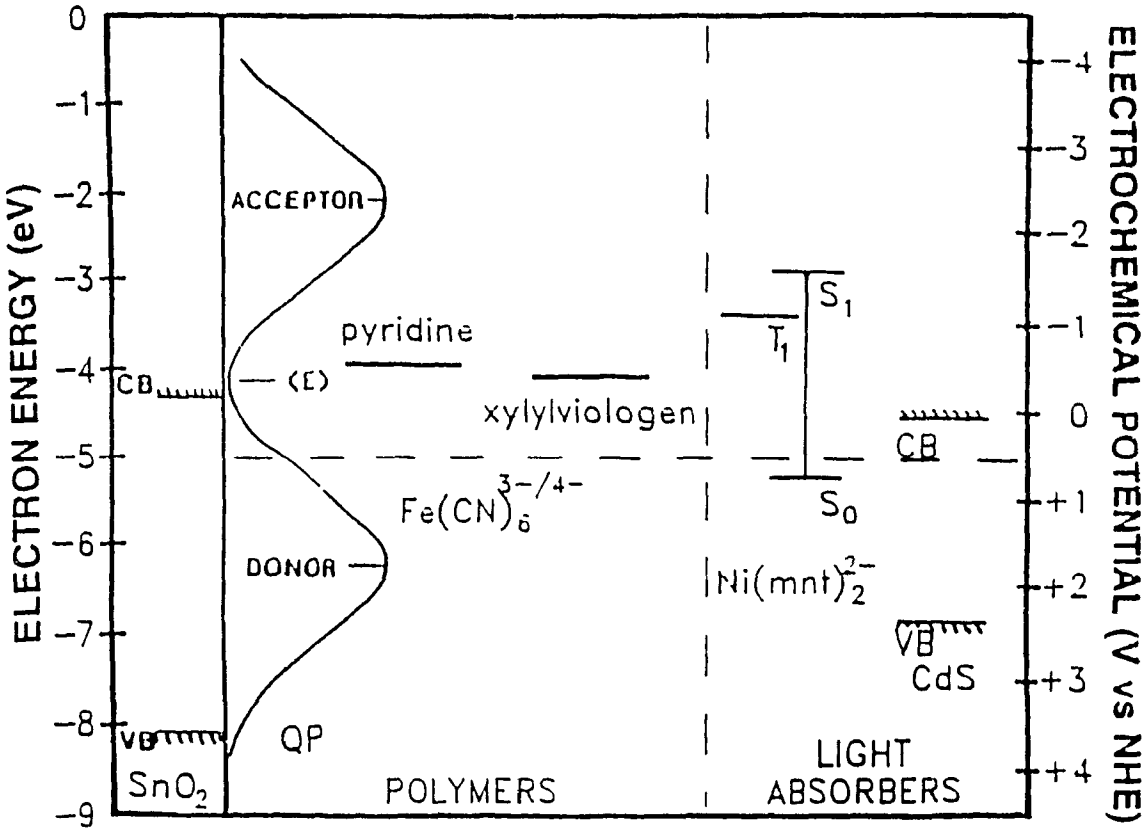

Figure 4.1 Energy level diagram. Distribution of acceptor and donor states of QP blend is shown relative to energy levels of species used in photovoltaic schemes here (SnO_2 electrode, $Fe(CN)_6^{3-/4-}$ redox couple, $Ni(mnt)_2$ dye, CdS particles and PXV, P4VP and QP polymers (adapted from (7)).

4.3 Electrode systems

A sensitized electrode studied in this laboratory and reported in 1986 (10) utilized the $Ni(mnt)_2$ dye and quaternized P4VP. This film permitted ion exchange of the complex and demonstrated larger photocurrents than observed for the dye in solution. The calculated diffusion coefficients for solution redox species used in the cell were of the order of 10^{-12} cm^2/s.

An advance on these films was made when a polymeric electrode coating consisting of a copolymer with quaternized ammonium derivatized methylstyrene moieties blended with poly(4-vinylpyridine-co-styrene) (**QP blend**) developed by Anson and coworkers (50) featured good ion exchange capabilities and calculated diffusion coefficients for electro-active species within an order of magnitude of solution values. These polymers would spontaneously segregate into hydrophobic and hydrophilic domains, supporting electronic conduction through the hydrophobic domains and ionic conduction through the hydrophilic domains. For films into which metal maleonitriledithiolates, phthalocyanines, and porphyrins were incorporated diffusion coefficients were similarly high (6-8). Also, in the case of the metal maleonitriledithiolates short-circuit photocurrents increased by a factor of a hundred (8) over that in quaternized P4VP. Temporal response in these systems, however, was slow, the electronic conduction being limited by electron traps within the hydrophobic domain of the QP blend. Realization of this fact led to efforts to exploit the ion conducting matrix of the QP blend while growing polypyrrole, a conducting polymer from the electrode surface (52). For electrons to travel along the conducting polymer

close orientation of the dye and the conductor should be obtained. An improvement was noted, but was not sufficiently large to suggest close coupling of the dye and conducting polymer.

Section 3.3 described a conducting polymer that was found to form a charge transfer complex with the $Ni(mnt)_2^{2-}$ dye. The PXV-$Ni(mnt)_2$ salt was found to be hydrophobic, therefore films did not show very large diffusion coefficients. Favourable positioning of the visible region absorption of the dye and acceptor levels of the polymer (the $PXV^{2+ \rightarrow 1+}$ reduction) as well as good conduction in the polymer led to rapid temporal response, but moderate photocurrents (9) about a tenth of that reported for the dye in the ion conducting QP blend (51, Chapter 4.4). This suggested that ion conductivity was the limit of the PXV-$Ni(mnt)_2$ system.

The promise of the PXV-$Ni(mnt)_2$ charge transfer salt behaviour led to strategies to improve ion conductivity within these films. Creating a swollen PXV modifying layer as a gel (section 3.4) to permit greater ion diffusion was of limited success. Gels would not allow significant in-partitioning of solution redox species. In a small number of cases for gels having an extreme concentration ratio of polymer to swelling solvent, a relatively loose polymer film structure and a larger capability for in-partitioning of redox species was realized. Photocurrents of about a factor of two larger than the PXV-$Ni(mnt)_2$ film system of section 3.3 were observed. Regrettably, the performance of these electrodes deteriorated quickly and most electrodes gave small trap controlled photocurrents. This again pointed to the importance of sustaining ionic as well as electronic conduction. The gels permitted a solvent swollen PXV

polymer structure showing large diffusion coefficients for solution species, but these species had poor solubility in the swelling solvent of the gel. The swollen polymer also appeared not to have favourable overlap of adjacent polymer chains since the temporal response of most electrodes demonstrated trap control switching behaviour.

The gel research, proving to be unsuccessful, stimulated further efforts to incorporate the PXV polymer into an ion conducting matrix. Section 3.2 outlined the characterization of the neat dye/QP blend system which formed a starting point for the modified films. Of particular note is the fact that the films produced during this work demonstrated the same reported diffusion coefficients (51, Chapter 4.2), but only reached *ca.* a tenth of the observed photocurrents under similar conditions. Spectroscopic data for the present QP blend matched that previously obtained. Elemental analysis showed a large discrepancy for the stoichiometric ratios of the monomers of the QP as compared to previous work (51, Chapter 2), but an anomalously low carbon value could have led to overestimation of oxygen content and hence an over inflated ethanolamine contribution to the calculation of monomer percentages. Discrepancies in carbon content for repeat analyses suggest that deviation in monomer percentages may not be significant.

Moderate dry cell photocurrent was observed for the dye/QP blend films as was seen in Figure 3.8a implying that the film did exhibit electronic conductivity. Charge transport is believed to involve trapping of photoexcited dye electrons by a broad distribution of trap states within the QP blend (7). The nature of the electron transfer between excited dye and polymer is not well characterized. From Figure 4.1.

the energetics of charge tranfer from an excited state of the $Ni(mnt)_2$ to the pyridine or the broad distribution of acceptor states of the QP blend is possible, but little evidence was found here to suggest that the dye and pyridine moiety couple or that electron transfer procedes via an $Ni(mnt)_2$ to pyridine route. Resonance raman and IR data reported in section 3.2.1 as well as experiments observing the effect on photocurrent of varying the degree of protonation of pyridine moieties within the film (see Figure 3.5) have shown no evidence of physical or electronic coupling of the pyridine to the dye. What was observed was an increase in rise and decay times for the electrodes at increasing pH indicating, not surprisingly that the P4VP contributes to the conduction pathway. Overlap of donor and acceptor species seems to be poor in the electrode films studied here and appears to limit the films.

4.4 PXV modified films

Notwithstanding the problem with reproducibility of the QP blend films, they were employed in efforts to incorporate conductors into a solvent swollen atmosphere to circumvent the poor conductivity noted for the QP blend's hydrophobic domains, which was a limit to the previously reported system, anyway (7,8). The fact that PXV formed charge transfer salts with the $Ni(mnt)_2$ was an encouraging starting point for these efforts. The PXV^{2+} was incorporated into the QP blend casting solutions, films cast from these did not show the structure of the QP blend favourable to high ionic conductivity. These films would allow high concentrations of the dye to be immobilized in the electrode film, but the structure of the film did not permit either electronic

or ionic conduction. This result pushed incorporating the PXV into preformed QP blend films. This was accomplished by either direct cathodic deposition or codeposition with a crosslinking agent. The former technique produced films of small PXV concentration which showed a potential for conducting photocurrent, but in a structure that either broke down or dissolved from the electrode pores into solution. Crosslinked PXV displayed good adherence of the PXV within the film. Unfortunately, immobilization of PXV depended upon reaction of the fully reduced, neutral viologen with a crosslinking agent. This oxidation state of the polymer is not reversibly reoxidized and it is well known that it is the 2+ -> 1+ reduction that is responsible for the redox self exchange conductivity in this polymer. The crosslinked films were electrically resistant and would be produced close to the electrode. If the dye was coupled to the viologens only very small capacitive SCPC's were observed. If the dye remained coupled to the QP blend SCPC's similiar to the neat QP blend films of section 3.2 would be observed.

The PXV did not prove a good choice for growing a conductive element through the QP blend. Electrodepostion did not afford films of sufficient thickness for use considering the thickness of our modifying layers were between 10 and 20 μm. The polymer is known to be composed of 8 - 9 repeat units and macroscopic conduction relies upon overlap of many separate chains. Attachment of the viologen moiety to an electropolymerizable functionality could increase the low concentration of PXV obtained here.

4.5 Semiconductor particle modified electrodes

An alternative tact was to obviate the troublesome coupling of light absorber to conductor by incorporating semiconductor particles into the QP blend film. These would offer the advantage of high extinction coefficients and high suface area while offering conductivity from particle to particle. Growing the particles within the film gave, in a few cases surprisingly large short-circuit photocurrents. These would not persist since the method of growing the particles was very harsh and electrode films would decompose a short time after being exposed to solution.

Preformed particles were incorporated into the polymer films. Directly incorporating commercially available high quality CdS gave moderate currents characteristic of trap controlled conduction. These particles would not necessarily reside at the interface of the hydrophobic and hydrophilic domains of the blend, which is where most efficient coupling of electronic and faradaic process would be expected to occur. The slow temporal response implied that charge was shuttled to the electrode through the hydrophobic domains of the QP blend instead of along the semiconductor, which defeats our purposes. Growing smaller particles with functionalities upon their surfaces would hopefully coordinate them to the blend at the interface of the two domains. Results showed poor size control as well as somewhat ambiguous surface derivatization. Short-circuit photocurrents were again moderate and trap controlled. The anionic functionalities upon the surface of these particles could also create a problem of intercluster communication as the repulsion of the like charged surface could restrict the distance to which the particles could approach one another.

4.6 Conclusions

In preparing chemically modified electrodes one must keep in mind that the net chemical, electrochemical or photoelectrochemical activity of the electrode is not so much a question of presence, but of accessibility of active sites. Of importance in wet junction cells is the distribution of any active species throughout the modifying matrix in such a way as to permit both electronic and faradaic processes to occur. If substrate diffusion is rate determining, only a small fraction of the film at the film/-solution interface will be used. On the other hand, if charge diffusion is rate determining, the catalytic reaction can take place only in a film fraction close to the electrode surface. Each of these effects will render parts of the film superfluous, and it is obvious that in either case there is no sense in designing very thick redox films.

The films studied here succeeded in coupling more than a monolayer of sensitizer to the surface of the SnO_2 electrode, but the QP blend film demonstrated some combination of poor electron accepting characteristics and poor conductivity in limiting performance of the system. The ion conducting polymer blend would retain the anionic $Ni(mnt)_2$ species while at the same time incorporating a substantial concentration of charged solution species.

The strategies pursued in this thesis may not have demonstrated the improvement in electronic conductivity initially hoped for, but they do point to possible future directions to this end. The PXV polymer while showing good conductivity in forms that permitted close overlap of the polymer chains (in a compressed state of poor ionic conductivity (section 3.3)), demonstrated an inability to form extended overlapping

chains when deposited through the solvent channels of the QP blend. A polymer of longer chain length could improve conductivity. In situ formation of semiconductor particles assured that particles grew in the solvent channels of the QP blend. A more robust, perhaps chemically crosslinked blend could resist the harsh conditions of particle preparation. The corrosion of the semiconductor particles prepared in this way seemed to be reduced upon surface derivatization, but this also reduced overall photocurrents. Attempts to passivate the surface of these particles with a conducting polymer such as polypyrrole within the QP blend could help reduce corrosion while maintaining a high photocurrent.

References

1 Archer, M.D.; Bolton, J.R. *J. Phys. Chem.* **1990**, *94*, 8028.

2 Lewis, N.S. *Acc. Chem. Res.* **1990**, *23*, 176.

3 Grätzel, M. *Energy Resources Through Photochemistry and Catalysis*; Academic Press: New York, **1983**.

4 Parkinson, B. *J. Chem. Ed.* **1983**, *60*, 338.

5 Bard, A.J. *J. Phys. Chem.*, **1982**, *86*, 172.

6 Crouch, A.M.; Langford, C.H. *J. Electroanal. Chem.* **1987**, *83*, 221.

7 Crouch, A.M.; Ordonez, I.; Langford, C.H.; Lawrence, M.F. *J. Phys. Chem.* **1988**, *92*, 6058.

8 Biro, D.A.; Langford, C.H. *Inorg. Chem.* **1988**, *27*, 3601.

9 Lefebvre, M.C.; Biro, D.A.; Langford, C.H. *Can. J. Chem. in press.*

10 Persaud, L.; Langford, C.H. *Inorg. Chem.* **1986**, *25*, 3438.

11 Bettelheim, A.; White, B.A.; Raybuck, S.A.; Murray, R.W. *Inorg. Chem.* **1987**, *26*, 1009.

12 Vlachopolous, N.; Liska, P.; Augustybski, J.; Grätzel, M. *J. Am. Chem. Soc.* **1988**, *110*, 1216.

13 Gosh, P.; Spiro, T.G. *J. Am. Chem. Soc.* **1980**, *102*, 5543.

14 Nosaka, Y.; Kuwabara, A.; Miyama, H. *J. Phys. Chem.* **1986**, *90*, 1465.

15 Gastonguay, L.; Dodelet, J.P.; Côté, R.; Lawrence, M.F.; Gravel, D.; *Can. J. Chem.* **1990**, *68*, 202.

16 Gningue, D.; Horowitz, G.; Garnier, F. *Ber. Bunsenges. Phys. Chem.* **1987**, *91*, 402.

17 Barendrecht, E. *J. Applied. Electrochem.* **1990**, *20*, 175.

18 Zameraev, K.I.; Parmon, V.N. In *Energy Resources Through Photochemistry and Catalysis*; Grätzel, M., Ed.; Academic Press: New York, **1983**; Chapter 5.

19 Turner, A.P.F.; Karube, I.; Wilson, G.S. *Biosensors*; Oxford Press: London, **1987**.

20 Chen, Y.L.; Guan, Y.J.; Mai, Y.L.; Li, W.; Liang, Z.X. *J. Macromol. Sci., Chem.* **1988**, *A25(2)*, 201.

21 Natan, M.J.; Wrighton, M.S. *Prog. in Inorg. Chem.* **1989**, *37*, 391.

22 Merz, A. In *Topics in Current Chemistry*; Steckhan, E., Ed.; Springer-Verlag: Berlin, **1990**; p49.

23 Bargon, J.; Mohmand, S.; Waltman, R.J. *IBM J. Res. Develop.* **1983**, *27*, 330.

24 Ikenoue, Y.; Saida, Y.; Kira, M.; Tomozawa, H.; Yashima, H.; Kobayashi, M. *J. Chem. Soc., Chem. Commun.* **1990**, 1694.

25 Creager, S.E.; Fox, M.A. *J. Electroanal. Chem.* **1989**, *258*, 431.

26 Deronzier, A.; Essakalli, M. *J. Chem. Soc., Chem. Commun.* **1990**, 242.

27 Oyama, N.; Anson, F.C. *J. Electrochem. Soc.* **1980**, *127*, 640.

28 Murray, R.W. In *Electroanalytical Chemistry*; Bard, A.J., Ed.; Dekker: New York, **1984**; *13*, p191.

29 Piechowski, A.P.; et. al. *J. Phys. Chem.* **1984**, *88*, 934.

30 Sartain, D.; Truter, M.R. *J. Chem. Soc., Chem. Commun.* **1966**, 382.

31 Eisenberg, R.; Ebers, J.A.; Clark, R.J.H.; Gray, H.B. *J. Am. Chem. Soc.* **1964**, *86*, 113.

32 Persaud, L. *PhD. Thesis*; Concordia University, Montreal, Que, Canada, **1985**.

33 Dooley, D.M.; Patterson, B.M. *Inorg. Chem.* **1982**, *21*, 4330.

34 Lianos, P.; Thomas, J.K. *Chem. Phys. Lett.* **1986**, *125*, 299.

35 Wang, Y.; Herron, N. *J. Phys. Chem.* **1987**, *91*, 257.

36 Henglein, A. *Chem. Rev.* **1989**, *89*, 1861.

37 Fendler, J.H. *Chem. Rev.* **1987**, *87*, 877.

38 Wang, Y. *J. Phys. Chem.* **1991**, *95*, 1119.

39 Towey, T.F.; Khan-Lodhi, A.; Robinson, B.H. *J. Chem. Soc., Farad. Trans.* **1990**, *86*, 3757.

40 Steigerwald, M.L.; Brus, L.E. *Acc. Chem. Res.* **1990**, *23*, 183.

41 Dalas, E.; Sakkopoulos, S.; Kallitsis, J.; Vitoratos, E.; Loutsoukos, G. *Langmuir* **1990**, *6*, 1356.

42 Spialter, L.; Pappalardo, J.A. *The Acyclic Tertiary Amines*; Macmillan: New York, **1965**; p14.

43 Christian, G.D. *Analytical Chemistry* 3rd ed.; Wiley and Sons: Toronto, **1980**. p240.

44 Factor, A.; Heinsohn, G.E. *Polym. Lett.* **1971**, *9*, 289.

45 Lawrence, M.F., *personal communication.*

46 Campaigne, E.; Meyer, W.W. *J. Org. Chem.* **1962**, *27*, 2835.

47 Steigerwald, M.L; Alivisatos, A.P.; Gibson, J.M.; Harris, T.D.; Kortan, R ; Muller, A.J.; Thayer, A.M.; Duncan, T.M.; Douglass, D.C.; Brus, L.E. *J. Am. Chem. Soc.* **1988**, *110*, 3046.

48 Chang, H-C.; Osawa, M.; Matsue, T ; Uchida, I. *J. Chem. Soc., Chem. Commun.* **1991**, 611.

49 Smothkin, E.S.; Brown, R.M.; Rabenberg, L.K.; Salomon, K; Bard, A.J.; Campion, A.; Fox, M.A.; Mallouk, T.E.; Webber, S.E.; White, J.M. *J. Phys. Chem.* **1990**, *94*, 7543.

50 Montgomery, D.D.; Anson, F.C. *J. Am. Chem. Soc.* **1985**, *107*, 3431.

51 Biro, D.A. *PhD. Thesis*, Concordia University, **1989**, Montreal, Que., Canada.

52 Biro, D.A.; Langford, C.H. *to be published.*

53 McCleverty, J.A. *Prog. Inorg. Chem.* **1968**, *12*, 49.

54 Rao, C.N.R. *Chemical Applications of Infrared Spectroscopy*; Academic Press: New York, **1963**, Chapters 2&6.

55 Sakai, Y.; Sadaoka, Y.; Fukumoto, H. *Sens. Actu.* **1988**, *13*, 243.

56 Schlapfer, C.W.; Nakamoto, K. *Inorg. Chem.* **1975**, *14*, 1338.

57 Langford, C.H.; Snoeck, T.L.; Stufkens, D.J. *to be published.*

58 Raghvan, R.; Iwamoto, R.T. *J. Electroanal. Chem.* **1978**, *92*, 101.

59 Abruna, H.D. *Coord. Chem. Rev.* **1988**, *86*, 135.

60 Adams, R.N. *Electrochemistry at Solid Electrodes*; Marcel Dekker: New York. **1969**, p219.

61 Inoue, T.; Anson, F.C. *J. Phys. Chem.* **1987**, *91*, 1519.

62 Liang, Z.; Lui, W.; Li, W.; Li, M. *Polym. Mat. Sci. Eng.* **1987**, *57*, 593.

63 Hester, R.E.; Suzuki, S. *J. Phys. Chem.* **1982**, *86*, 4626.

64 Sato, H.; Tamamura, T. *J. Appl. Polym. Sci.* **1979**, *24*, 2075.

65 Kosower, E.M.; Cotter, J.L. *J. Am. Chem. Soc.* **1964**, *86*, 5524.

66 Tsou, Y.M.; Hui, H.Y.; Bard, A.J. *J. Electrochem. Soc.* **1988**, *135*, 1669.

67 Sumi, K.; Anson, F.C. *J. Phys. Chem.* **1986**, *90*, 3845.

68 Audebert, P.; Divisia-Blohorn, B.; Kern, J.M.; Aldebert, P.; *J. Chem. Soc.. Chem. Commun.* **1989**, 939.

69 Bard, A.J. *J. Phys. Chem.* **1982**, *86*, 172.

70 *Unpublished results.*

71 Kutal, C. *J. Chem. Ed.* **1983**, *60*, 882.

72 Heinze, J. In *Topics in Current Chem;* Steckhan, E., Ed.; Springer-Verlag: Berlin, **1990**, p1.

73 Silinsh, E.A. *Organic Molecular Crystals*: Springer-Verlag: Berlin, **1980**.

74 Duke, C.B.; Fabish, T.H.; Paton, A. *Chem. Phys. Lett.* **1977**, *49*, 133.

75 Duke, C.B.; Fabish, T.J. *Phys. Rev. Lett.* **1976**, *37*, 1075.

76 Duke, C.B. *Surf. Sci.* **1978**, *70*, 674.

77 Fabish, T.J.; Saltsburg, H.M.; Hair, M.L. *J. Appl. Phys.* **1976**, *47*, 930.

78 Duke, C.B.; Salaneck, W.R.; Fabish, R.J.; Ritsko, J. .; Thomas, H.R.; Paton, A. *Phys. Rev., B* **1978**, *18*, 5717.

79 Duke, C.B.; Fabish, T.J. *J. Appl. Phys.* **1978**, *49*, 316.

80 Ordonez, I.D. *PhD. Thesis*, Concordia University, **1989**, Montreal, Que., Canada.

81 Davison, A.; Holm, R.H. *Inorg. Synth.* **1967**, *10*, 8.